Synthesis and Photoluminescent Properties of Linear and Starburst Compounds Based on Benzimidazole, 2-(2'-pyridyl)benzimidazole and 2,2'-dipyridylamine

By

Wade M. White

A thesis submitted to the Department of Chemistry

in conformity with the requirements for

the degree of Master of Science

Queen's University

Kingston, Ontario, Canada

July 2007

Abstract

The objective of this thesis was to explore the chemistry of series of linear and star shaped compounds based on benzimidazolyl, 2-(2'-pyridyl)benzimidazolyl, and 2,2'-dipyridylamino functional groups. These groups all possess Lewis base sites suitable for metal coordination, and are all known fluorophores.

The first compounds to be presented are the homo-substituted benzimidazolyl derivatives. Compounds 2.1-2.5 have been fully characterized and are all luminescent with emission energies in the UV region. While coordination complexes with these ligands have not been isolated, the effect of metal ion complexation on ligand luminescence has been explored via metal ion titration experiments. Furthermore, these compounds all have electron affinities greater than -3.0 eV and large optical bandgaps that range between 3.55 and 3.95 eV. These compounds also have high thermal and morphological stability. In light of this, compound 2.3 was selected as a representative example, and further characterized as an electron transport/hole blocking material for OLED applications. It has demonstrated a performance comparable to that of the well known electron transport material Alq_3 (q = 8-hydroxyquinolinate).

The second class of compounds, 3.2 and 3.3, represent a pair of hetero-substituted ligands with two different binding sites available for coordination chemistry. A copper (I) complex of 3.3 has been isolated and exhibits orange phosphorescence at room temperature and at 77 K. Furthermore, a series of metal titration experiments have been performed on 3.3 and 3.4, and have demonstrated the preference of different metal ions for either the 2,2'-dipyridylamino site, or the 2-(2'-pyridyl)benzimidazolyl binding site. The details of these explorations will be presented in the subsequent chapters.

Acknowledgements

I would like to extend my deepest and most sincere gratitude to Professor Dr. Suning Wang for her continued help and support throughout this research project. Her kindness, patience, encouragement, and understanding have been greatly appreciated. Without her assistance, none of this would have been possible.

I would also like to thank Professor Dr. Francoise Sauriol for her direction in recording variable temperature NMR and Dr. Ruiyao Wang for his continued assistance in collecting x-ray data and in solving the x-ray structures. Furthermore, I extend my thanks to Professor Dr. Philip Jessop and Professor Dr. Guojun Liu for being on my supervisory committee and for their continued assistance in this capacity.

Special thanks go to all of the members of the Wang group, including Dr. Wen-Li Jia, Dr. Junghyun Lee, Dr. Liu, Dr. Yi Sun, Dr. Yi Cui, Dr. Dongren Bai, Theresa McCormick, Yasmin Jessa, Shubin Zhao, Sanela Martic and Hazem Amarne for their continued assistance and support. I would also like to thank Xiaodong Feng, Sijin Han and Dr. Zhen-Hong Lu for the preparation and characterization of the devices prepared using compound 2.3.

Many thanks go to the other professors, staff members and fellow students who have helped me through my degree and to the National Sciences and Engineering Research Council, Queen's Graduate School and the Queen's Department of Chemistry for funding.

Finally, I can only hope to begin to thank my family and fiends for listening when I've been stressed, for encouraging me when I've been down and for giving me the strength and courage to finish this program.

Table of contents

List of Tables

List of Figures

List of Symbols and Abbreviations

A	ampere
Å	Angstrom
ABS	absorbance
Anal	analysis
C545T	10-(2-benzothiazolyl)-2,3,6,7-tetrahydro-1,1,7,7,-tetramethyl 1-1H,5H,11H-[1]benzopyrano [6,7,8,ij]quinolizin-11-one
Calc	calculated
CE	current efficiency
cm	centimeters
cd	candela
CH_3CN	acetonitrile
CH_2Cl_2	dichloromethane
d	doublet
dd	doublet of doublets
ddd	doublet of doublet of doublets
dt	doublet of triplets
DCM	4-(dicyanomethylene)-2-methyl-6-[4-(dimethylaminostyryl)-4H-pyran]
DFT	density functional theory
DMF	dimethylformamide
DNA	deoxyribonucleic acid
DPA	dipyridylamino
DSC	differential scanning calorimetry

EA	electron affinity
ETM	electron transport material
eV	electron volt
FLU	fluorescence
Hz	Hertz
HOMO	highest occupied molecular orbital
HRMS	high resolution mass spectrometry
HTM	hole transport material
HX	acid
IP	ionization potential
ISC	intersystem crossing
J	coupling constant, current density
K	kelvin
kV	kilovolts
L	liter, luminance
LCD	liquid crystal display
LLCT	ligand to ligand charge transfer
LUMO	lowest unoccupied molecular orbital
m	meter, multiplet
M	molar
mA	milliampere
mg	milligram
MHz	megahertz

mL	milliliter
MLCT	metal to ligand charge transfer
^{3}MLCT	triplet metal to ligand charge transfer
mmol	millimole
MO	molecular orbital
mol	mole
m. p.	melting point
mw	milliwatts
NBB	Fullerene
NPB	N,N’-diphenyl-N,N’-bis(1-naphthalenyl)-1,1’-biphenyl-4,4’-diamine
nm	nanometers
NMR	nuclear magnetic resonance
OLEDS	organic light emitting diodes
PBM	2-(2’-pyridyl)benzimidazolyl
PC	personal computer
PHOS	phosphorescence
PMMA	poly(methyl methacrylate)
q	8-hydroxyquinolate
s	seconds
S_0	singlet ground state
S_1	singlet excited state
Spec	spectrometry
t	triplet

T_1	triplet excited state
TAB	tris(N-7-azaindolyl)benzene
T_g	glass transition temperature
TBPI	1,3,5-tris(N-phenyl-benzimidazol-2-yl)benzene
TDAT	2,4,6-tris(dipyridylamino)-1,3,5-triazine
TGA	thermogravimetric analysis
THF	tetrahydrofuran
TIB	1,3,5-tris(N-indolyl)benzene
TLC	thin layer chromatography
TPD	N,N'-diphenyl-N,N'-bis(3-methylphenyl)-1,1'-biphenyl-4,4'-diamine
TSQ	N-(6-methoxy-8-quinolyl)-p-toluenesulfonamide
UV-Vis	ultraviolet-visible
V	volts
δ	chemical shift
μs	microsecond
λ	wavelength
ϕ	quantum yield
ϕ_a	anode work function
ϕ_c	cathode work function
τ	lifetime

Chapter 1:

Introduction

1.1 Organic Light Emitting Diodes

Organic light emitting diodes (OLEDs) represent an emerging display technology. A number of companies such as Kodak, Phillips Research and Cambridge Display Technology have begun to incorporate flat panel displays using OLEDs into some of their simple devices, such as cellular telephones and digital cameras.[1] The initial discovery of electroluminescence in organic materials was made by Pope *et al* in 1963 when a large crystal of anthracene emitted light while under the influence of a large potential difference.[2,3] Tang and van Slyke later demonstrated that by devoting different materials to electron transport, emission and hole transport, simple and efficient light emitting devices could be constructed. These devices are capable of efficiently producing various colors of light at low voltages making them potentially useful industrially.[2,4]

OLEDs are promising for a number of reasons. They operate at low voltages (3-10 V) and are capable of high luminance. Furthermore, device fabrication is simple, consisting of vacuum deposition by sublimation or spin coating of organic materials between layers of appropriate electrode materials. This can potententially lead to many different applications, including devices which are smaller and simpler than any that can be built using conventional cathode ray tube technology, or large and flexible displays prepared from polymer materials. Furthermore, because OLEDs are themselves emissive,

they offer considerably enhanced power efficiency when compared with liquid crystal display (LCD) technologies, which require an alternate light source and which are the current leader in flat panel display technologies.[5]

1.1.1 **Principles of Operation**

A generalized structure for a triple layer OLED device is depicted in Figure 1-1. A cathode injects electrons into an electron transport material (ETM), which transfers electrons to the emissive layer. Simultaneously, an anode injects holes into a hole transport material (HTM), which transports holes to the emissive layer. Ideally, holes and electrons combine in the emissive layer to generate excitons, which relax to produce light. This is ensured when the electron transport layer is effective in blocking holes, and the hole transport layer is effective in blocking electrons.

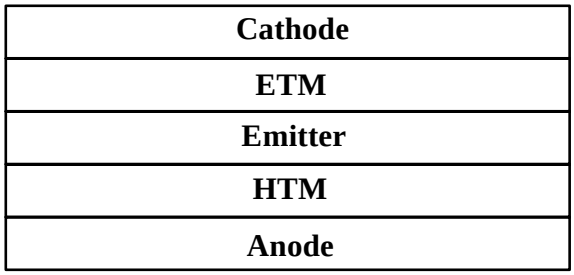

Figure 1-1: Standard device structure for a triple layer device. Organic layers are desposited onto an anode material by vacuum deposition, followed by deposition of the cathode material.

Triple layer devices tend to be the most efficient, with external quantum efficiencies of 4-5% having been reported by 1997. Simplified device designs also exist, in which only one to two layers of organic compounds are applied between the anode and the cathode. For example, the first device designed by Tang used Alq_3 (q=8-hydroxyquinolate) as both the emitter and ETM and produced green electroluminescence.

Double layer devices have also been designed in which hole transport and emission are combined into a single layer.[4]

The simplest design is of course the use of a single material for electron transport, emission, and hole transport. This is often challenging, because most organic materials do not transport electrons and holes with equal efficiency, resulting in charge recombination occurring close to one of the electrodes and reduction of overall efficiency. The simplicity of this design, however; makes this type of devices structure desirable. Schematic diagrams of the simplified device structures are illustrated below.[1,2,4,6]

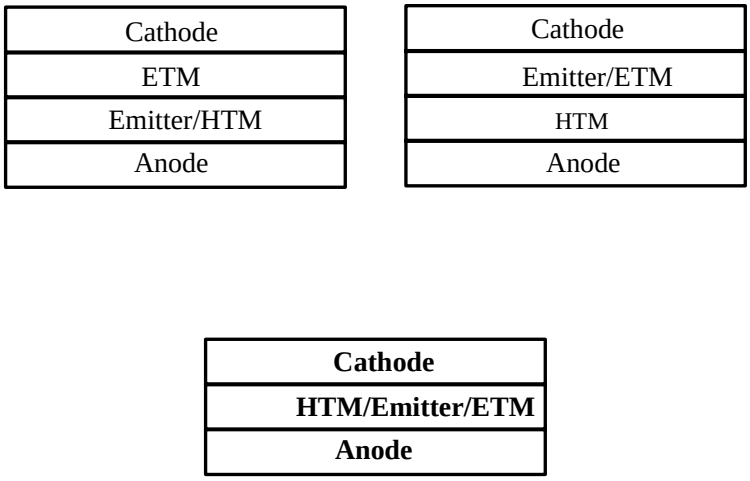

Figure 1-2:Device designs for simplified structures. Top left: double layer device combining the emitter material and the HTMs. Top right: double device combining the emitter material and the ETM. Bottom: single layer device combining the HTM, the emitter and the ETM.

1.1.2 Materials used in OLEDs

Materials suitable for OLEDs should have a number of properties in common. These include high glass transition temperatures (T_gs), good processability and high environmental stability. It is also advantageous for the morphology to be amorphous to

prevent light scattering and crystallization-induced degradation. Finally, they should be capable of efficient charge transport, efficient photoluminescence, or both. [1,7]

1.1.2.1 Emissive Materials

Good emissive materials play a pivotal role in OLED applications. Materials capable of efficiently emitting green, red and blue light are important in applications for flat panel displays, as these are the colors typically used to generate full color in most current display technologies.[8]

A number of different classes of molecules have been applied to each of these colors. Early red emitters include dopants such as Nile Red and 4-(dicyanomethylene)-2-methyl-6-[4-(dimethylaminostyryl)-4H-pyran] (DCM), displayed in Figure 1-3.[9] Good green emitters were among the first to be explored including Tang's Alq_3.[4] A variety of others have been tested, including other metal chelates such as those Figure 1-4.[,10]

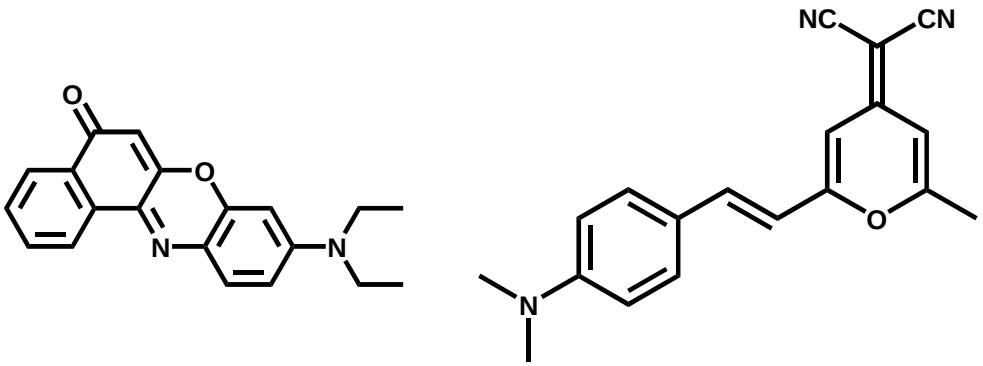

NILE RED (1.1 a) **DCM (1.1b)**

Figure 1-3: Red dopants frequently used as red emitters in OLEDs.

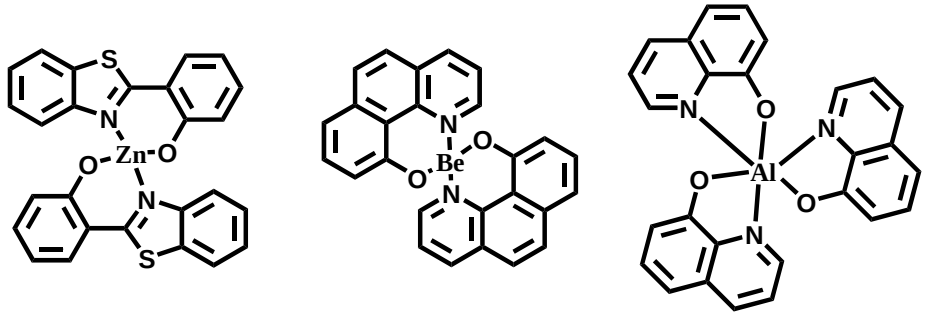

1.2a **1.2b** **Alq_3 (1.2c)**

Figure 1-4:Compounds known to possess useful green emission for application in OLEDs.[4,5,10]

Several different classes of compounds have been explored as good blue emitters. Obtaining bright and stable blue emission continues to be a challenge in OLED research because of the large band-gap energies which are necessary to obtain blue emission.[c,] Examples of compounds which have been explored as blue emitters include 3- and 4-coordinate boron compounds,[11,12] metal chelates using functionalized hydroxyquinolates and oxadiazole metal chelates.[13] Furthermore, phosphorescent iridium complexes[14] and extensively conjugated polyaromatic systems such as 2,2'-bistriphenylenyl (BTP)[c] and triazatruxene core oligomers[15] have also demonstrated blue luminescence . Some examples of these compounds are depicted in Figure 1-5**.**

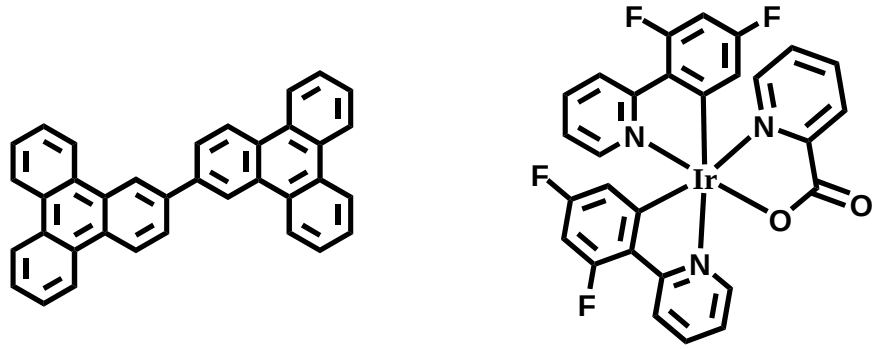

1.3a **1.3b**

Figure 1-5: Representative compounds explored as possible blue emitters in OLEDs. Left: extensively conjugated polyaromatic system[13c]. Right: iridium complex.

1.1.2.2: Materials Used for charge transport

In addition to good emitter materials, good charge transport materials are also important to OLED research. The key properties to be considered for charge transport are the energies of the HOMO and LUMO orbitals, the stability toward oxidation and reduction for HTM and ETM respectively and high charge mobility. Charge mobility refers to the ability of the material to transport charges, and is usually separated into hole mobility and electron mobility[1]

The energies of the HOMO and LUMO are often approximated by the magnitude of the oxidation and reduction potentials respectively.[1] For ETMs, the LUMO must be matched closely to the work function of the cathode to ensure good electron injection. Furthermore, the HOMO must be matched closely to the work function of the anode to maximize hole injection.[1,2,16] Figure 1-6 displays a diagram representing the HOMO and LUMO energies relative to the electrode work potentials

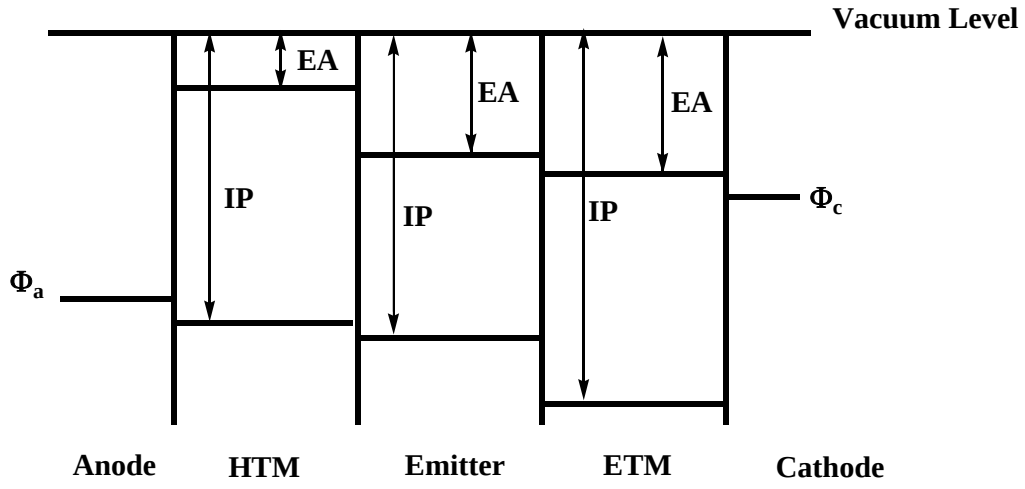

Figure 1-6: Energy level diagram comparing the HOMO and LUMO energy levels of OLED materials to the work functions of the electrode materials. In the above illustration, IP represents the ionization potential which is used to approximate the HOMO energy level, and EA represents the electron affinity, which is used to approximate the LUMO energy level. Φ_a and Φ_c represent the work functions for the anode and cathode respectively.

Heeger et al demonstrated the importance of this in their work on PPV. PPV has an electron affinity (EA) of approximately -2.7 eV. When the cathode material was changed from aluminum (ϕ_c = -4.3 eV) to calcium (ϕ_c = -2.9 eV), device performance improved remarkably with an order of magnitude increase in luminescent intensity. This improved performance is believed to be the result of improved electron injection at the cathode.[6]

The reversibility of the electrochemical processes is also important in charge transport materials. It should be noted that electron transport in organic molecules is poorly understood. In single crystals, band theory can be used to explain the movement of electrons across a sample. For amorphous films, electron transport appears to have more to do with carrier hopping between individual molecules. Therefore, charge transport in amorphous films is often considered to be a series of redox processes taking place within a material.[1,17] In the case of an ETM, for example, electrons are transferred via reversible reduction of adjacent molecules across a sample.[1]

This explains why reversibility of the reduction process is so important in the solid state. If, for example, a molecule used in an ETM cannot be reversibly reduced, it will decompose under the influence of an external current, resulting in device decay. Similarly, HTMs must be stable to reduction in order to prevent similar decay.[1]

1.1.2.2.1 Hole Transport Materials

For reasons that will be discussed in the next section, hole transport is generally more efficient in organic materials than electron transport. A number of good HTMS are known, and are mainly derived from triaryl amines.[18] Some examples of such compounds include N,N'-diphenyl-N,N'-bis(1-naphthalenyl)-1,1'-biphenyl-4,4'-diamine

(NPB) and N,N'-diphenyl-N,N'-bis(3-methylphenyl)-1,1'-biphenyl-4,4'-diamine (TPD). These compounds are electron rich, and possess low and reversible oxidations and good hole mobilities.' Initially these compounds were explored for applications in electrophotography, and were characterized to be good hole carriers, but poor electron carriers. More recently, they have found applications in OLED devices. Some examples of good hole carriers are illustrated in Figure 1-7.

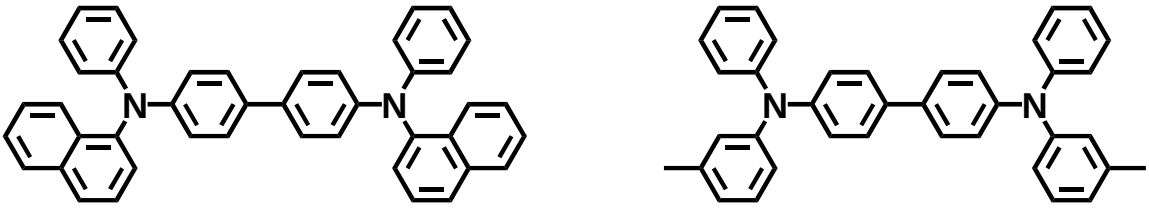

NPB (1.4a) **TPD (1.4b)**

Figure 1-7: Represenatative triarylamine based HTMs frequently used in OLED applications.

1.1.2.2.2 Electron Transport Materials

Good ETMs are more difficult to develop. The mobility of electrons appears to be considerably lower than that of holes in organic compounds. For example, the electron mobility in Alq_3, a well known ETM, has been determined to be approximately 1 X 10^{-5} $cm^2V^{-1}s^{-1}$, which is approximately one full order of magnitude lower than that of the well known HTM, TPD. This is largely because oxygen, moisture and other common impurities tend to trap electrons within these materials, and impede transport.[2,19] Also, there tends to be a considerably larger barrier to electron injection in OLEDs than to hole injection.[1] For these reasons, there is a greater need to develop better ETMs compared to HTMs.[2, 19]

Many different classes of molecules have been examined for applications as ETMs in OLEDs.[1] Among the most extensively studied are the oxadiazole molecules.[20] A variety of different types of oxadiazoles have been applied as ETMs, including simple oxadazioles such as 1.5a and more complex oxadiazoles employing dimeric and star topologies such as 1.5b-c (Figure 1-8).[20]

Devices based on monomeric structures, such as 1.5a suffer from crystallization because of low glass transition temperatures.[20a] Incorporation of additional oxadiazole units leads to an increases in glass transition temperature, and electron affinity (EA), thus better ETMs.[20] Herein we define the EA as an apprxoximation of the LUMO energy level. The monomeric compound, 1.5a has an EA of -2.16 eV,[20b] while the dimeric compound 1.5b has an EA of -2.8 eV[20c] and the star shaped trimer 1.5c has an EA of approximately -3.2 eV.[20d] Furthermore, the star shaped molecules display much higher T_g, at 142ºC for 1.5c versus 60ºC for 1.5a.[20d]

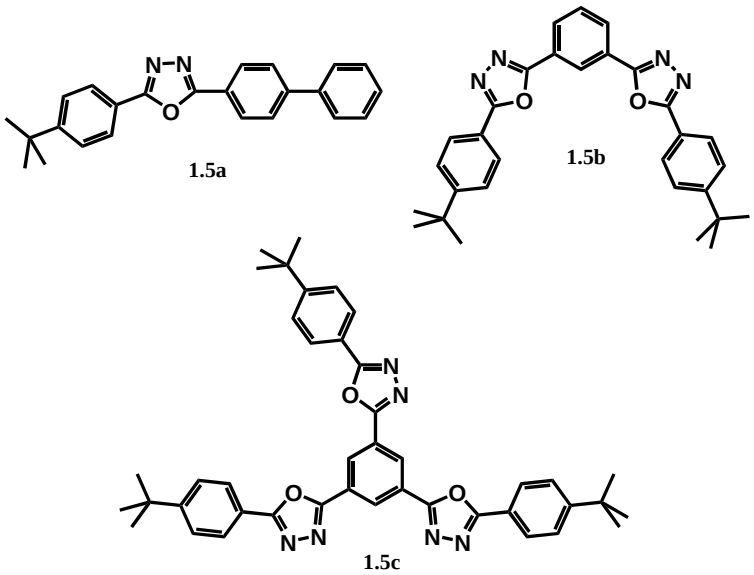

Figure 1-8: Representative oxadiazoles applied to electron transport in OLEDs.

Metal chelates, similar to Alq_3, also represent a promising class of ETMs. Because of its high EA (-3.0eV), IP (-5.95 eV) and T_g (172ºC), Alq_3 is one of the most extensively studied ETMs known.[4a] A variety of other related metal chelates have also been explored. Gaq_3 and Inq_3 both have remarkably reduced fluorescence efficiency, which results in an order of magnitude loss of brightness in devices employing these compounds as emitters.[21] Despite this, Inq_3 does have superior charge transport properties, such as a higher EA at -3.4 eV and a higher electron mobility compared to Alq_3, and does outperform Alq_3 when used strictly as the ETM.[21]

Metal chelates employing divalent metals such as zinc have also been employed. Zinc metal chelates generally produce yellow emitting devices, and are brighter than Alq_3.[22] Also, based on lower operating voltages in devices employing zinc chelates, it has been suggested that zinc complexes have better electron mobilities and electron injection.

Azoles are another important class of ETM. Compounds containing triazole, imidazole, oxazole, thiazole and thiadiazole derivativatives have been widely explored in OLED applications.[1] Among the most promising of the azole derivatives is the star shaped molecule, 1,3,5-tris(N-phenyl-benzimidazol-2-yl)benzene (TPBI, Figure 1-9). With an EA of -2.7 eV and an IP of approximately -6.2 eV, TPBI is useful as both an ETM and as a hole blocking material. It has been used in a variety of applications, both as an ETM and as a host material for luminescent molecules.[8] It should also be noted that because of its larger optical bandgap, TBPI can also be used as a host or ETM for bright blue emitters.[8] For example, bright blue emission (11,000 cd/m^2) was observed using TBPI as the ETM and a phenylene vinylene oligomer as the emitter.[8]

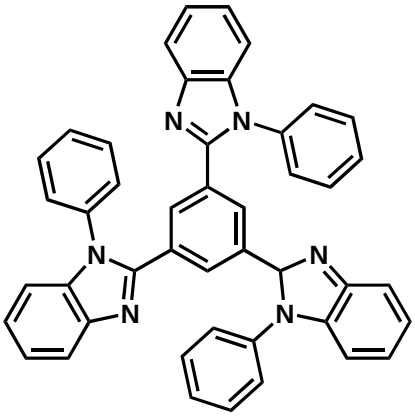

1.6

Figure 1-9: Molecular Structure of TPBI

Finally, three-coordinate organo-boron containing compounds are also of interest as ETMs.[,23] The empty p_z orbital on the boron center makes them potential electron acceptors, and allow them to function effectively as ETMs. The incorporation of two mesityl groups provide sufficient kinetic stability to the three-coordinate boron center. Some examples of boron compounds used as ETMs are displayed in Figure 1-10.[,]

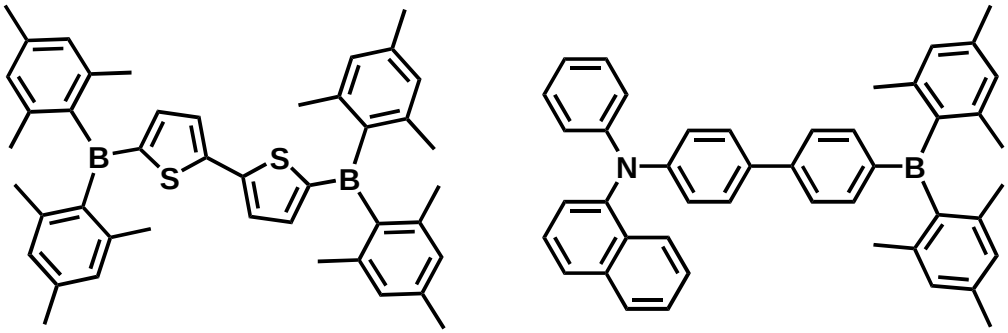

1.7a **1.7b**

Figure 1-10: Organoboron compounds used as ETMs for OLED devices. The EA for 1.7a and 1.7b are -2.58 eV, and -2.13 eV respectively.[11,23]

Development of new ETMs and stable blue emitters remain two of the major challenges in OLED research. Hence, one of the goals of this thesis is to develop a new class of ETMs and demonstrate their utility in device applications.

1.2 Luminescence

1.2.1 Principles of Luminescence

Luminescence is a term commonly used to refer to the generation of light. For luminescence to occur, a molecule that is capable of emitting light must first be excited via absorption of energy from an external source. The excited molecule then releases the excess energy and relaxes through one of three processes: non-radiative decay, fluorescence, or phosphorescence.[24]

In the case of non-radiative decay, relaxation does not result in luminescence. The excited molecule relaxes through a series of vibrational modes, returning to its original ground state. This process is generally fast, occurring on a picosecond timescale.[24]

Fluorescence is one alternative to non-radiative decay. In this case, the relaxation process is radiative, and does produce light. The singlet excited state (S_1) returns to the singlet ground state (S_0) and a photon with an energy corresponding to the difference in energy between the ground and excited states will be produced. Fluorescence is therefore a spin allowed transition, and can typically be observed on a nanosecond timescale.[24]

Phosphorescence is another example of radiative decay in which a photon is produced. In this case, the S_1 state undergoes an intersystem crossing to a lower energy triplet excited state (T_1). Relaxation from a triplet state to a singlet state is spin forbidden, resulting in prolonged excited states, and longer radiative lifetimes. Phosphorescence can

often take place on a microsecond timescale, unless assisted by the presence of a heavy atom such as a metal center.[24] This is represented schematically in the Jablonskii diagram in Figure 1-11.

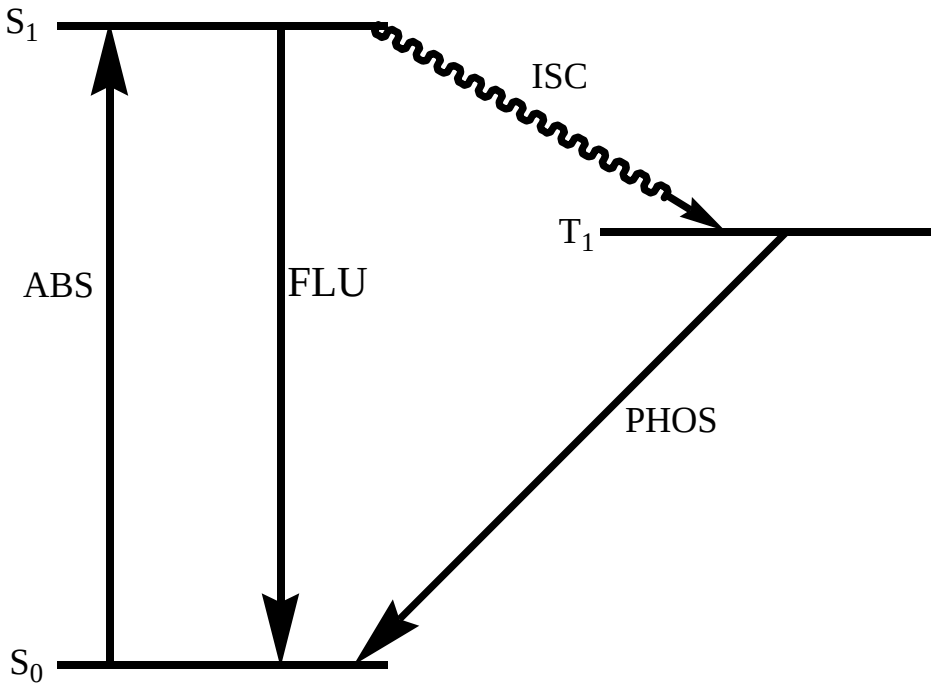

Figure 1-11:Jablonskii diagram for luminescent decay from an excited state.

1.2.2 Luminescence in Transition Metal Complexes

The effect of transition metal coordination on ligand luminescence has been widely studied. In general, one of three effects is observed: fluorescent quenching, fluorescent enhancement or phosphorescent enhancement. Some metal ions such as Ag(I)[34,35,36,37] quench luminescence by the heavy atom effect, while others such as Zn(II)[35-37] have demonstrated fluorescent enhancement. Phosphorescent enhancement will be discussed in greater detail below.

Phosphorescent enhancement is important to OLED research because it leads to a considerable increase in theoretical internal quantum efficiency. As described above, phosphorescence originates from a formally spin forbidden triplet to singlet transition, whereas fluorescence originates from a spin allowed singlet to singlet transition.[24] In OLED devices, electron-hole recombination results in formation of both singlet and triplet excitons, with triplet exciton formation being statistically three times more probable. This limits fluorescent emitters to maximum internal quantum efficiencies of approximately 25%, as emission can only occur from the singlet excitons.[25] Incorporation of transition metal ions enhances mixing of singlet and triplet states, and facilitates emissive relaxation of triplet excitons. This greatly improves the theoretical internal quantum efficiency to 100%.

Phosphorescent enhancement can be achieved through one of three effects: direct enhancement of ligand based phosphorescence, metal to ligand charge transfer (MLCT) or ligand to ligand charge transfer (LLCT). In principle, complexation to any non-paramagnetic metal ion should result in enhancement of phosphorescence by spin orbit coupling. Complexes with metal ions such as Ir(III) and Pt(II), such as compounds 1.8a and 1.8b (Figure 1-12) commonly display this type of phosphorescence.[26]

Alternatively, a MLCT excitation and emission can occur. MLCT has often been observed in ligand complexes with ions such as Ru(II), Cu(I), and Pt(II). Compounds 1.9a-c in Figure 1-12 are representative examples of such complexes.[27,28,47] Finally, phosphorescent enhancement can occur via ligand to ligand charge transfer, in complexes with ions such as Ir(III) and Os(II). Compounds 1.10a and 1.10b are two examples of complexes known to demonstrate LLCT.[29]

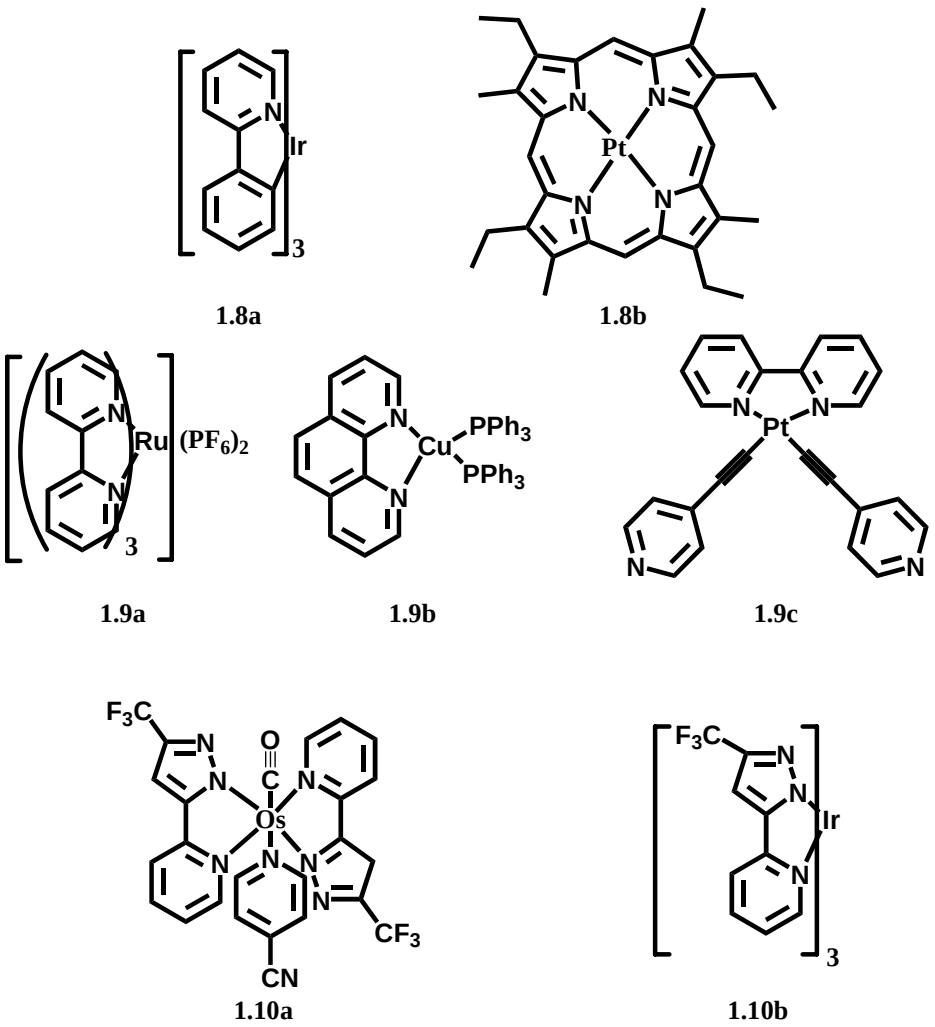

Figure 1-12:Different types of phosphorescent complexes used in OLED research. Compounds 1.8 a and b exhibit enhancement of ligand based phosphorescence by spin orbit coupling. Compounds 1.9 a-c all enhance phosphorescence by MLCT,[27,28,47] while compounds 1.10 a and 1.10b enhance phosphorescence through LLCT excited states.[29]

1.2.2.1 Luminescence in Copper Complexes

Copper complexes with bidentate nitrogen ligands are widely known. Copper complexes containing functionalized phenanthroline ligands are particularly well explored.[30,31] Copper (I) compounds with bidentate nitrogen donor ligands typically show metal MLCT states with absorption spectra ranging between 350 and 650 nm and

extinction coefficients ranging between 10^3 and 10^4 $M^{-1}cm^{-1}$. When excited, the copper center donates an electron from its highest filled d-orbital to a π* orbital on the ligand, resulting in a formal +2 oxidation state on the copper, and -1 oxidation state on the ligand.[30] This is presented schematically in the figure below.

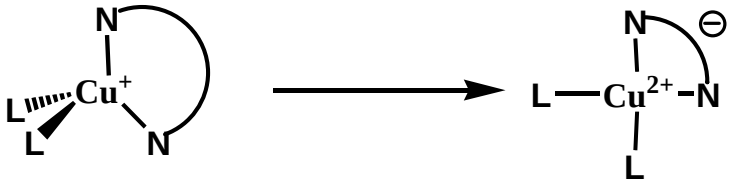

Figure 1-13: Upon excitation of the ground state molecule (left) to the excited state molecule (right) the oxidation state of the copper atom increases by one and the oxidation state of the ligand decreases by one.

Early work on phenanthroline complexes by the McMillin group has given a great deal of insight into the factors which impact this type of phosphorescence. Cu(I) complexes generally exhibit a tetrahedral coordination geometry around the copper center, which is typical for a d^{10} complex. Upon excitation, it is generally believed that the change in oxidation state results in a change to a square planar coordination geometry (Figure 1-14), creating an open coordination site in the axial position. The presence of this open site is believed to be the cause of the solution state quenching of phosphorescent copper complexes. [30, 31, 33]

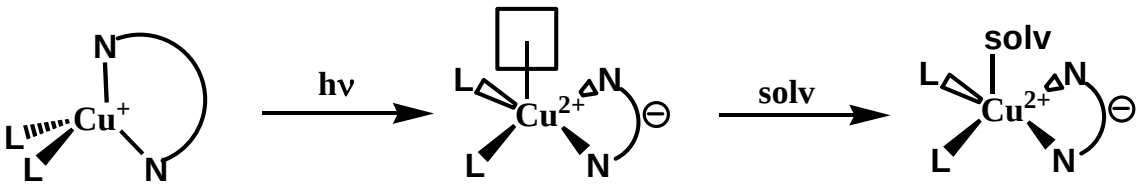

Figure 1-14: Change in coordination geometry around a copper center upon photo-excitation. The square planar geometry opens an additional coordination site on the copper center, which can permit formation of the emission quenching eciplex the far right.

Copper complexes of this type have been widely explored for a number of applications including solar energy conversion,[30] sensing[30] and display technology.[27,30] Copper complexes offer less expensive and more environmentally friendly alternatives to other metals with similar properties, such as ruthenium, rhenium and osmium.[27,31a]

For example, copper-phenanthroline complexes with phosphine based supporting ligands have been explored as emissive materials for OLEDs. A series of complexes were developed using different 2,9 substituted phenanthroline ligands (Figure 1-15). These compounds were used to develop yellow-orange OLED devices with performances comparable to devices prepared using well known Ir(III) complexes.[27]

It should be noted that increasing the steric bulk on the phenanthroline ligands lead to an increase in quantum yield and excited state lifetime, as well as to a hypsochromic shift in emission. The additional steric strain appears to impede the above-described geometric relaxation in the excited state. This destabilizes the excited state, thereby widening the band gap, and reducing non-radiative decay.[27]

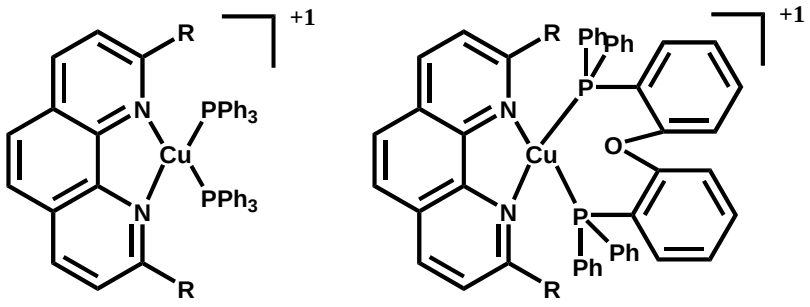

1.11a-c **1.12a-c**

Figure 1-15: Phenanthroline ligands employed by Zhang *et al* in exploration of copper(I) complexes as emitters in OLED applications. R = H (a), CH_3 (b), or $(CH_2)_3CH_3$ (c).

Recently, our group has reported a series of studies on four coordinate copper(I) complexes using a variety of different ligand systems (Figure 1-16). When coordinated to 2-(2'-pyrdyl)benzimidazolyl derivative ligands, the MLCT generally results in an orange phosphorescence. The phosphorescent lifetimes of these complexes are on the order of 100-500 μs in doped PMMA and 100 -300 μs in methylene chloride at 77K.[32,33] Copper complexes with the linear shaped ligands demonstrate weak room temperature emission when dissolved in non-coordinating solvents such as methylene chloride. Complexes with the starburst ligands were entirely non-emissive in solution.[32]

Room temperature phosphorescent emission in the solution state has been observed previously for McMillin's $Cu(phen')_2^+$ systems, where phen' can be any functionalized phenanthroline ligand.[31] In non-coordinating solvents, such as methylene chloride, the Cu^{2+} excited state is generally unable to form an emission quenching exciplex, and emission is not suppressed. In weakly coordinating solvents, such as acetonitrile, acetone and methanol, emission can also be observed if the phen' ligand is sufficiently bulky to stabilize the four-coordinate Cu^{2+} center. If steric demand of the ligand is insufficient, these solvents also have a quenching effect and reduce emission. The more strongly coordinating the solvent, the stronger the quenching effect.[31]

The luminescent properties of Cu^+ centers are interesting because of the nature of the resulting MLCT and because of the phosphorescent emission. The luminescent properties of a novel copper complex will be presented herein.

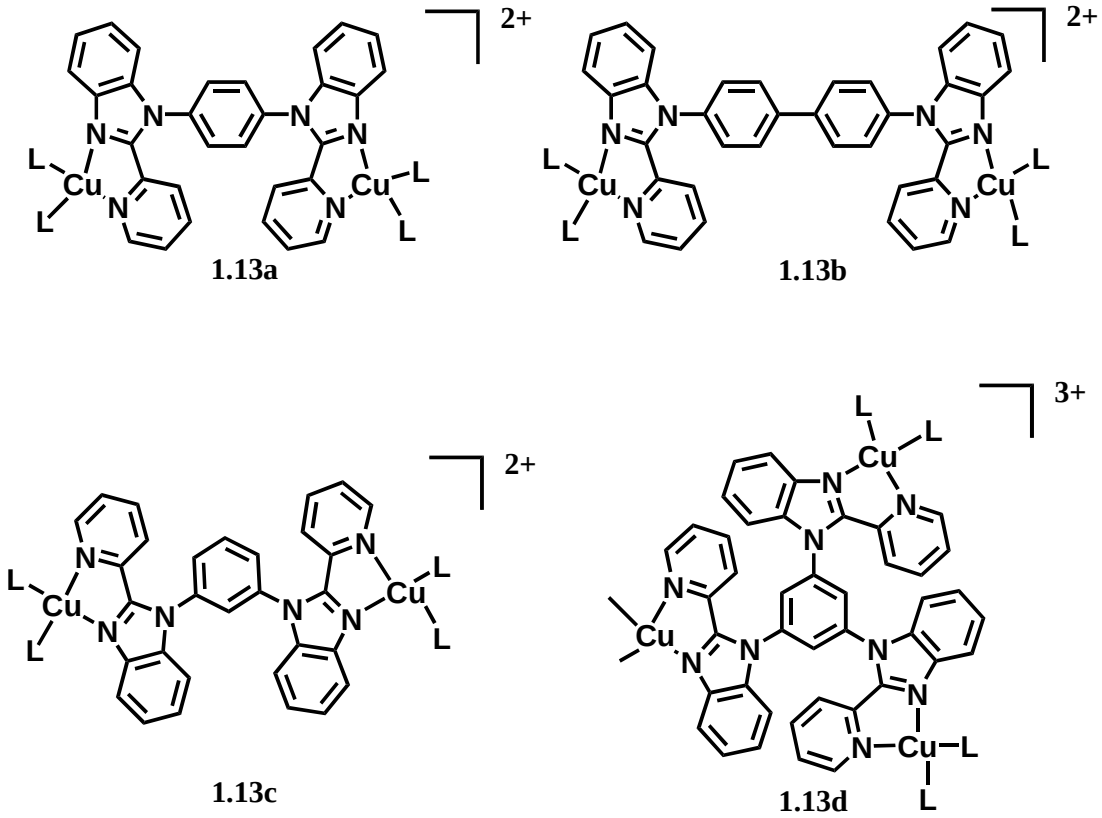

Figure 1-16: Linear and starburst molecules used to make phosphorescent copper (I) coordination complexes. 1.13a and b show room temperature phosphorescence in solution, 1.13 c and d do not.

1.2.2.2 Impact of Zinc(II) and Ag (I) on Fluorescent Emission

Zinc complexes with nitrogen donor ligands generally exhibit coordination numbers between four and six, and a variety of different coordination geometries.[34,35,36,37] Luminescent properties of complexes of this type are generally best described as ligand based fluorescence, with varying effects on intensity. For example, addition of zinc(II) ions to a dipyridylamine derivative ligand (compound 1.14a), resulted in a significant decrease in fluorescent intensity while addition of zinc to compounds 1.14b and 1.14c, (based on a ruthenium terpyridine chromophore and a trispyrazolylborate respectively) caused fluorescent enhancement. The structures for

these compounds are depicted in Figure 1-17. Similar enhancement of fluorescence has been observed elsewhere.[36]

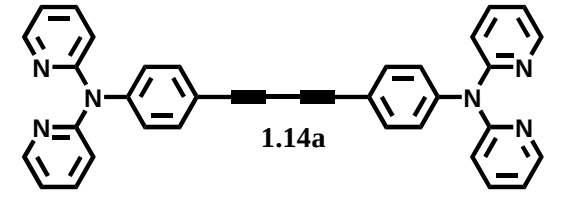

1.14a

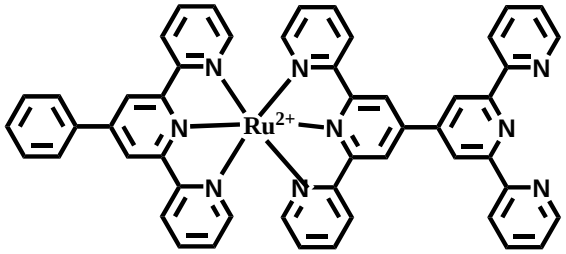

1.14b

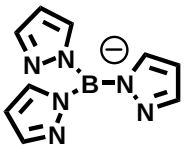

1.14c

Figure 1-17: Chemical structures of representative chromophores which have shown changes in luminescence when titrated with zinc.

Silver(I), like copper(I) and zinc(II) is a d^{10} metal center which has been widely explored in coordination chemistry. Compared to copper, silver shows a much wider variation in coordination number and geometry. Coordination numbers typically vary between two and six, and geometries range between linear or bent structures, to distorted octahedral, depending on coordination number.[38, 39]

The impact of silver on luminescence has also been studied. Similar to zinc, ligand based fluorescent emission is generally observed for silver complexes. As mentioned previously, Ag(I) ions generally quench fluorescence. For example, 2,2',3''-tripyridylamine (compound 1.15a) complexes reported by Seward *et al* display a decrease

in intensity to approximately 50 % upon silver complexation[34,38] and Jia *et al* report quenching to a final value of 4% of the original luminescence for compound 1.15b. The ligands are depicted in the figure below.

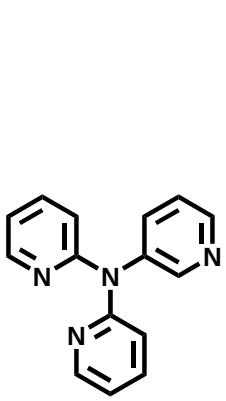

1.15a

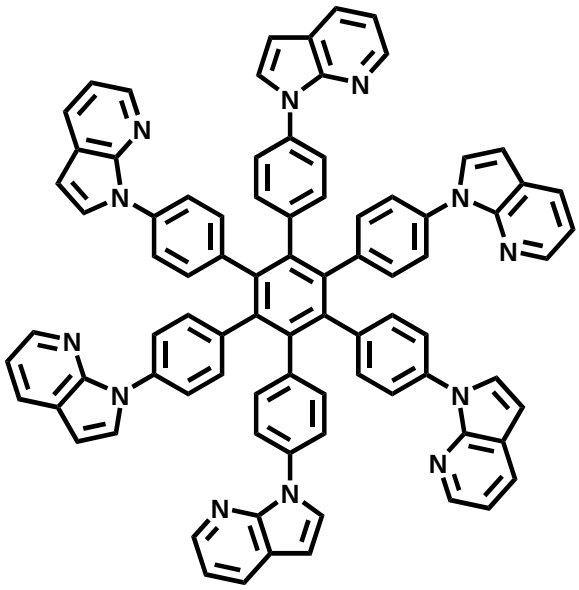

1.15b

Figure 1-18: Compounds 1.10a and 1.10b. Both compounds have demonstrated fluorescent quenching in the presence of silver(I) ions.

1.2.3: Applications of Luminescent Ligands: Zinc Sensors

Luminescent organic compounds and their coordination complexes have been used in a number of applications, substrate sensing being among the most important of these. The Zn(II) cation is important for a number of biological processes, including DNA synthesis, apoptosis, gene expression and protein structure.[40,41] In light of this, fluorescent sensing of zinc has received a great deal of attention.[37]

The first known zinc fluorophore was TSQ (N-(6-methoxy-8-quinolyl)-p-toluenesulfonamide, Figure 1-19). It was used widely because it functions selectively in the presence of other biologically relevant cations such as Ca^{2+} and Mg^{2+}. Despite this,

TSQ is not an ideal sensor for zinc. In vitro, 2:1 TSQ:Zn complexation generally occurs. In the presence of protein bound zinc, 1:1 complexation is often observed, if the protein binds zinc sufficiently strongly. This makes quantitative analysis of zinc in vivo challenging when using TSQ. Moreover, fluorescent quantum yield is moderate, making an accurate determination of zinc concentration challenging.[37]

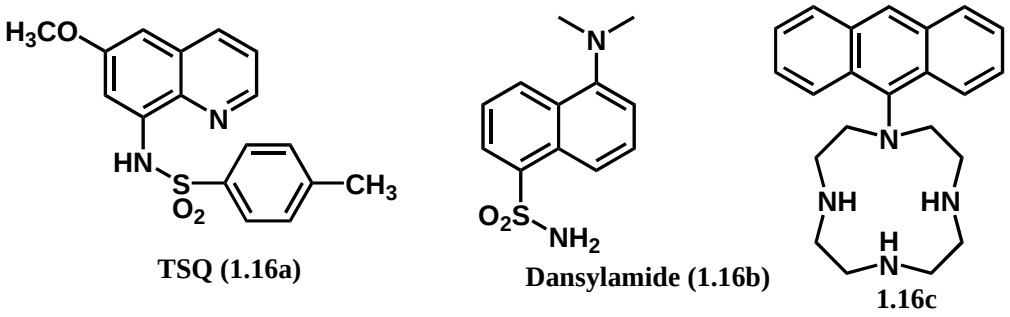

Figure 1-19: A representative sample of compounds used as zinc sensors. TSQ on the left was the first known zinc fluorophore. Dansylamide and compound 1.11c represent two promising possibilities for classes of more efficient zinc sensors.

Subsequent work followed, and a number of other fluorophores have been used in zinc sensing (Figure 1-19). Examples include macrocycle 1.16c which demonstrates a chelation enhanced fluorescence, and dansylamide[37]. Dansylamide is especially useful because upon complexation with zinc, a 112 nm blue shift in emission is observed, along with a concomitant increase in fluorescent quantum yield from 5.5% to 84%.[37]

Our group has also explored this area. Two 2-(2'-pyridyl)benzimidazolyl based ligands were titrated with a series of divalent group 12 metal ions and the fluorescent response was observed. The ligands demonstrated a very clear response to both Cd and Zn, resulting in a red shift in emission, and an increase in emission intensity. This clearly demonstrates the potential of these chelating ligands as sensor molecules.[40]

1.3 Benzimidazolyl Functionalized Ligands.

Benzimidazole is an aromatic bicyclic heterocycle which has received a great deal of attention in recent literature. Much of this interest is a result of the persistence of this moiety in a variety of biologically relevant molecules. It has been observed in derivatives of vitamin B_{12}, and several metaloproteins.[41] Furthermore, compounds of these types have also proven to be biologically relevant, behaving as anti-cancer and anti-fungal agents.[42]

The presence of nitrogen atoms in the 1- and 3- positions, and facile modification of the carbon in the 2- position has led to the generation of a plethora of benzimidazolyl derivatives with various functions.[41]

One of the most common means of modification is the attachment of a Lewis base group to the carbon in the 2 position. For example, the attachment of a pyridyl or quinolyl group to generate a chelation site in this position has been widely explored.[43, 44] In addition, ligands in which two and three benzimidazolyl units are bridged by a pyridyl group and a trimethyleneamine group respectively have been synthesized. In each of these cases, the ligands are modified in such a way as to promote chelation to a variety of metal centers such as chromium(III),[44] ruthenium(II) and osmium(II).[45]

Furthermore, considerable attention has been paid to modification at the amine nitrogen position. Linear molecules and molecular stars with a variety of cores have been prepared, employing the 2-(2'-pyridylbenzimidazolyl) group as both a luminophore and as a ligand for metal chelation. Some of the examples have been presented above, and additional information will be given in the follow section. [47,48]

1.3.1 Applications of Benzimidazole Compounds in OLEDS

Benzimidazole compounds have found a number of applications in OLED devices. One of the most well known examples is the application of TPBI as an electron transport and hole blocking material, as described above.[1,8]

In addition to their capacities as ETMs, benzimidazolyl derivative compounds have been used as luminescent materials in OLEDs. For example, early work by our group demonstrated that complexing benzimidazolyl derivatives to diphenylborates resulted in blue/green luminescent materials.[46] Furthermore, the effect of varying the electronic nature of the substituent in the 5-position of the benzimidazolyl ligand was also explored, and a bathochromic shift in emission color was observed with increased electron donation. The related structures are illustrated in Figure 1-20.[46]

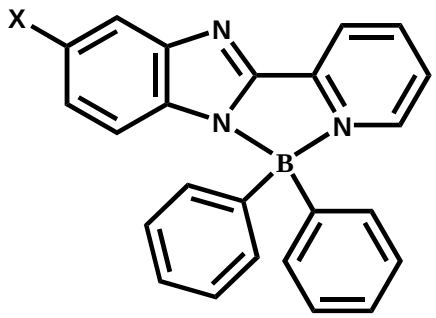

1.17a-c

Figure 1-20: Boron Complexes explored as electron transport and emissive materials for OLED applications. X= F for 1.17a, Cl for 1.17b and OCH_3 for 1.17c.

Furthermore, Chen and coworkers complexed two other benzimidazolyl ligands to 4-coordinate boron centers to create emissive compounds. Both compounds were stable and bright. It is noteworthy that compound 1.18a (Figure 1-21) produced white emission

when used as the emitting layer in a device with Alq_3 and NPB as the ETM and HTM respectively. The structures of the compounds and the white emitting device are depicted in Figure 1-21 and Figure 1-22. [44]

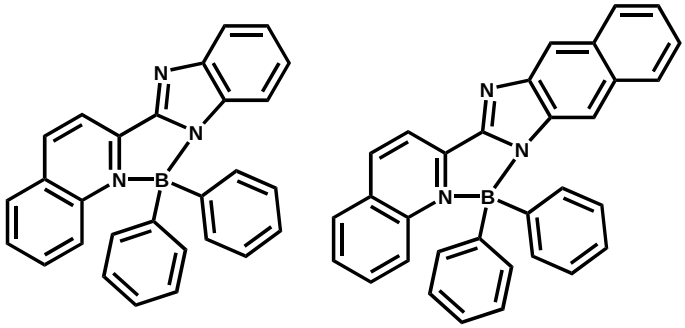

1.12a **1.12b**

Figure 1-21: Structures of boron compounds explored by Chen *et al* as materials for OLED applications.

Mg/Ag
Alq_3
1.12a
NPB
ITO

Figure 1-22: Device structure used by Chen *et al* to observe bright white emission.

O-(*N*-phenyl-2-benzimidazolyl)phenol has been demonstrated to be useful in OLED applications when coordinated to both aluminum and beryllium (Figure 1-23). The aluminum compound was used as a combined emissive and electron transport layer in a device using copper picrate as the hole injection layer and NPB as the hole transport layer. The device produced bright blue emission at 216 cd/m^2 under a driving voltage of 11V, indicating that this compound is useful as both a blue emitter and as an electron transport material. The beryllium compound proved to be even more promising when

applied in a similar device, and displayed a light output of 504 cd/m^2 under a lower driving voltage of 8.7 V.[5]

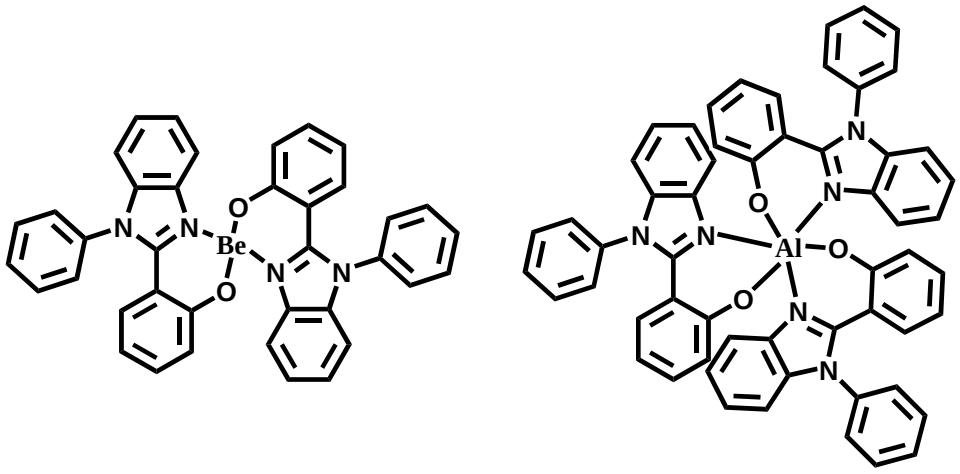

1.19a **1.19b**

Figure 1-23: Beryllium and aluminum complexes of *o*-(*N*-phenyl-2-benzimidazolyl)phenol used as blue emitters and ETMs.

Finally, our group has also explored coordination complexes of Ru(II) and Pt(II) with ligands based on the 2-(2'-pyridyl)benzimidazolyl moiety.[47,48] The structures of the ruthenium and platinum complexes are illustrated in the figures below.

The Ru(II) complexes reported by Jia *et al* displayed the typical MLCT based red phosphorescent emission. The reported compounds were used to prepare red emitting devices, and their performance compared to identical devices using $[Ru(bpy)_3][PF_6]_2$ as the emitter. The devices constructed from the benzimidazolyl derivatives were generally brighter, and more efficient than their $[Ru(bpy)_3](PF_6)_2$ analogues.[47]

Incorporation of Pt(II) in the 2-(2'-pyridyl)benzimidazolyl functionalized molecular stars resulted in red-orange emission. Time-resolved phosphorescence spectroscopy was used to observe the phosphorescent emission of both the free ligands and the resulting complexes. The ligand's phosphorescence occurred in the blue-green

region of the visible spectrum. Since the phosphorescent emission of the complex was significantly red shifted compared to that of the free ligand, the red-orange emission is believed to result from the MLCT transition. Although no devices were prepared, these complexes are believed to be applicable as phosphorescent emitters in OLED devices.[48]

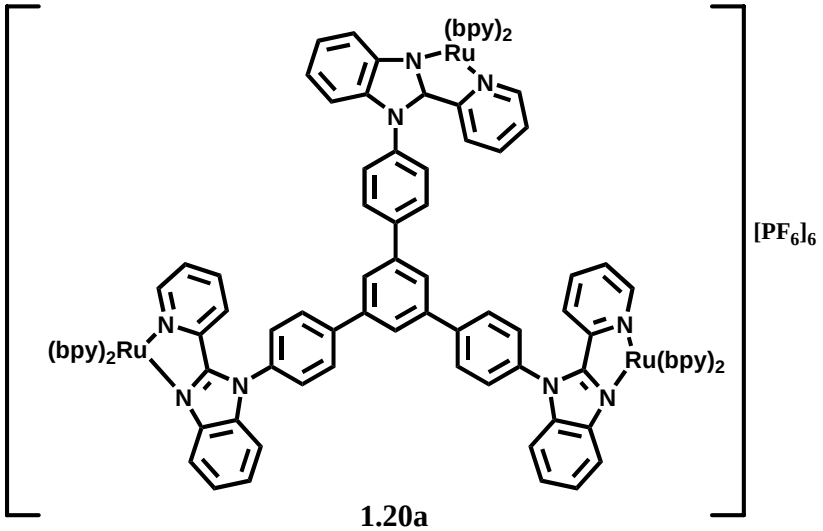

1.20a

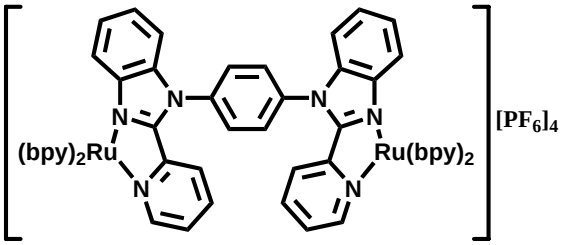

1.20b

Figure 1-24: Representative ruthenium (II) complexes with 2-(2'-pyridyl)benzimidazolyl functionalized ligands applied to light emitting devices.

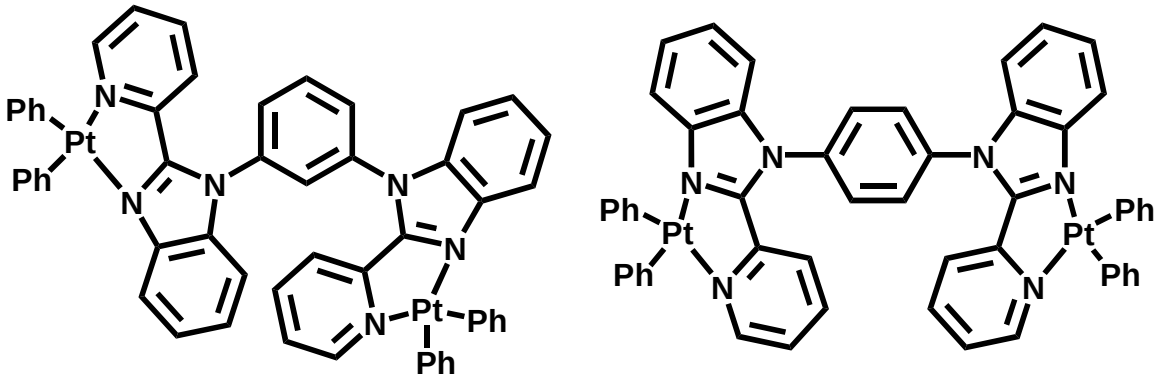

1.21a **1.21b**

Figure 1-25: Representative platinum (II) complexes with 2-(2'-pyridyl)benzimidazolyl functionalized ligands. All complexes were observed to be bright orange emitters.

1.4 Scope of This Thesis

As discussed above, the benzimidazolyl moiety has been used widely in a number of different applications. Compounds of this type have been explored for both electron transport and emissive materials in OLED applications with promising results. Furthermore, the presence of the neutral nitrogen atom in the 3 position has lead to an abundance of coordination complexes with interesting photophysical and electronic properties. In light of this, a series of new benzimidazolyl derivative compounds have been prepared and their potential applications have been explored.

In chapter 2, the synthesis of a series of starburst benzimidazolyl derivatives and their subsequent characterization will be discussed. Their potential applications as electron transport materials in OLED devices will be presented, as well as their interactions with metal ions. Chapter 3 will focus on the synthesis of a novel pair of compounds, each possessing two completely different binding sites. The effect of coordination a copper (I) center will be examined, as will the effect of metal ion titrations.

Finally chapter 4 will draw some general conclusions and briefly discuss possible future work to expand on the topics previously discussed.

1 A. P. Kulkarni, C. J. Tonzola, A. Babel, S. A. Jenekhe. *Chem. Mater.* 2004, **16,** 4556.

2 A. Dodabalapur. *Solid State Commun*. 1997, **102**, 259.

3 M. Pope, H. P. Kallman, P. J. Magnante. *Chem Phys.* 1963, **38,** 2042.

4 a) C. W. Tang, S. A. VanSlyke. *Appl. Phys. Lett.* 1989, **51,** 3610; b) C. W. Tang, S. A. VanSlyke, C. H. Chen. *J. Appl. Phys.* 1989, **27,** L713.

5 a) C. H. Chen, J. Shi. *Coord. Chem. Rev.* 1998, **171,** 161. b) W. E. Howard, F. Prache, *IBM J. Res. & Dev.* 2001, **45,** 116.

6 D. Braun, A. J. Heeger. *Appl. Phys. Lett.* 1991, **58**, 1982

7 G. Yu, W. Yin, Y. Liu, Z. Shuai, D. Shu. *J. Am Chem. Soc.* 2003, **125,** 14816.

8 a) Z. Gao, C. S. Lee, I. Bello, S. T. Lee, R.–M. Chen, T. –Y. Luh, J. Shi, C. W. Tang. *Appl. Phys. Lett.* 1999, **74**, 865. b) T. D. Anthopoulos, J. P. J. Markham, E. B. Namdas, I. D. W. Samuel, S. –C. Lo, P. L. Burn. *Appl. Phys. Lett.* 2003, **82,** 4824. c) H.–T. Shih, C.–H. Lin, H.–H. Shih, C.–H. Cheng. *Adv. Mater.* 2002, **14,** 1409.

9 C.–T. Chen. *Chem. Mater.* 2004, **16,** 4389.

10 C. Liu, J. Li, B. Li, Z. Hong, F., Zhao, S. Liu, W. Li. *Appl. Phys. Lett.* 2006, **89,** 243511

11 a) D. Tanaka, T. Takeda, T. Chiba, S. Watanabe, J. Kido. *Chem. Lett.* 2007, **36,** 262. b) S. Kappaun, S. RentenBerger, A. Pogantsch, E. Zojer, K. Mereiter, G. Trimmel, R. Saf, K. C. Moller, F. Stelzer, C. Slugovc. *Chem. Mater.* 2006, **18,** 3539. c) W.–L. Jia, M. J. Moran, Y.–Y. Yuan, Z. H. Lu, S. Wang. *J. Mater. Chem.* 2005, **15,** 3326. d)W.–L. Jia, X. D. Feng, D. R. Bai, Z. H. Lu, S.Wang, G. Vamvounis. *Chem. Mater.* 2005, **17,** 164.

12. e) X. T. Tao, H. Suzuki, T. Wada, S. Miyata, H. Sasabe. *J. Am. Chem. Soc.* 1999, **121,** 9447.

13 a) Y. Liu, J. Guo, J. Feng, H. Zhang, Y. Li, Y. Wang. *Appl. Phys. Lett*. 2001, **78**, 2300. b) N.–X. Hu, M. Esteghamatian, S. Xie, Z. Popovic, A.–M. Hor, B. Ong, S. Wang. *Adv. Mater.* 1999, **11,** 1460.

14 C.–H. Yang, Y.–M. Chen, Y. Chi, C.–J. Hsu, F.-C. Fang, K.–T. Wong, P.–T. Chou, C.–H. Chang, M.–H. Tsai, C.–C. Wu. *Angew. Chem. Intl. Ed.* 2007, **46,** 2418.

15 P. A. Levermore, R. Xia, W. Lai, X. H. Wang, W. Huang, D. D. C. Bradly. *J. Phys. D: Appl Phys*. 2007, **40,** 1896.

16 I. D. Parker. *J. Appl. Phys.* 1994, **75,** 1656.

17 a) R. G. Kepler. *Phys. Rev.* 1960, **119,** 1226., b) A. Babel, S.A. Jenekhe. *J. Am Chem. Soc.* 2003, **125,** 13656

18 a) M. Stolka, J. F. Yanus, D. M. Pai, *J. Phys. Chem.* 1984, **88,** 4707; b) C. Adachi, K. Nagai, N. Tamato. *Appl. Phys. Lett.* 1995, **65,** 2697.

19 R. G. Kepler, P. M. Beeson, S. J. Jacobs, R. A. Anderson, M. B. Sinclair, V.S. Valencia, P. A. Cahill. *Appl. Phys. Lett.* 1995, **66,** 3618.

20 a) C. Adachi, T. Tsutsui, S. Saito. *Appl. Phys. Lett.* 1990, **56,** 799. b) J. Pommerehne, H. Vestweber, W. Guss, R. F. Mahrt, H. Bassler, M. Porsch, J. Daug, *Adv. Mater*. 1995, **7,** 551. c) D. O'Brien, A. Bleyers, D. G. Lidzey, D. D. C. Bradley, T. Tsutsui, *J. Appl. Phys.* 1997, **82,** 2662. d) J. Bettenhausen, P. Strohriegl, W. Brutting, H. Tokuhisa, T. Tsutsui, *J. Appl. Phys.* 1997, **82,** 4957. e) M.–K. Leung, C.–C. Yang, J.–H. Lee, H.–H. Tsai, C.-F. Lin, C.–Y. Huang, Y. O. Su, C.–F. Chiu. *Org. Lett.* 2007, **9,** 235. f) K. T.

Kamtekar, C. W. Wang, S. Bettington, A. S. Batsonov, I. F. Perepichka, M. R. Bryce, J. H. Ahn, M. Rabinal, M. Petty. *J. Mater. Chem.* 2006, **16,** 2823.

21 a)B. J. Chen, X. W. Sun, Y. K. Li. *Appl. Phys. Lett.* 2003, **82,** 3017. b) P. E. Burrows, L. S. Sapochak, D. M. McCarty, S. R. Forrest, M. E. Thompson. *Appl. Phys. Lett.* 1994, **74,** 2718.

22 Y. Hamada, T. Sano, M. Fujita, T. Fujii, Y. Nishio, K. Shibata. *Jpn. J. Appl. Phys.* 1993, **32,** L514

23 a) T. Noda, Y. Shirota. *J. Am. Chem. Soc.* 1998, **120,** 9714. b) Y. Shirota, M. Kinoshita, T. Noda, K. Okumoto, T. Ohara. *J. Am. Chem. Soc.* 2000, **122,** 11021.

24 a) P. Suppan and N. Ghoneim in *Solvatochromism.* Chapter 1.The Royal Society of Chemistry, Cambride, UK. **1997**. b) R. C. Ropp. in *Luminescence and the Solid State.* Chapter 1. Elsevier, New York, NY. **1991**.

25 M. A. Baldo, S. Lamansky, P. E. Burrows, M. E. Thompson, S. R. Forrest. *Appl. Phys. Lett.* 1999, **75,** 4.

26 R. C. Kwong, S. Sibley, T. Duboyov, M. Baldo, S. R. Forrest, M. E. Thompson. *Chem. Mater.* 1999, **11,** 3709.

27 Q. Zhang, Q. Zhou, Y. Cheng, L. Wang, D. Ma., X. Jing, F. Wang. *Adv. Mater.* 2004, **16,** 432.

28 T. K. Ronson, T. Lazarides, H. Adams, S. J. A. Pope, D. Sykes, S. Faulkner, S. J. Coles, M. B. Hursthouse, W. Clegg, R. W. Harrington, M. D. Ward. *Chem. Eur. J.* 2006, **12,** 9299.

29 a) P.–T. Chou, Y. Chi. *Chem. Eur. J.* 2007, **13,** 380. b) P.–T. Chou, Y. Chi. *Chem. Eur. J.* 2006, 3319.

30 a) D. V. Scaltrito, D. W. Thompson, J. A. O'Callaghan, G. J. Meyer, *Coord. Chem. Rev.* 2000, **208,** 243. b) N. Armaroli. *Chem. Soc. Rev.* 2000, **30,** 113. c) D. R. McMillin, K. M. McNett. *Chem. Rev.* 1998, **98**, 1201.

31 a) S**.–**M. Kuang, D. G. Cuttell, D. R. McMillin, P. E. Fanwick, R. A. Walton. *Inorg. Chem.* 2002**, 41,** 3313. b) A. Juris, R. Ziessel. *Inorg. Chim. Acta.* 1994, **225,** 251. c) M. K. Eggleston, D. R. McMillin, K. S. Koenig, A. Pallenberg. *Inorg. Chem.* 1997, **36,** 172. d)J. R. Kirchhoff, D. R. McMillin, W. R., Robinson, D. R. Powell, A. T. McKenzie, S. Chen. *Inorg. Chem.* 1985, **24,** 3928. e) K. Saito, T. Arai, N. Takahashi, T. Tsukuda, T. Tsubomura. *Dalton Trans.* 2006, 4444. f) K. Saito, T. Tsukuda, T. Tsubomura, *Bull. Chem. Soc. Jpn.* 2006, **79,** 437.

32 W.–L. Jia, T. M. McCormick, Y. Tao, J.–P. Lu, S. Wang. *Inorg. Chem.* 2005, **44,** 5706.

33 T. M. McCormick, W.–L. Jia, S. Wang. *Inorg. Chem.* 2006, **45,** 147.

34 a)Y. Kang, C. Seward, D. Song, S. Wang. *Inorg. Chem.* 2003, **42**, 2789. b) D. Song, S. Wang. *Eur. J. Inorg. Chem.* 2003, 3774.

35 a) M. H. Keef, K. D. Benkstein, J. T. Hupp. *Coord. Chem. Rev.* 2000, **205**, 201. b) D. Song, W.–L. Jia, G. Wu, S. Wang. *Dalton Trans.* 2005, 433

36 Q. D. Lui, R. Wang, S. Wang. *Dalton Trans.* 2004, 2073

37 a) E. Kimura, T. Koike. *Chem. Soc. Rev.* 1998, **27**, 179. b) E. M. Nolan, J. Jaworski, K.–I. Okamoto, Y. Hayashi, M. Sheng, S. J. Lippard. *J. Am. Chem. Soc.* 2005, **127,** 16812.

38 a)C. Seward, J. Chan, D. Song, S. Wang. *Inorg. Chem.* 2003, **42,** 1112. b)Y.–B. Dong, T. M. J.–P. Sung, X.–X. Zhao, R. –Q. Huang. *Inorg. Chem.* 2006, **45,** 10613. c) R. P. Feazell, C. E. Carson, K. K. Klausmeyer. *Eur. J. Inorg. Chem.* 2005, 3287,

39 W.–L. Jia, R.–Y. Wang, D. Song, S. J. Ball, A. B. McLean, S. Wang, *Chem. Eur. J.* 2005, **11,** 832.

40 L. De. La Durantaye, T. M. McCormick, X.–Y. Liu, S. Wang. *Dalton Trans.* 2006, 5676.

41 R. J. Sundberg, R. B. Martin. *Chem. Rev.* 1974, **74**, 471.

42 a) C. Zhou, A. Hassner. *Carbohydr. Res.* 2001, **333,** 313. b) R. Zou, J. C. Drach, L. B. Townsend. *J. Med. Chem.* 1997, **40,** 802. c) K. S. Godmundsson, J. Tidwell, N. Lippa, G. W. Koszalka, N. van Draanen, R. G. Ptak, J. C. Drach, L. B. Townsend. *J. Med. Chem.* 2000, **43,** 2464.

43 T.–R. Chen, R.–H. Chien, A. Yeh, J.–D. Chen, *J. Organomet. Chem.* 2006, **691**, 1998.

44 A. E. Ceniceros-Gomez, N. Barba-Behrens, M. E. Quiroz-Castro, S. Bernès, H. Noth, S. E. Castillo-Blum. *Polyhedron.* 2000, **19**, 1821.

45 a) M. M. H. Khalil, H. A. Mohamed, S. M. El-Medani, R. M. Ramada. *Spectrochim. Acta A.* 2003, **58.** 1341. b) M. M. H. Khalil, S. A. Ali, R. A. Ramada. *Spectrochim. Acta A.* 2001, **57,** 1017. c) M. M. H. Khalil. *Transition. Met. Chem.* 2000, **25,** 358.

46 Q.-D. Liu, M. S. Mudadu, H. Schmider, R. Thummel, Y. Tao, S. Wang. *Organomet.* 2002, **21,** 4743.

47 W.–L. Jia, Y.–F. Hu, J. Gao, S. Wang, *Dalton Trans.* 2006, 1721.

48 Q.–D. Liu, W.–L. Jia, S. Wang. *Inorg. Chem.* 2005, **44**, 1332.

Chapter 2:

Homo-substituted Benzimidazolyl Derivatives: Syntheses, Photophysical Properties and Applications In OLEDs

2.1 Introduction

Starburst or star-shaped molecules are an important class of molecules for OLEDs because they often possess high glass transition temperatures, thus high thermal and morphological stability.[1,2,3,4] Moreover, the starburst topology offers the opportunity to create individual molecules that have multiple binding sites or multiple chromophores.[5,6,7,8] One such example is 1,3,5-tris(*N*-phenyl-2-benzimidazolyl)benzene (TBPI), a well known molecular star that has been widely used as an electron transport material (ETM) in organic light emitting devices (OLEDs).[9] Our recent investigation has focused on the development of simple benzimidazolyl functionalized linear and star-shaped molecules, motivated primarily by the industrial demand for new ETMs that can also function as effective hole blocking materials.[4b] The most commonly used electron transport material in OLEDs is Alq_3 where q is the 8-hydroxyquinolate anion. However, it is a green emitter and cannot block holes effectively. Herein is a report of the synthesis of several new linear and star-shaped benzimidazolyl derivative compounds and their uses as non-emissive electron transport/hole blocking materials in OLEDs.

This new group of molecules are closely related to the indolyl and 7-azaindolyl functionalized linear and star-shaped molecules with similar central cores.[9,10] However, the benzimidazolyl derivatives display strikingly different photophysical properties from the 7-azaindolyl analogues which enable their use as highly effective ETMs in OLEDs.

A careful comparison between the benzimidazolyl compounds and their 7-azaindolyl analogues will be made using both empirical data and theoretical calculations. Finally, the effect of metal coordination to the ligands will also be explored.

2.2 Experimental

2.2.1 General

All starting materials were purchased from the Aldrich Chemical Company and used without further purification. 1,3,5-tris(*p*-bromophenyl)benzene and hexakis(*p*-bromophenyl)benzene were synthesized using literature procedures.[9,13]

TLC was carried out on silica gel. Column chromatography was carried out on silica (silica gel 60, 70-230 mesh). ^{1}H and ^{13}C NMR spectra were recorded on Bruker Avance 300, 400 or 500 MHz spectrometer. Excitation and emission spectra were recorded on a Photon Technologies International QuantaMaster Model C-60 spectrometer. Elemental analyses were performed by Canadian Microanalytical Service Ltd., Delta, British Columbia, Canada.

2.2.2 Electrochemical Studies

Cyclic voltammetry was performed using a BAS CV-50W analyzer with scan rates of 2 V s^{-1}. The electrolytic cell used was a conventional three compartment cell, in which a Pt working electrode, a Pt auxiliary electrode, and Ag/AgCl reference electrode were employed. The CV measurements were performed at room temperature using 0.10 M tetrabutylammonium hexafluorophosphate as the supporting electrolyte and dry CH_3CN or DMF as the solvent. The ferrocenium/ferrocene (E^o = 0.45 V in CH_3CN, 0.57 V in DMF) couple was used as the standard for converting the redox potentials to absolute energy (eV).

2.2.3: Thermal Studies

Thermogravimetric analysis was performed on a Perkin Elmer Thermogravimetric Analyzer TGA 7 under nitrogen with a temperature scanning rate of 10 ºC per minute using approximately 3 mg of sample for each compound. Differential scanning calorimetry was performed on a Perkin Elmer Differential Scanning Calorimeter DSC 6. All experiments were run with approximately 3 mg of sample with a heating and cooling rate of 10 ºC/minute.

2.2.4: Computational Studies

The molecular orbital calculations were performed for compounds 2.1, 2.2 and 2.3, and on 1,3,5-tris (*N*-indolyl)benzene and 1,3,5-tris(*N*-7-azaindolyl)benzene using the Gaussian Suite of programs (Gaussian 03). The geometries for all compounds were calculated and optimized. The calculations were performed with the B3LYP/6-311^{++}G** basis set employing a DFT level of computation. The orbital diagrams were generated using Chem3D Ultra 8.0.3.

2.2.5: Synthetic Procedures

Synthesis of 4,4'-bis(benzimidazolyl)-1,1'-biphenyl (2.1): A flask was charged with 4,4'-dibromo-1,1'-biphenyl (0.78 g, 2.5 mmol), CuI (0.10 g, 0.05 mmol), Cs_2CO_3 (3.25 g, 10 mmol), 1,10-phenanthroline (0.18 g, 1.0 mmol), benzimidazole (0.91g, 7.5 mmol) and 4 mL of DMF. The suspension was heated to 165ºC for 24 hours under a dry nitrogen atmosphere. The resulting oil was poured into water and extracted using methylene chloride (3 x 60 mL) and purified by column chromatography using methanol-ethyl acetate (1:3) as the eluting solution. A colorless powder of 2.1 was obtained (310 mg, yield 32%). ^{1}H NMR (300 MHz, $CDCl_3$, 298 K, ppm) δ: 8.22 (s, 2H), 7.94 (dd, 2H,

J_1 = 3.0 Hz, J_2 = 6.0 Hz), 7.88 (d, 4H, J = 8.4 Hz), 7.69 (d, 4H, J = 8.4 Hz), 7.65 (dd, 2H, J_1 = 3.0 Hz, J_2 = 6.0 Hz), 7.41 (dd, 4H, J_1 = 3.0 Hz, J_2 = 6.0 Hz). ^{13}C NMR (100 MHz, CD_2Cl_2, 298 K, ppm): δ 144.7, 142.7, 139.8, 136.5, 134.1, 129.0, 124.8, 124.0, 123.1, 120.8, 110.9. Anal Calc for $C_{26}H_{18}N_4$: C 80.8; H 4.7; N, 14.5. Found C 80.3; H 4.4; N 14.5. m.p. > 300ºC.

Synthesis of 1,3,5-tribenzimidazolylbenzene (2.2): A flask was charged with 1,3,5-tribromobenzene (0.49 g, 1.58 mmol), benzimidazole (0.55 g, 6.32 mmol), Cs_2CO_3 (2.6 g, 7.9 mmol), CuI (0.045 g, 0.23 mmol), 1,10-phenanthroline (0.091 g, 0.474 mmol) and 3 mL of DMF. The reaction mixture was heated to 165 ºC for 14 hours under a nitrogen atmosphere. The resulting oil was poured into water and extracted using methylene chloride (3 x 50 mL) and isolated via column chromatography using chloroform-methanol (7:1) as the eluent. A colorless solid of 2.2 was isolated (0.055 g, yield 8%). The compound was recrystallized from CH_2Cl_2 and hexane. ^{1}H NMR (300 MHz, CH_2Cl_2, 298 K, ppm) δ: 8.71 (s, 3H), 8.12 (s, 3H), 7.88 (d, 3H, J = 8.1 Hz), 7.81 (d, 3H, J = 8.1 Hz), 7.45 (dd 3H, J_1 = 7.2 Hz, J_2 = 7.2 Hz), 7.40 (dd, 3H, J_1 = 7.2 Hz, J_2 = 7.2 Hz). ^{13}C NMR (100 MHz, DMSO, 298 K, ppm) δ: 144.9, 142.6, 139.4, 133.7, 124.7, 123.8, 120.9, 118.0, 118.0, 112.1. Anal Calc for $C_{27}H_{18}N_6$: C, 76.0; H, 4.5; N 20.1. Found: C, 75.5; H, 4.3; N, 19.7. m.p. >300ºC.

Synthesis of 2,4,6-trisbenzimidazolyl-1,3,5-triazine (2.3): Compound 2.3 was previously reported by Elguero *et al*, but was synthesized herein by a procedure previously applied by our group.[13] Cyanuric chloride (0.51 g, 2.71 mmol) was dissolved in 35 mL of toluene and slowly added to a suspension of benzimidazole (1.44 g, 12.2 mmol) in 20 mL of toluene. The suspension was stirred for 30 minutes before addition of

sodium hydroxide (0.433 g, 10 mmol) and then warmed to 110 ºC for 16 hours. The resulting mixture was washed with water and the product was isolated from the toluene layer. The crude product was recrystallized from hot methylene chloride, to produce a colorless solid of 2.3 (0.62 g, yield 53%). ^{1}H NMR (300 MHz, CD_2Cl_2, 298 K, ppm) δ: 9.36 (s, 3H), 7.86 (dd, 6H, J_1 = 3.3 Hz, J_2 = 6.3 Hz), 7.66 (dd, 6H, J_1 = 3.3 Hz, J_2 = 6.3 Hz). ^{13}C NMR data were not obtained because of poor solubility of the compound. HRMS *calcd* for $C_{24}H_{15}N_{9:}$ 429.1450 *Found*: 429.1463 m.p. > 300ºC.

Synthesis of 1,3,5-tris(p-benzimidazolylphenyl)benzene (2.4): A flask was charged with a mixture of 1,3,5-tris(p-bromophenyl)benzene (0.32 g, 0.552 mmol), benzimidazole (0.41g, 3.2 mmol), $CuSO_4$ (0.04 g, 0.16 mmol), KOH (0.29 g, 5.3 mmol) and K_2CO_3 (0.44 g, 3.2 mmol). The flask was heated, in the absence of solvent, to 210 ºC for 16 hours under a dry nitrogen atmosphere. The resulting mixture was poured into water and extracted using methylene chloride and washed with water. The water layer was washed with methylene chloride (3 x 40 mL). The organic layers were combined and the solvent evaporated producing a brown oil. The product was isolated by column chromatography using ethyl acetate-methanol (7:1) as a pale yellow solid (84 mg, yield 23%). The solid was further purified by recrystallization from CH_2Cl_2 and hexane. ^{1}H NMR (400 MHz, CD_2Cl_2, 298 K, ppm) δ: 8.25 (s, 3H), 8.04 (s, 3H), 8.04 (d, 6H, J = 8.5 Hz), 7.90 (d, 3H, J = 7.5 Hz), 7.77 (d, 6H J = 8.5 Hz), 7.71 (d, 3H, J = 7.5 Hz), 7.40-7.43 (m, 6H). ^{13}C NMR (100 MHz, CD_2Cl_2, 298 K, ppm) δ: 142.7, 141.9, 140.7, 136.6 129.3, 125.8, 124.8 123.1, 120.9 110.9. HRMS *calcd* for $C_{45}H_{30}N_{6:}$ 654.2532 *Found*: 654.2546 m.p. 294-296ºC.

Synthesis of hexakis(p-benzimidazolylphenyl)benzene (2.5): A flask was charged with hexakis(p-bromophenyl)benzene (0.82 g, 1.02 mmol), CuI (0.16 g, 0.82 mmol), Cs_2CO_3

(4.0 g, 12.2 mmol), 1,10-phenanthroline (0.32 g, 1.8 mmol), benzimidazole (1.00 g, 8.52 mmol) and 4 mL of DMF. The suspension was heated to 165 ºC for 2 days, under a dry nitrogen atmosphere. The resulting mixture was poured into water and extracted with methylene chloride and washed with water. The methylene chloride layer was washed with water (3 x 100 mL). The solvent was evaporated to produce a brown oil. The compound was isolated using column chromatography, using methylene chloride: triethylamine (10:1) as the mobile phase (0.45 g, yield 37 %). The solid was further purified by repeated washing with methanol, and recrystallization from methylene chloride and methanol. ^{1}H NMR (300 MHz, $CDCl_3$, 298 K, ppm) δ: 8.41 (s, 6H), 7.71 (d, 6H, J = 8.1 Hz), 7.40 (s, 24H) 7.22-7.26 (m, 12H), 6.95 (dd, 1H, J_1=6.5Hz, J_2 = 6.5 Hz). ^{13}C NMR (100 MHz, CD_2Cl_2, 298 K, ppm):140.1,139.6, 134.4, 132.9, 123.5, 122.9, 120.4, 110.1 Anal Calc for $C_{84}H_{54}N_{12}\cdot 0.3\ CH_2Cl_2\cdot H_2O$: C, 80.42, H, 4.53, N, 12..35 Found C, 80.39, H, 4.33, N, 12.35. m.p. >300ºC.

2.2.6: Fabrication of Electroluminescent Devices

The EL device of compound 2.3 was fabricated on a gold substrate. Organic layers were deposited on the substrate by conventional vacuum deposition. Fullerene doped copper phthalocyanine (CuPc/NBB) was used as the hole injection layer (HIL). N,N'-Bis(1-naphthyl)-N,N'-diphenylbenzidine (NPB) was deposited as the hole transport layer. Alq_3 doped with 1% of 10-(2-benzothiazolyl)-1,1,7,7-tetramethyl-2,3,6,7-tetrahydro-1H,5H,11H-[l]benzo-pyrano[6,7,8-ij]quinolizin-11-one (C545T) was used as the emitting layer. Alq_3 and compound 2.3 are used as the hole blocking/electron transport layer for devices **A** and **B**, respectively. Fullerene (NBB) was used as the electron transport layer for both devices. Luminance-current density-voltage (L-J-V)

characteristics were recorded in ambient atmosphere using a HP 4140B pA meter and a Minolta LS-110 meter.

2.2.7: X-ray Crystallographic Analysis: Single crystals of 2.1 and 2.2 were obtained from slow diffusion of hexane into a CH_2Cl_2 solution. Single crystals for 2.5 were obtained by slow diffusion of methanol into a CH_2Cl_2 solution. Data were collected on a Siemens P4 single-crystal X-ray diffractometer with a Smart 1000 detector for 2.1, and a Bruker Apex II X-ray diffractometer for 2.2 and 2.5 with graphite-monochromated Mo Kα radiation, operating at 50 kV and 30 mA at 25°C and -93ºC respectively. Data were processed on a PC using Bruker SHELXTL software package[11] (version 6.14). Crystals of 2.1, 2.2 and 2.5 belong to the monoclinic space group C2/c, the orthorhombic space group $Pca2_1$, and the monoclinic space group $P2_1/c$ respectively. The absolute structure of 2.2 cannot be determined reliably. All structures were solved by direct methods. All non-hydrogen atoms were refined anisotropically. The positions of all hydrogen atoms were calculated and their contributions were included. The crystallographic analysis details are provided.

2.2.8: Metal Titration Experiments

For the titration of compound 2.1 with metal salts, a solution of 2.1 was prepared in methylene chloride (1.8×10^{-5} M). Another solution containing a metal ion (1.1×10^{-2} M) was also prepared. The metal ion solutions used in this study include $Zn(CF_3COO)_2$ in THF and $AgNO_3$ in acetonitrile. The emission and excitation spectra for the 2.1 were measured prior to addition of metal ions. A 0.1 equivalents of the metal salt was added to the stock solution of 2.1, and allowed to diffuse for 5 minutes. The emission spectrum was measured, and then the solution was left to stand for another 5 minutes before the

emission spectrum was measured again. This procedure was repeated until three identical emission spectra were collected, and then subsequent 0.1 equivalents of metal ions were added. The titration experiments employing compound 2.5 were done in a similar manner. Solutions of 2.1, 2.5 and of the metal salts were prepared such that the addition of the salts resulted in a total change in volume of less than 1% at the end of the experiment. The excitation wavelengths employed were 303 nm and 301 nm for 2.1 and 2.5 respectively.

2.3 Results and discussions

2.3.1 Synthesis and characterization

Four new benzimidazolyl derivative molecules were synthesized using modified Ullmann condensation methods where either CuI with 1,10-phenanthroline or $CuSO_4$ was used as the catalyst and a base was used to scavenge HX. Another known derivative, compound 2.3[13] was synthesized by a different route, using direct substitution facilitated by sodium hydroxide. The starting materials, 1,3,5-tris(*p*-bromophenyl)benzene and hexakis(*p*-bromophenyl)benzene for compounds 2.4 and 2.5, respectively, were synthesized using literature procedures.[2,8] The synthetic procedures for compounds 2.1 – 2.5 are summarized in Figure 2-1.

A common problem we encountered in the syntheses of the benzimidazolyl derivative compounds is that these compounds generally exhibit poor solubility in common organic solvents such as THF and CH_2Cl_2, making the purification and separation of some of the compounds difficult, resulting in low yields.

All five compounds were fully characterized by NMR and either elemental analyses or high resolution mass spectrometry. ^{13}C NMR data were not obtained for

compound 2.3, because of poor solubility. For compounds 2.1 and 2.2 and 2.5, single crystals were obtained and their structures were determined by X-ray diffraction methods.

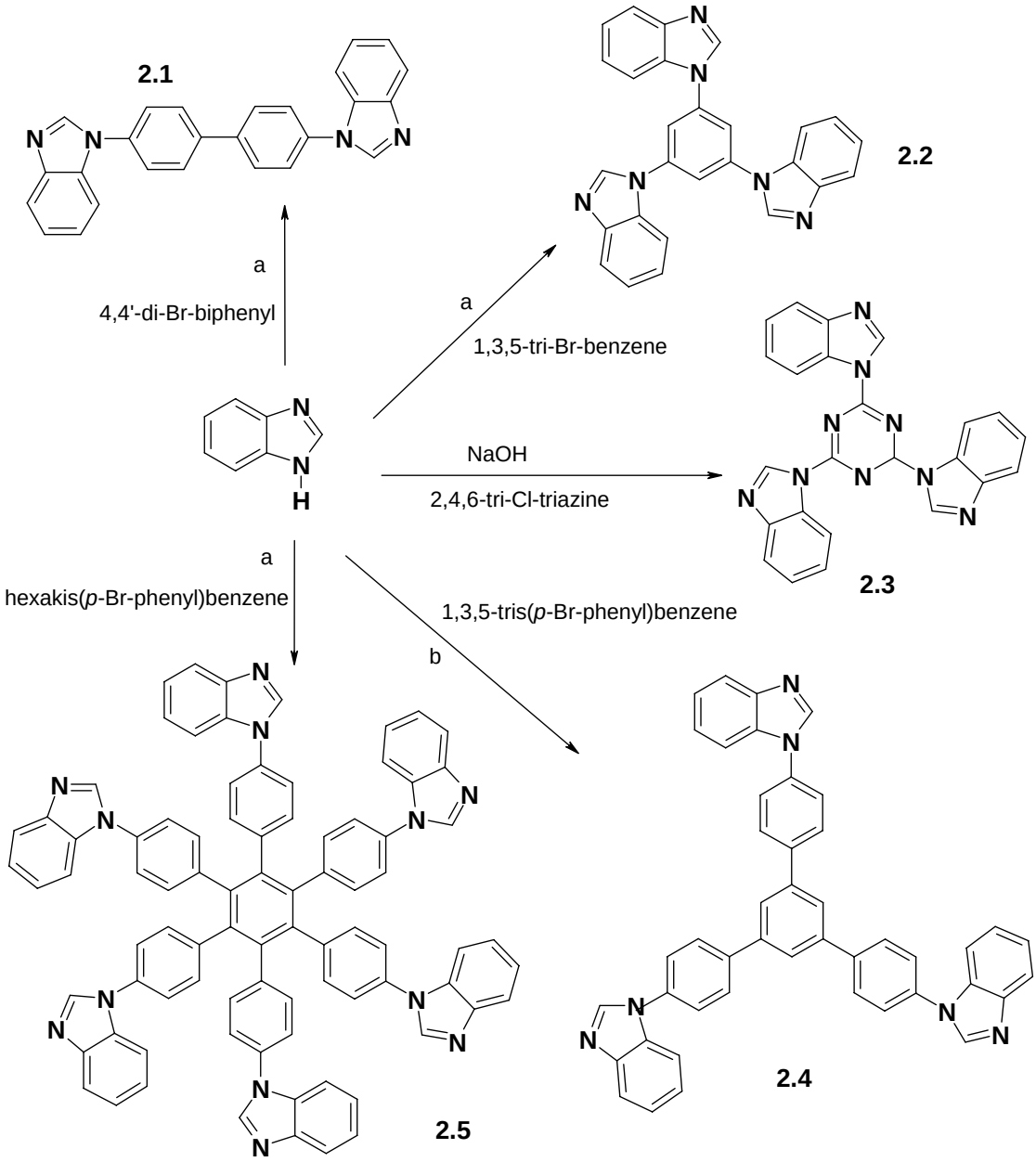

Figure 2-1: Synthetic scheme for compounds 2.1-2.5. a) CuI, 1,10-phenanthroline, Cs_2CO_3. b) $CuSO_4$, KOH

Table 2-1: Crystal data and structure refinement for compound 2.1

Identification code	2.1	
Empirical formula	$C_{26}H_{18}N_4$	
Formula weight	386.44	
Temperature	296(2) K	
Wavelength	0.71073 Å	
Crystal system	Monoclinic	
Space group	C2/c	
Unit cell dimensions	a = 19.548(6) Å	α= 90°.
	b = 7.058(2) Å	β= 90.886(6)°.
	c = 13.842(4) Å	γ = 90°.
Volume	1909.6(10) $Å^3$	
Z	4	
Density (calculated)	1.344 Mg/m^3	
Absorption coefficient	0.081 mm^{-1}	
F(000)	808	
Crystal size	.05 x .2 x 0.4 mm^3	
Theta range for data collection	2.08 to 28.23°.	
Index ranges	-25<=h<=26, -8<=k<=8, -16<=l<=17	
Reflections collected	4443	
Independent reflections	2121 [R(int) = 0.0554]	
Completeness to theta =28.23°	89.8 %	
Absorption correction	SADABS	
Refinement method	Full-matrix least-squares on F2	
Data / restraints / parameters	2121 / 0 / 172	
Goodness-of-fit on F2	0.718	
Final R indices [I>2sigma(I)]	R1 = 0.0521, wR2 = 0.0777	
R indices (all data)	R1 = 0.1917, wR2 = 0.0982	
Largest diff. peak and hole	0.136 and -0.140 $e.Å^{-3}$	

Table 2-2: Crystal data and structure refinement for compound 2.2

Identification code	2.2	
Empirical formula	$C_{27}H_{18}N_6$	
Formula weight	426.47	
Temperature	298(2) K	
Wavelength	0.71073 Å	
Crystal system	Orthorhombic	
Space group	$Pca2_1$	
Unit cell dimensions	a = 16.7712(18) Å	α= 90°.
	b = 16.6183(18) Å	β= 90°.
	c = 7.4205(8) Å	γ = 90°.
Volume	2068.2(4) $Å^3$	
Z	4	
Density (calculated)	1.370 Mg/m^3	
Absorption coefficient	0.085 mm^{-1}	
F(000)	888	
Crystal size	0.30 x 0.20 x 0.10 mm^3	
Theta range for data collection	2.43 to 21.51°.	
Index ranges	-17<=h<=17, -16<=k<=17, -7<=l<=7	
Reflections collected	11047	
Independent reflections	2013 [R(int) = 0.0609]	
Completeness to theta = 21.51°	86.1 %	
Absorption correction	SADABS	
Refinement method	Full-matrix least-squares on F^2	
Data / restraints / parameters	2013 / 1 / 298	
Goodness-of-fit on F2	1.032	
Final R indices [I>2sigma(I)]	R1 = 0.0345, wR2 = 0.0803	
R indices (all data)	R1 = 0.0461, wR2 = 0.0840	
Absolute structure parameter	-3(3)	
Largest diff. peak and hole	0.180 and -0.173 e.$Å^{-3}$	

Table 2-3: Crystal data and structure refinement for compound 2.5

Identification code	2.5	
Empirical formula	$C_{84}H_{54}N_{12}\cdot CH_2Cl_2\cdot H_2O$	
Formula weight	1334.36	
Temperature	180(2) K	
Wavelength	0.71073 Å	
Crystal system	Monoclinic	
Space group	P2(1)/c	
Unit cell dimensions	a = 13.2011(16) Å	α= 90°.
	b = 9.2379(11) Å	β= 93.0210(10)°.
	c = 56.398(7) Å	γ = 90°.
Volume	6868.2(14) $Å^3$	
Z	4	
Density (calculated)	1.288 Mg/m^3	
Absorption coefficient	0.154 mm^{-1}	
F(000)	2768	
Crystal size	0.35 x 0.20 x 0.06 mm^3	
Theta range for data collection	1.45 to 25.00°.	
Index ranges	-15<=h<=15, -10<=k<=10, -67<=l<=67	
Reflections collected	64309	
Independent reflections	12064 [R(int) = 0.0453]	
Completeness to theta = 25.00°	100.0 %	
Absorption correction	SADABS	
Refinement method	Full-matrix least-squares on F^2	
Data / restraints / parameters	12064 / 1 / 922	
Goodness-of-fit on F^2	1.093	
Final R indices [I>2sigma(I)]	R1 = 0.1008, wR2 = 0.2695	
R indices (all data)	R1 = 0.1263, wR2 = 0.2902	
Largest diff. peak and hole	0.692 and -1.130 e.$Å^{-3}$	

Table 2-4: Selected bond lengths [Å] and angles [°] for 2.1.

C(8)-N(2)	1.426(3)	C(6)-N(2)-C(8)-C(9)	48.1°
C(11)-C(11)#1	1.487(5)	N(1)-C(7)-N(2)	114.5(3)

Table 2-5: Selected bond lengths [Å] and angles [°] for 2.2.

N(1)-C(22)	1.431(5)	C(6)-N(1)-C(22)	126.4(3)
N(3)-C(26)	1.411(4)	C(20)-N(4)-C(24)	127.5(3)
N(4)-C(24)	1.428(5)	C(13)-N(3)-C(26)	126.9(2)

Table 2-6: Selected bond lengths [Å] and angles [°] for 2.5

C(10)-N(1)	1.431(5)	C(49)-N(7)	1.438(1)
C(23)-N(3)	1.423(3)	C(62)-N(6)	1.436(5)
C(36)-N(5)	1.421(6)	C(75)-N(11)	1.427(3)

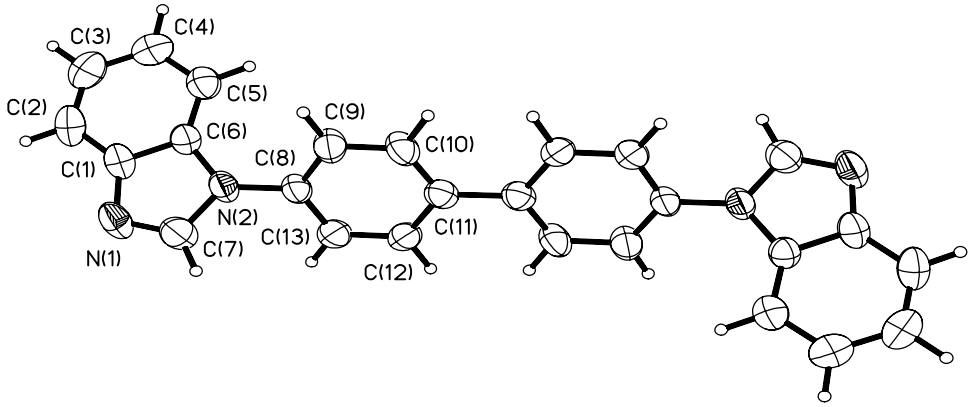

Figure 2-2: Crystal structure for compound 2.1

As shown in Figure 2-2, the central biphenyl core in compound 2.1 is coplanar. However, the benzimidazolyl rings are not coplanar with the central core as evident by the dihedral angle of 48.1° between the benzimidazolyl ring and the biphenyl core. In the crystal lattice, the molecules of 2.1 stack along the b axis with extensive π–π stacking interactions between the benzimidazolyl rings of neighboring molecules (Figure 2-3).

The shortest atomic contact distance between two neighboring benzimidazolyl rings is ~3.3 Å.

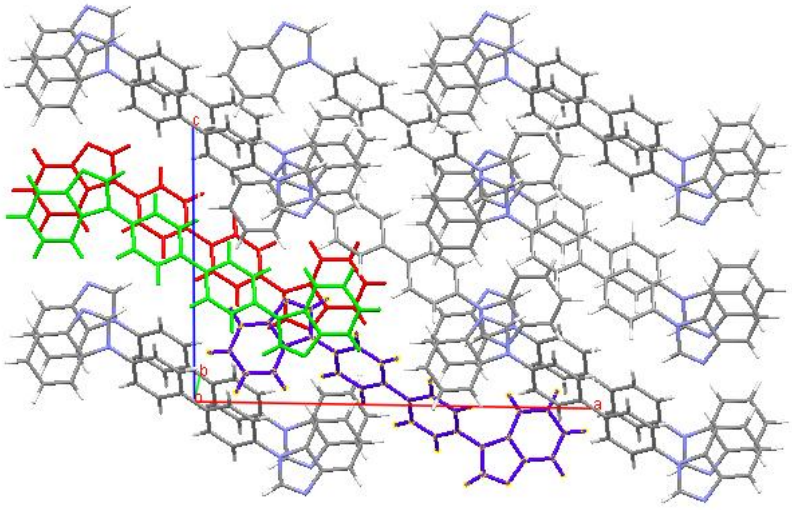

Figure 2-3: Unit cell packing diagram for compound 2.1 projected down the b-axis.

Compound 2.2 belongs to the chiral orthorhombic space group $Pca2_1$. As illustrated in Figure 2-4, compound 2.2 has an approximate propeller structure. The dihedral angles between the benzimidazolyl rings and the central benzene ring range from 37.1° to 56.7°. One of the benzimidazolyl rings is involved in intermolecular π - π interactions with the same benzimidazolyl ring from neighboring molecules with the shortest atomic contact distance being ~3.5 Å. As a result of these π - π interactions, the molecules of compound 2.2 stack along the *c* axis in the crystal lattice (Figure 2-5). The propeller structure of 2.2 resembles that of 1,3,5-tris(*N*-7-azaindolyl)benzene (TAB).[12] However, unlike 2.2 where the intermolecular stacking occurs through one of the benzimidazolyl groups in the crystal lattice, the molecules of TAB stack on top of each other through the entire structure.[12]

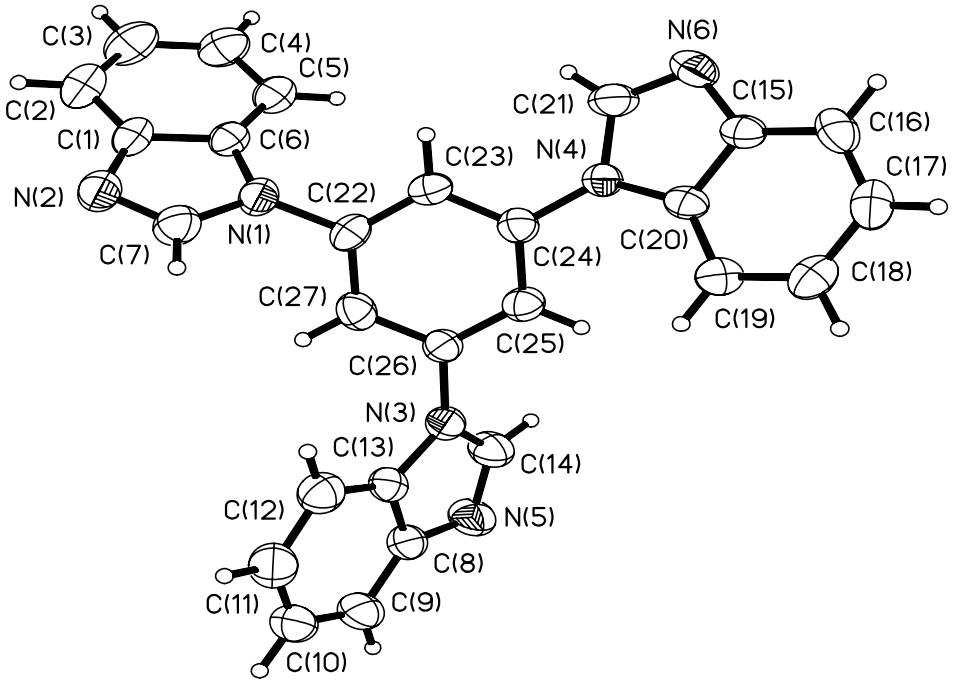

Figure 2-4: Molecular structure of compound 2.2 with labeling scheme.

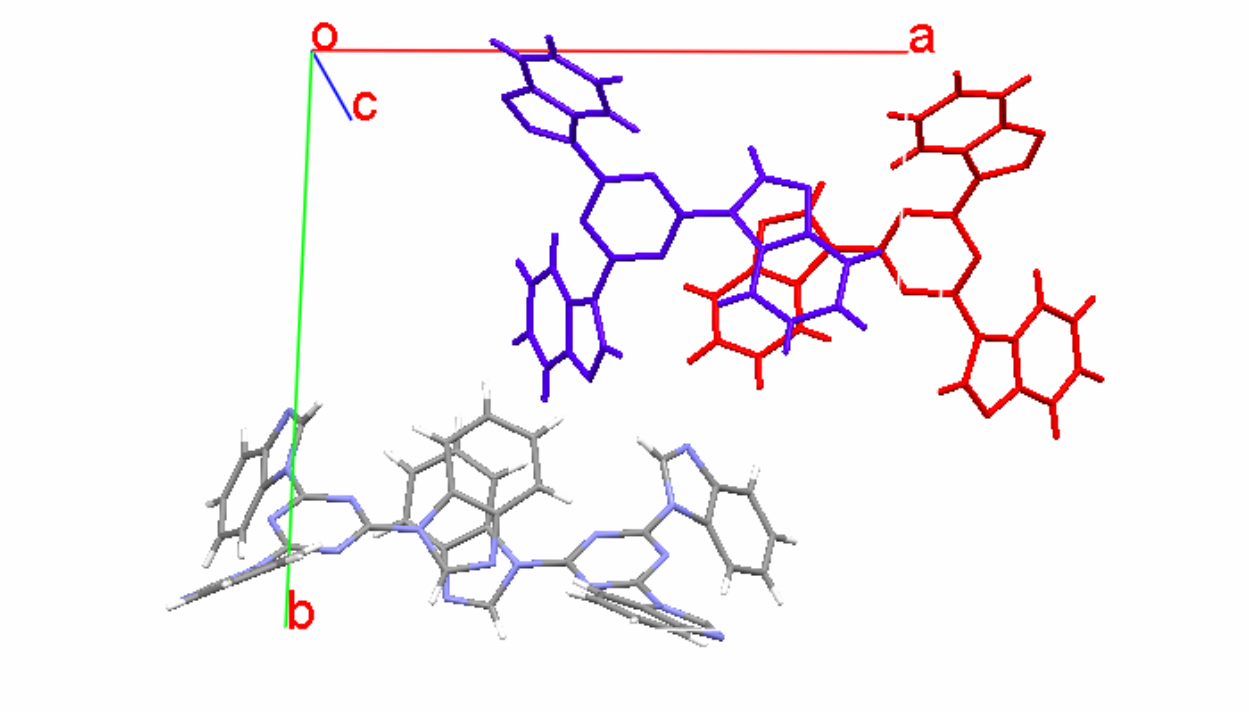

Figure 2-5: Unit cell packing diagram of 2.2 projected down the c axis.

Compound 2.5 crystallizes in the monoclinic space group $P2_1/c$ and is depicted in Figure 2-6, with the packing scheme displayed in Figure 2-7. A molecule of methylene chloride and a disordered molecule of water are both present in the structure. The dihedral angles between the benzimidazolyl groups and the phenyl linkers range between 26.3º and 67.1º, while the dihedral angles between the central benzene core and the phenyl groups range between 52.0º and 88.9º. This suggests that the degree of conjugation throughout molecule is small. It is also noteworthy that there are π–π interactions between two of the benzimidazolyl moieties and the phenyl linkers in two of the adjacent molecules with the shortest atomic contact distance being ~ 3.4 Å (Figure 2-8). As a result of this, the molecules stack along the *b* axis.

This structure differs markedly from the 7-azaindole analogue previously reported.[8] The coexistence of solvent molecules in the structure of 2.5 causes significant distortion in the dihedral angles compared to the 7-azaindolyl analogue, where all of the 7-azaindolylphenyl legs lie perpendicular to the benzene core. Furthermore, the 7-azaindolyl molecule demonstrates a two-dimensional layered structure,[8] which is not apparent in 2.5. Again, this is likely a result of the incorporation of solvent in the molecule, which prevents orderly packing.

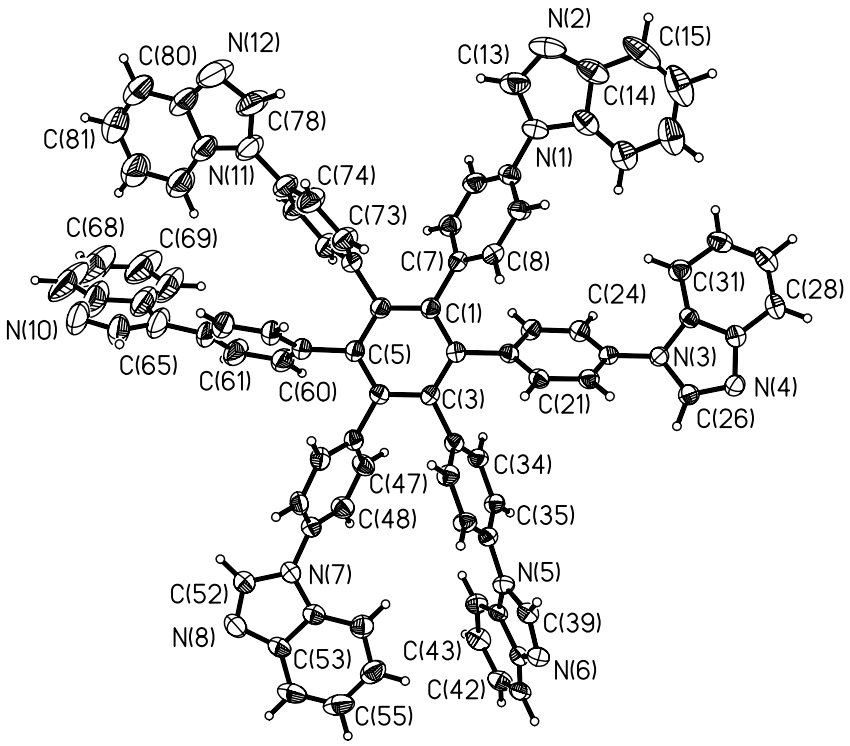

Figure 2-6: Crystal structure for compound 2.5 in with labeling scheme. The solvent molecules have been omitted for clarity.

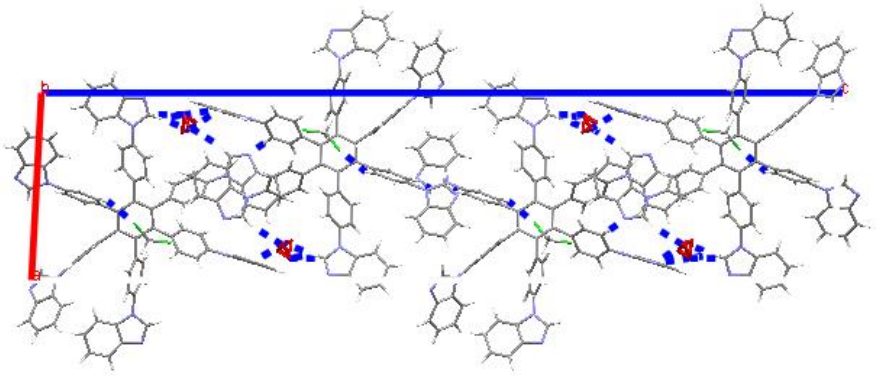

Figure 2-7: Unit cell packing diagram of 2.5 projected down the b-axis.

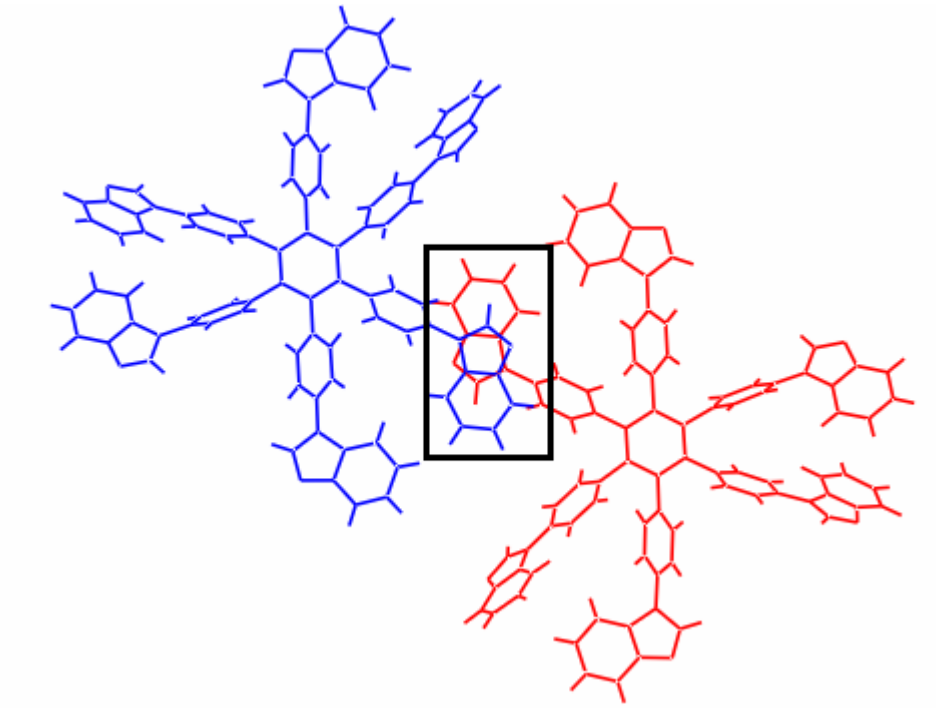

Figure 2-8: Illustration of the intermolecular interactions present in the crystal structure for compounds 2.5. The π–π interaction between benzimidazolylphenyl legs is emphasized in the black box in the middle of the figure.

2.3.2 Thermal Properties

The thermal properties of the new compounds were first examined by thermogravimetric analysis under nitrogen with a heating rate of 10 ºC per minute. All compounds are stable up to at least 300 ºC under these conditions. All compounds, except 2.1, display small percentage of weigh loss at temperatures below 200 °C which were attributed to the loss of solvent molecules trapped inside the samples. Compound 2.3 undergoes decomposition at ~300 °C while the other four compounds appear to undergo sublimation at high temperatures (~370 °C for 2.2 and 2.3, ~500 °C for 2.4 and 2.5), as evidenced by the rapid and complete weight loss of these samples (Figure 2-9).

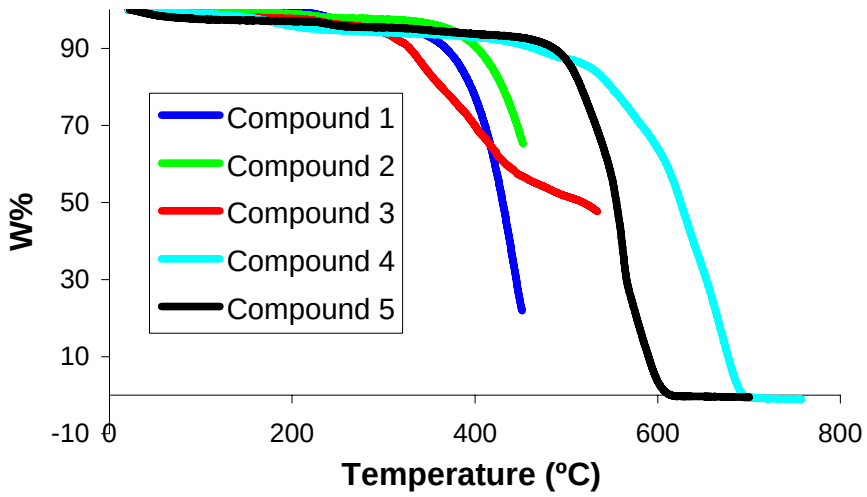

Figure 2-9: TGA diagrams for compounds 2.1 -2.5.

Compounds 2.2 and 2.3 have similar structures with the former having a benzene core and the latter a triazine core. The relatively lower thermal stability of 2.3 is clearly associated with the triazine core, which is unexpected because earlier work on 2,2'-dipyridylamino functionalized compounds indicated that compounds with a triazine core are in general thermally more stable than the benzene core analogues.[2,13]

Compounds 2.1 - 2.5 were further examined using differential scanning calorimetry under an argon atmosphere with the heating and cooling rate of 10 ºC per minute. These compounds have high melting temperatures, generally greater than 300ºC and glass transitions were only observed for compounds 2.3 and 2.4 at 145 ºC and 195 ºC respectively, an indication that these two molecules are morphologically stable. Relatively high glass transition temperatures have been observed previously in star-shaped molecules based on either benzene or triazine cores with 7-azaindolyl or 2,2'-dipyridylamino groups.[7]

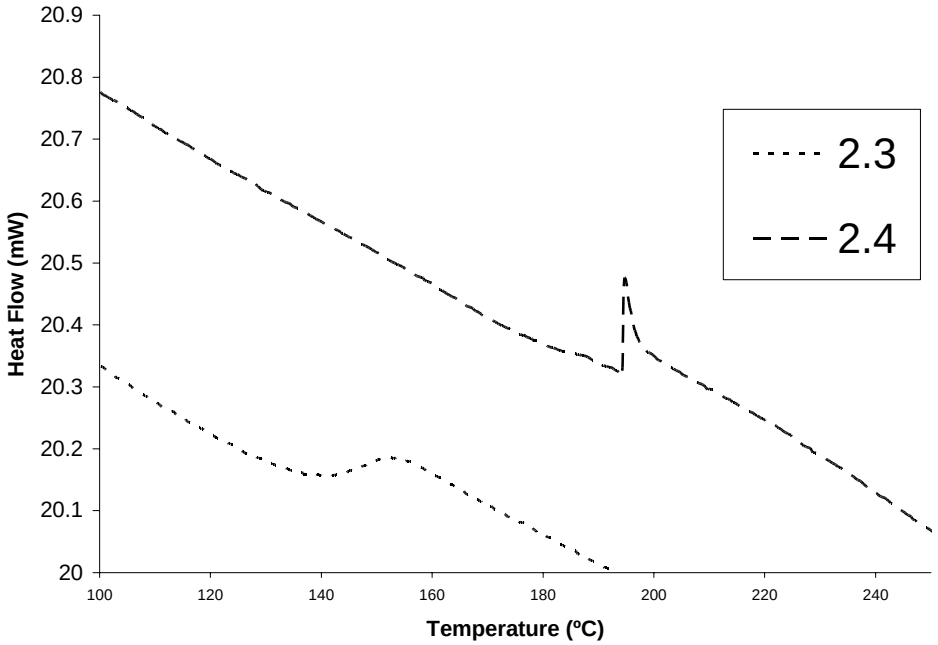

Figure 2-10: DSC curves for compounds 2.3 and 2.4.

2.3.3 Photophysical properties

As demonstrated by Figure 2-11, the absorption spectra for compounds 2.1 – 2.5 in CH_2Cl_2 appear in the 200 – 350 nm region and all possess similar features. The notable difference is between compound 2.2 and compound 2.3. Despite the structural similarity between these two molecules, 2.2, with a benzene core has a much higher absorption energy than that of 2.3 which has a triazine core. This is in fact consistent with the general trend observed previously for 7-azaindolyl or 2,2'-dipyridylamino group functionalized benzene or triazine molecules.[7]

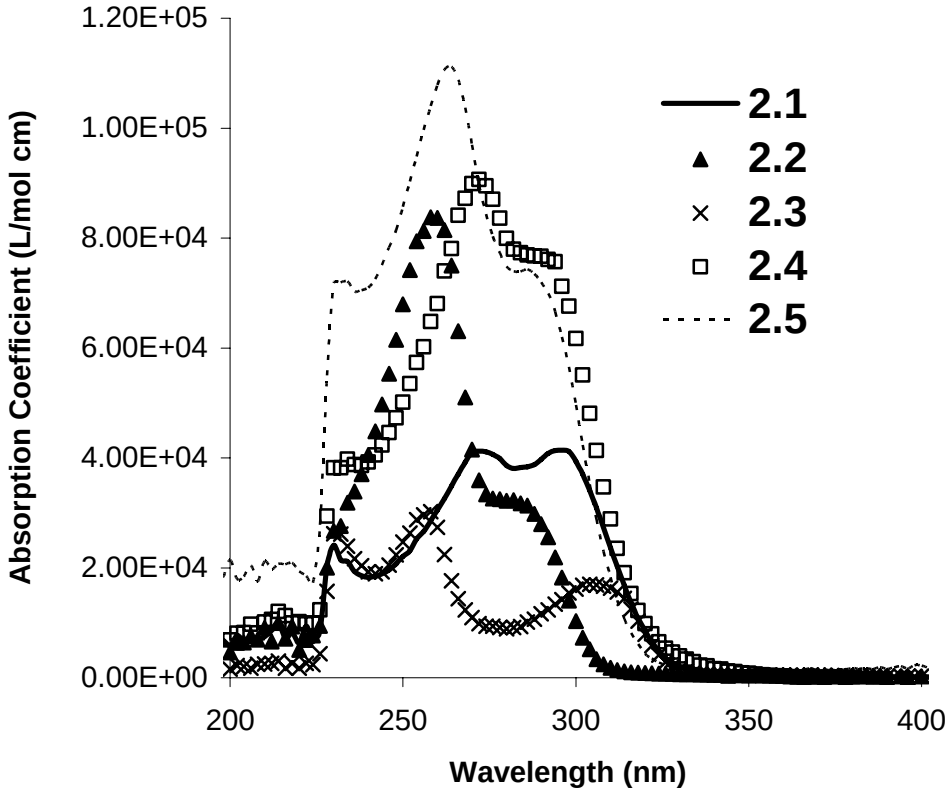

Figure 2-11: UV-Vis spectrum for compounds 2.1-2.5 in CH_2Cl_2 at a concentration of $10^{-5} – 10^{-6}$ M.

Furthermore, compared to compounds 2.1, 2.4 and 2.5 where the benzimidazolyl groups are separated by at least two phenyl rings, compound 2.2 has the highest absorption energy. This can be attributed to the fact that the benzimidazolyl groups in 2.2 are only separated by a single phenyl ring, and are therefore less conjugated.

It is also interesting that the spectrum of the hexa-substituted compound 2.5 is significantly blue shifted when compared to the spectrum to the tri-substituted 2.4. This is clearly a consequence of the loss of conjugation between the *p*-benzimidazolylphenyl

group and the benzene core in 2.5, resulting from the increased steric strain in this molecule.

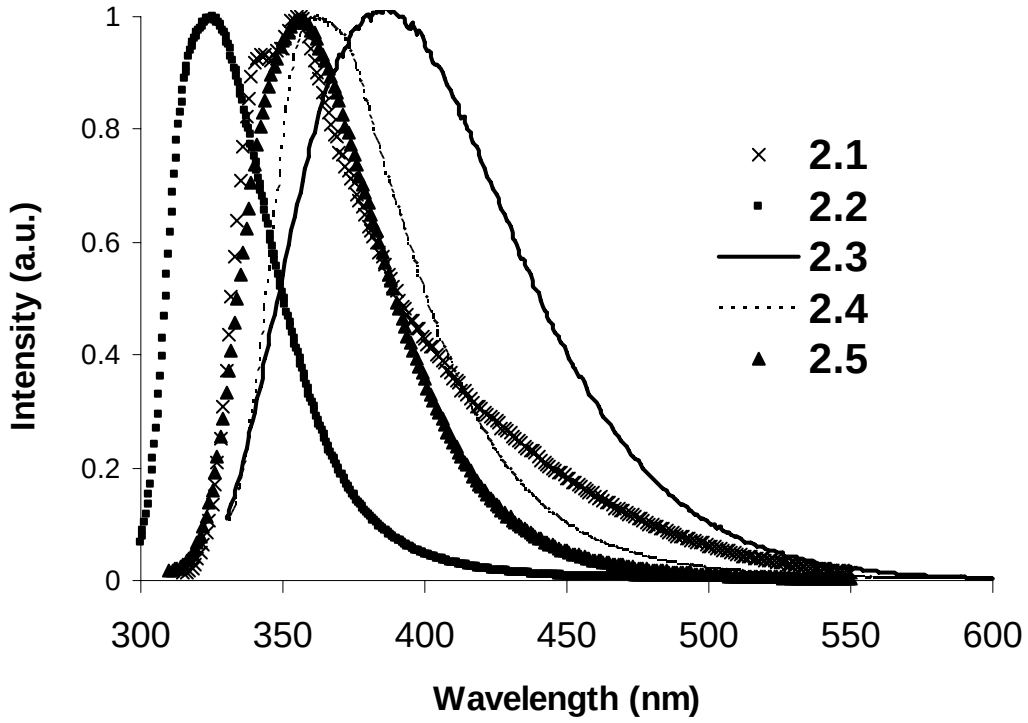

Figure 2-12: Emission Spectra for compounds 2.1-2.5 (10^{-6}M) in CH_2Cl_2.

Compounds 2.1 – 2.5 are luminescent in the blue-violet region with the emission wavelength maxima ranging from ~325 nm (2.2) to ~ 384 nm (2.3) when irradiated by UV light (Figure 2-12). The triazine derivative 2.3 displays the longest emission wavelength, compared to the benzene derivatives, which is again consistent with previous observations on related systems.[7] The emission quantum efficiency varies between 8% (2.5) and 27% (2.4). The luminescent data and optical bandgaps are summarized in Table **2-7**.

Despite the presence of six *p*-benzimidazolylphenyl chromophores in the molecule, compound 2.5 has the lowest quantum efficiency. This can be attributed to steric interactions between the *p*-benzimidazolylphenyl groups. The additional substitution about the benzene core increases the number of interleg quenching modes available to the molecule, and facilitates non-radiative decay of the excited state. This effect is particularly apparent when compared to the much less crowded 2.4, which has the highest quantum efficiency.

The emission energy of 2.5 (355 nm) is about 30 nm blue shifted, compared to that of hexakis(para-*N*-(7-azaindolyl)phenyl)benzene, which again demonstrates the impact of the location of the nitrogen atoms in the heterocycle. The low emission quantum efficiency of 2.5 is also consistent with that of hexakis(para-*N*-(7-azaindolyl)phenyl)benzene.

Table 2-7: Photophysical and electrochemical data for compounds 2.1-2.5.

	λ_{em} (nm)[a]	Φ[a]	E_{red} (V)[b]	Optical energy-gap (eV)[a]	HOMO (eV)	LUMO (eV)	HOMO-LUMO gap[c] (eV)
2.1	356	0.12	-1.05	3.55	-6.84	-3.29	4.40
2.2	326	0.14	-1.20	3.95	-7.09	-3.14	4.80
2.3	384	0.16	-0.87	3.55	-7.04	-3.49	4.50
2.4	362	0.27	-.1.00	3.45	-6.79	-3.34	
2.5	355	0.08	-1.17	3.76	-6.88	-3.12	
TAB	410	0.50		3.76	-5.95	-2.13	4.70

[a]Measured in CH_2Cl_2 at a concentration or 10^{-6} M. Anthracene was used as the reference for all quantum yield measurements. [b]For 2.1, 2.2, and 2.4 measured in CH_3CN, for 2.3 and 2.5, measured in DMF. [c]Obtained from theoretical molecular orbital calculations. The reduction potentials were estimated using the half wave potentials, and then compared to ferrocene to estimate the LUMO energy levels. HOMO energy levels were estimated based on the optical bandgap obtained from the UV-Vis spectrum.

2.3.4 Electrochemical properties

The electrochemical properties of compounds 2.1 – 2.5 were examined by cyclic voltammetry experiments. Freshly distilled acetonitrile was used as the solvent for 2.1, 2.2 and 2.4. Due to the poor solubility of compounds 2.3 and 2.5 in acetonitrile, DMF was used as the solvent. All five compounds display a half wave reduction potentials between ~ -0.80 V and -1.2 V, relative to AgCl/Ag reference electrode (Figure 2-13).

After calibration with the $FeCp_2/FeCp_2^+$ oxidation potential, the observed reduction potentials were used to estimate the LUMO energy levels for each compound. The results are shown in Table 2-7. The HOMO energy levels were estimated by using the optical band gap, as determined by UV-Vis spectroscopy.

As shown in Table 2-7, compounds 2.1 – 2.5 all have high electron affinities that are below -3 eV, with compound 2.3 being the lowest at -3.49 eV, attributable to the electronegative triazine core in 2.3. This is consistent with previously reported triazine derivatives, which often display high electron affinities.[14]

It is noteworthy that the LUMO level (-3.14 eV) of 1,3,5-tris(*N*-benzimidazolyl)benzene (2.2) is about 1 eV lower than its isoelectronic analogue, 1,3,5-tris(*N*-7-azaindolyl)benzene.[b] The location of the electronegative nitrogen atom in the heterocycles clearly has a significant impact on the energy level of HOMO and LUMO. This is consistent with the previous observation that the LUMO level of 2-(2'-pyridyl)benzimidazole is considerably lower than that of the corresponding 2-(2'-pyridyl)-7-azaindole analogue.[2,15] The LUMO levels of compounds 2.1 – 2.5 are lower than those of the well-known ETMs TPBI (2.7 eV),[16] and Alq_3 (3.0 eV).[17] The exceptionally low LUMO levels for this class of molecules is a strong indication that they

may be prone to good electron injection, and therefore useful as ETMs for OLED devices. Furthermore, high ionization potentials suggest that these compounds may function well as hole blocking materials.

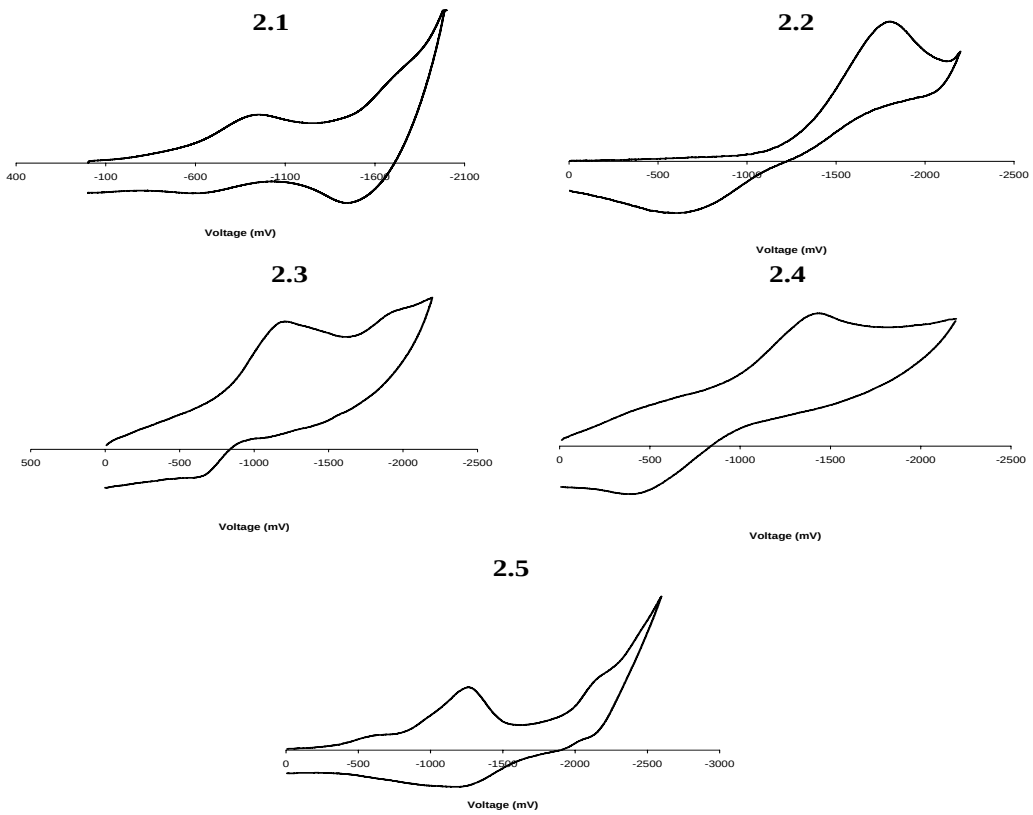

Figure 2-13: Cyclic voltammograms showing the reduction potentials for compounds 2.1-2.5 vs the Ag/AgCl reference electrode. All data were collected in acetonitrile, except 2.3 and 2.5 which was done in DMF.

2.3.5 Molecular Orbital Calculations

Molecular orbital calculations have been performed on compounds 2.1, 2.2 and 2.3 to further understand their electronic properties. Furthermore, calculations on 1,3,5-tris(N-(7-azaindolyl))benzene (TAB) and 1,3,5-tris(N-indolyl)benzene (TIB) were also

carried out for comparison with 2.3. The structures are displayed in Figure 2-14. Calculations were performed using DFT at the B3LYP level of theory with the 6-311^{++}G** basis set.

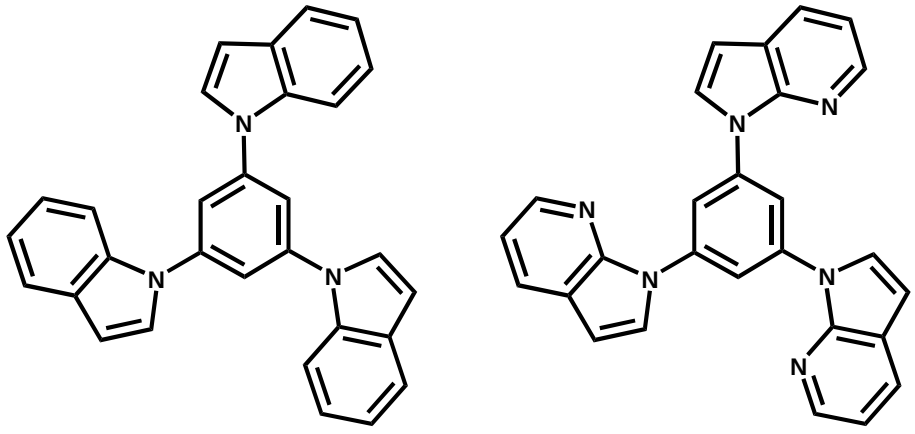

TIB **TAB**

Figure 2-14: Chemical Structures for 1,3,5-tris(N-indolyl)benzene (TIB) and 1,3,5-tris(N-(7-azaindolyl))benzene (TAB).

Table 2-8:Theoretically calculated HOMO and LUMO energy levels for compounds 2.1-2.3.

	2.1	**2.2**	**2.3**
HOMO (eV)	-6.3	-6.7	-6.9
LUMO (eV)	-1.9	-1.9	-2.4

For compounds 2.1-2.3, the calculated trends of the HOMO and LUMO energy levels and the HOMO-LUMO energy gaps are in moderate agreement with the experimental values obtained from electrochemical and UV-Vis spectroscopic measurements. For example, compound 2.1 has the highest HOMO while compound 2.3 has the lowest LUMO (Table 2-8). It is noteworthy that the phenyl rings are coplanar for 2.1, similar to the X-ray structure. For 2.1, the HOMO level has contributions from the

entire molecule while the LUMO level is dominated by the central biphenyl ring (Figure 2-15). For 2.2 and 2.3 the LUMO levels are similar with dominating contributions from the central core and some contributions from the benzimidazolyl rings. However, as depicted by Figure 2-4, the HOMO levels for 2.2 and 2.3 are distinctly different. For 2.2, the HOMO shows significant contribution from the entire molecule, while in 2.3 there is minimal contribution from the triazine ring. Therefore, the lowest electronic transition can be described as a $\pi \rightarrow \pi^*$ for 2.1 and 2.2, but as charge transfer from the benzimidazolyl ring to the central triazine ring for 2.3. The calculated results demonstrate that the LUMO level for all three molecules includes the electronegative benzimidazolyl moiety which is clearly responsible for the observed low LUMO energy of these molecules.

Figure 2-15: HOMO (bottom) and LUMO (top) diagrams for compound 2.1.

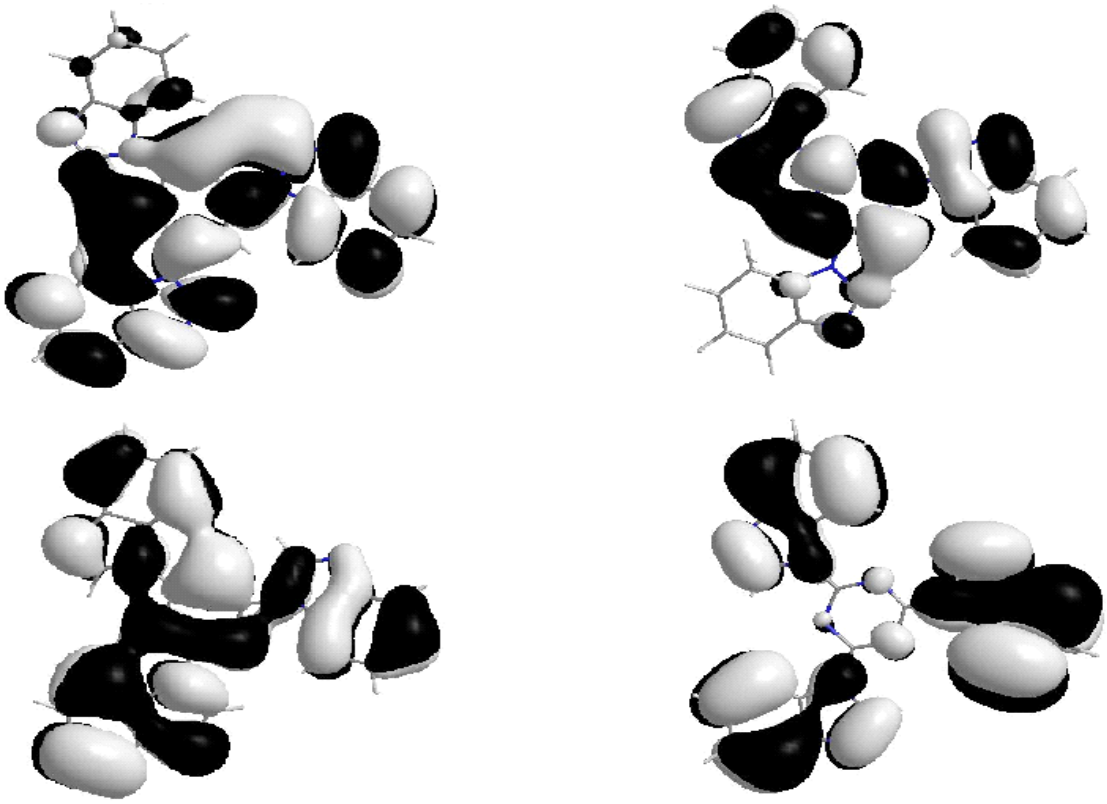

Figure 2-16: HOMO (bottom) and LUMO (top) diagrams for 2.2 (left) and 2.3 (right).

The MO calculations were performed on TIB and TAB, for comparison with compound 2.2. The MO diagrams for the HOMO and LUMO orbitals are shown in Figure 2-17 and clearly illustrate the similarities between the three molecules In all cases, the lowest electronic transition can be described as $\pi \rightarrow \pi^*$. It is also apparent that inclusion of the additional nitrogen atom in the functional group changes the shape of the HOMO orbital considerably. The HOMO in TIB only displays contributions from two of the luminophores, while in TAB there is considerably more contribution from the third azaindolyl group. The trend continues, with the HOMO showing equal contribution from the entire molecule in compound 2.2.

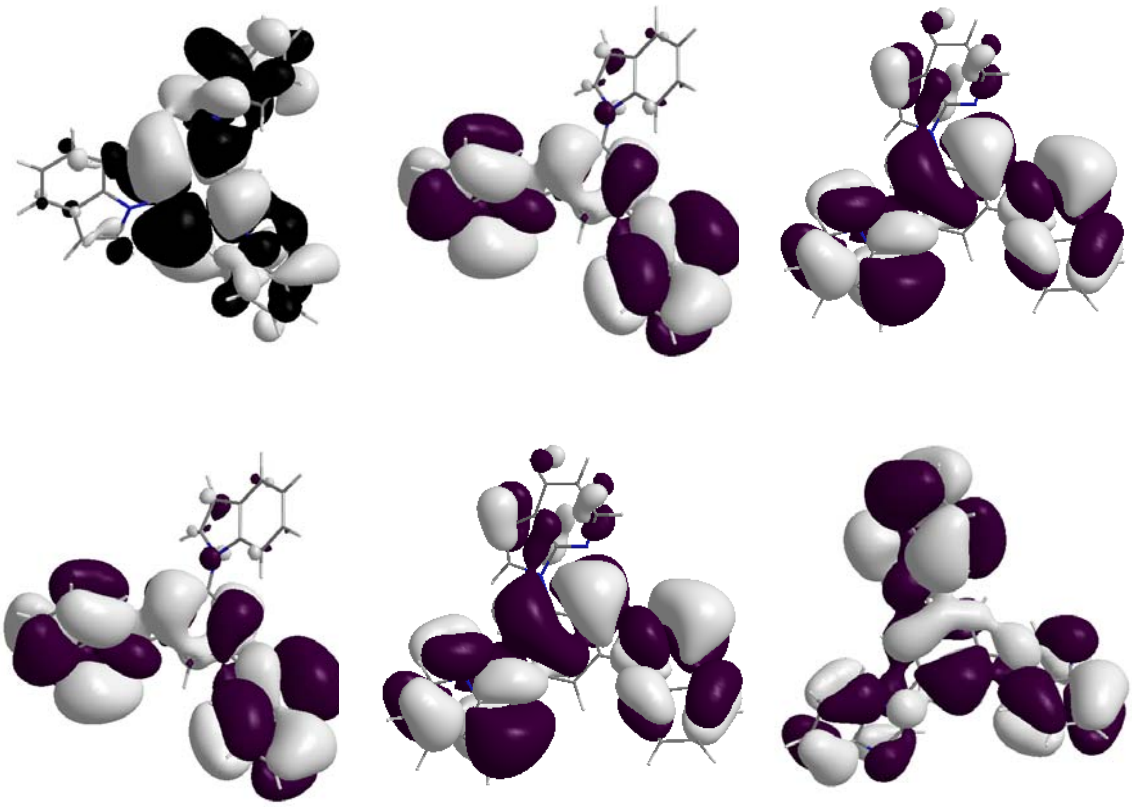

Figure 2-17: Molecular orbital diagrams generated from theoretical calculations on TIB(left), TAB (middle) and 2.2 (right). The HOMO orbital diagrams are illustrated on the bottom, and the LUMO diagrams on the top.

It is also interesting to note the effect of the additional nitrogen atom on the energies of the orbitals. Indole, having only one heteroatom in its structure, has the smallest HOMO-LUMO gap (Table 2-9). Substitution of the methine in the seven position with the more electronegative nitrogen atom, as in TAB, results in a widening of the HOMO-LUMO gap. This is justified as an electron withdrawing effect, removing electron density from the HOMO orbital, hence lowering its energy.

The location of the nitrogen atom is also relevant. Moving the nitrogen from the 7- position to the 3- position concentrates the electron withdrawing effect, further lowering the HOMO energy level, and further increasing the HOMO-LUMO gap.

Table 2-9: Calculated energy levels for tri-substituted molecular stars with a benzene core.

	TIB	TAB	2.2
HOMO (eV)	-5.9	-6.0	-6.7
LUMO (eV)	-1.3	-1.3	-1.9
Bandgap (eV)	4.6	4.7	4.8

This effect is consistent with previously reported data. The photo and electrochemical properties of TIB have not been reported hitherto, and are therefore unavailable for comparison. However, TAB has been fully characterized.[10b] The HOMO-LUMO gap for TAB has been estimated through the use of UV-Vis spectroscopy, and was found to be 3.76 eV. Comparison of these values with the data in Table 2-7 shows that the empirical trends match those theoretically calculated. Moreover, these trends between TAB and 2.2 appear to be generally true in comparing 7-azaindolyl derivatives to benzimidazolyl derivatives. 7-azaindolyl analogues for compounds 2.1 and 2.4 have also been reported, and a similar increase in the HOMO-LUMO gap is observed in both instances.[10b]

2.3.6 Compound 2.3 as an Electron Transport/Hole Blocking Material in Electroluminescent Devices

Because compound 2.3 has the highest electron affinity among the five new compounds, it was selected for evaluation as an electron transport/hole blocking material

in OLEDs and its performance was compared to that of Alq_3. Because fullerene (NBB) has been demonstrated recently to be an effective electron injection/transport material,[18] it was used as an electron injection material in our devices.

Two EL devices, **A** and **B** were constructed. To compare the performance of Alq_3 and compound 2.3, these two molecules were used as the electron transport/hole blocking layer in devices **A** and **B**, respectively (Figure 2-19). The emitting layer (25 nm) is Alq_3 doped with a green dye (C545T, 1 wt%). NPB was used as the hole transport layer (45 nm) while fullerene-doped (30 wt.%) copper phthalocyanine (16 nm) was used as the hole transport/hole injection layer in both devices. The anode is made of gold and the cathode is made of LiF/Al bilayer. The details of this type of Au anode devices have been described previously.

The performance of both devices is comparable, as shown by the L-V diagram in Figure 2-20, and current efficiency (CE)-L diagram in Figure 2-21. The brightness and the turn-on voltage (~3.0 V) of device B are very similar to those of device A. Further, both devices show extremely high luminance > 100,000 cd/m^2 without device breakdown. The current efficiency for both devices is similar, in particular in high luminance (>10000 cd/m^2). Devices A and B produce the same emission color that is characteristic of the C545T dye doped Alq_3 layer as shown by Figure 2-22, which indicates that, unlike Alq_3, compound 2.3 behaves strictly as an electron transport layer and does not influence the emission characteristics of the device. The large HOMO-LUMO gap and the fact that compound 2.3 is a colorless material and does not emit in the visible region make it possible to use this compound as an electron transport/electron injection layer in broad range of electroluminescent devices.

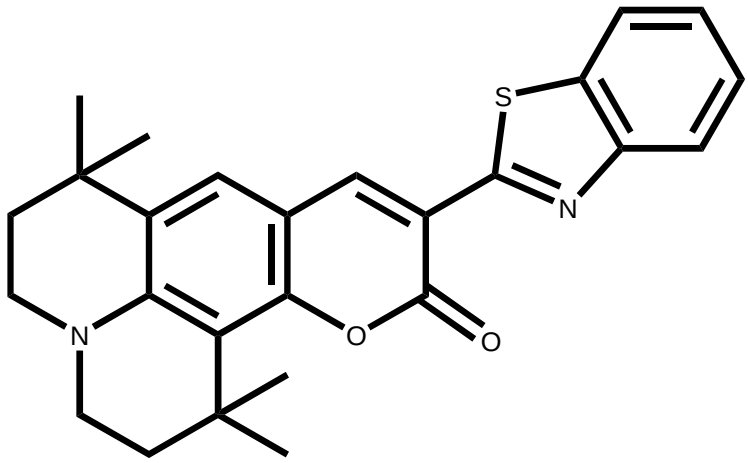

Figure 2-18: Chemical structure for 10-(2-benzothiazolyl)-2,3,6,7-tetrahydro-1,1,7,7,-tetramethyl 1-1H,5H,11H-[1]benzopyrano [6,7,8,ij]quinolizin-11-one (C545T).

Al (100 nm)
LiF (1.5 nm)
NBB (15 nm)
Alq_3 (5nm)
Alq_3: 1 wt % C545T (25 nm)
NPB (45 nm)
CuPc:30% NBB (16 nm)
Au (20 nm)

Device A

Al (100 nm)
LiF (1.5 nm)
NBB (15 nm)
Compound 3 (5 nm)
Alq_3: wt % C545T (25 nm)
NPB (45 nm)
CuPc: 30 % NBB (16 nm)
Au (20 nm)

Device B

Figure 2-19: Device structures for A and B.

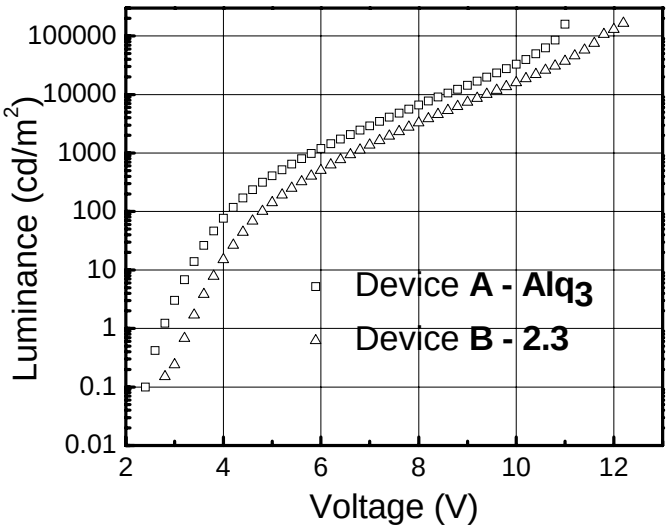

Figure 2-20: Luminance-Voltage diagrams for devices A and B.

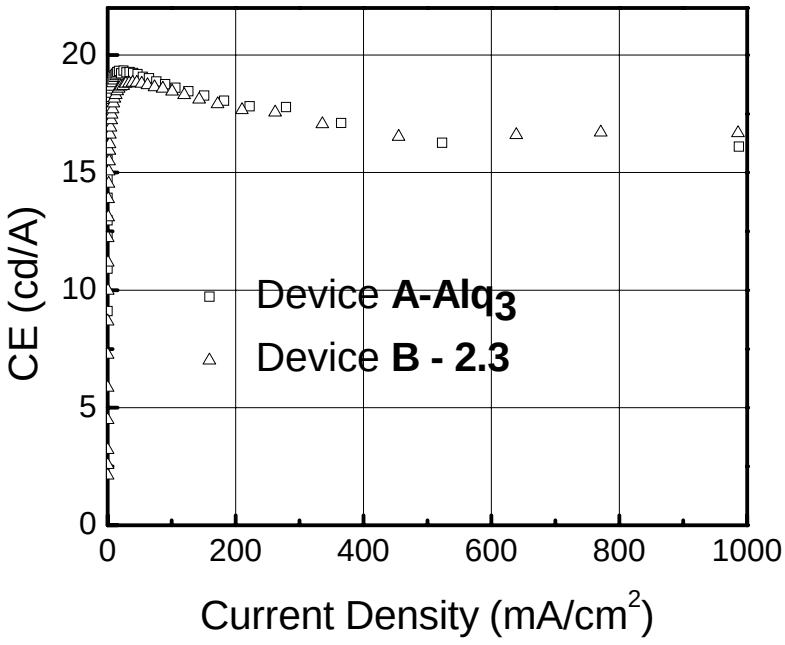

Figure 2-21: Current Efficiency – Luminance Diagram for Devices A and B.

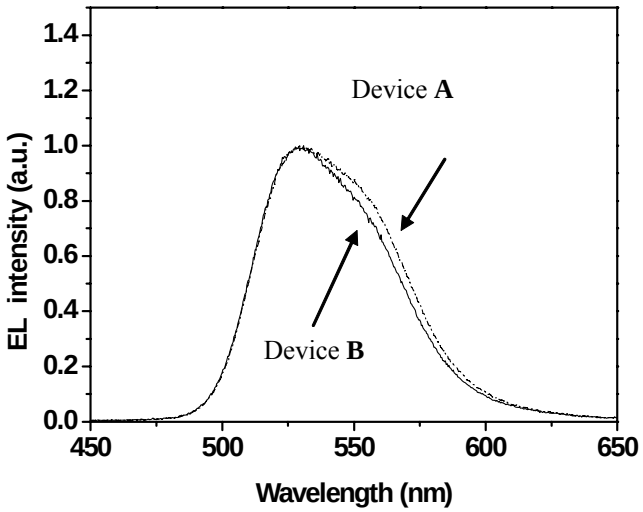

Figure 2-22: Electroluminescent Spectra for devices A and B.

2.3.6: Metal Ion Titrations

The effect of metal coordination on the luminescent properties of these compounds is also of interest Coordination complexes with the ligands were not successfully isolated, therefore metal titration experiments were performed to determine the effects. Silver nitrate and zinc trifluoroacetate were used as titrants. Silver(I) and zinc(II) are interesting because both metals display a variety of coordination modes in the presence of nitrogen donor ligands.[19] Furthermore, as discussed in chapter 1, compounds which are useful as zinc sensors are also important, since zinc(II) is a biologically relevant cation.[20]

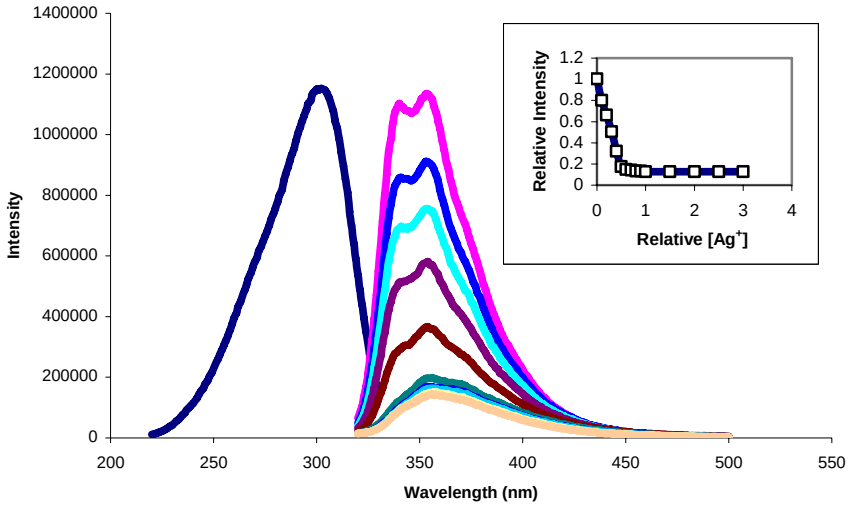

Figure 2-23: Fluorescent titration data for the titration of compound 2.1 (1.8 x 10^{-5} M) in CH_2Cl_2 with $AgNO_3$ (1.1 x 10^{-2} M) in acetonitrile. Inset: Stern-Volmer plot showing the change in relative fluorescent intensity at 354 nm with addition of $AgNO_3$. 0.1 Equivalents of $AgNO_3$ was added between each measurement until saturation was reached.

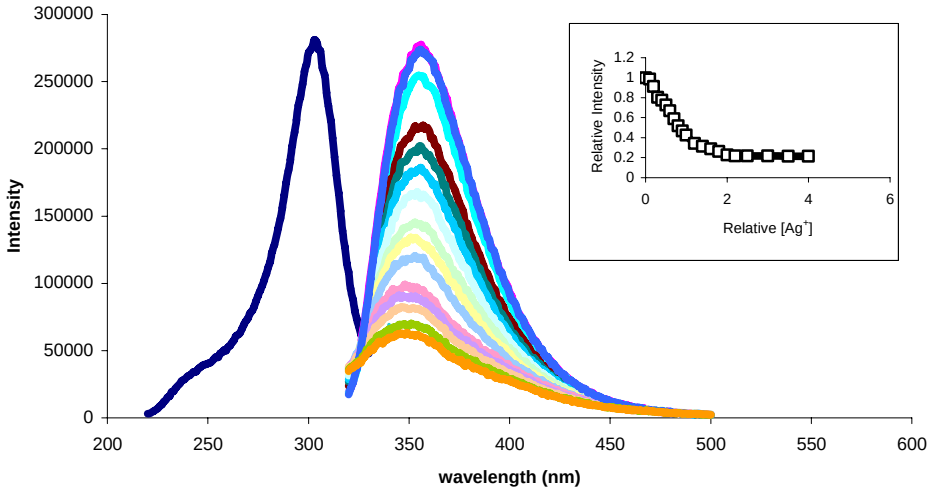

Figure 2-24: Fluorescent titration data for the titration of compound 2.5 (2.1 x 10^{-5} M) in CH_2Cl_2 with $AgNO_3$ (1.1 x 10^{-2} M) in acetonitrile. Inset: Stern-Volmer plot showing the change in relative relative fluorescent intensity at 356 nm with addition of $AgNO_3$. 0.1 Equivalents of $AgNO_3$ was added between each measurement until saturation was reached.

Both compounds 2.1 and 2.5 show a fluorescent quenching response to addition of $AgNO_3$, as illustrated in Figure 2-23 and Figure 2-24. Similar to its 7-azaindolyl analogue, 2.5 shows sensitivity to the addition of up to 2 full equivalents of $AgNO_3$, after which no further change is observed. The change in fluorescence in compound 2.1, however; is complete when 0.8 equivalents of $AgNO_3$ have been added. This discrepancy is a logical result of the difference in structures between the 2.1 and 2.5. Because 2.5 contains a greater number of individual luminophores, it makes sense that a larger number of silver ions should be required to achieve saturation and complete fluorescent quenching.

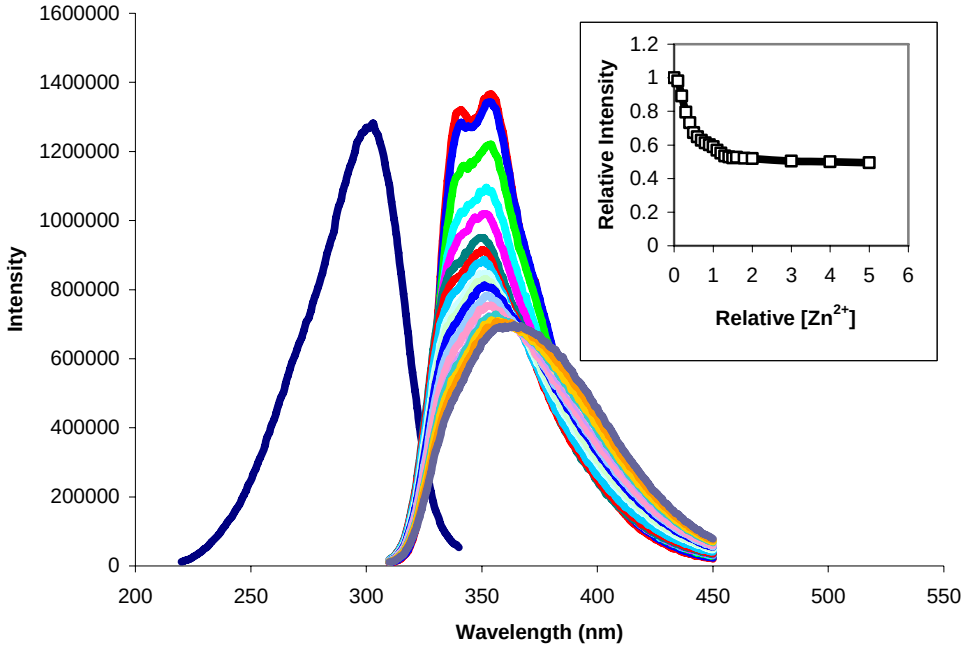

Figure 2-25: Fluorescent titration data for the titration of compound 2.1 (1.8×10^{-5} M) in CH_2Cl_2 with $Zn(CF_3COO)_2$ (1.1×10^{-2} M) in THF. Inset: Stern-Volmer plot showing the change in relative relative fluorescent intensity at 355 nm with addition of $Zn(CF_3COO)_2$. 0.1 Equivalents of $Zn(CF_3COO)_2$ was added between each measurement until saturation was reached. The excitation spectrum prior to titration is shown on the left.

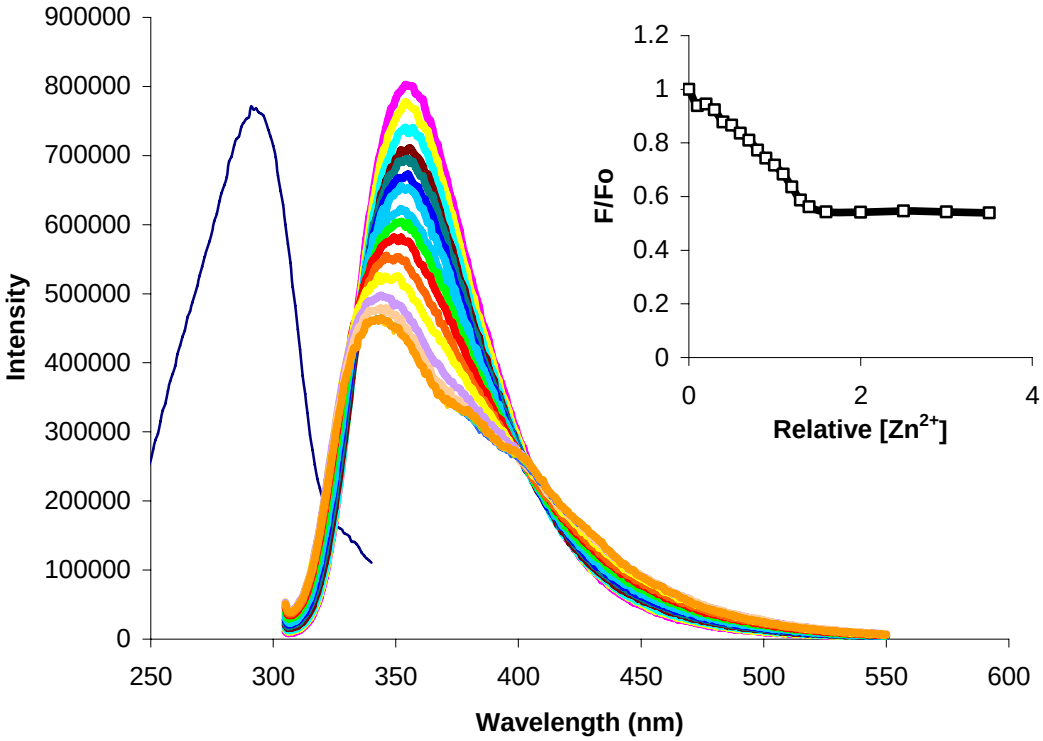

Figure 2-26: Fluorescent titration data for the titration of compound 2.5 (2.1×10^{-5} M) in CH_2Cl_2 with $Zn(CF_3COO)_2$ (1.1×10^{-2} M) in THF. Inset: Stern-Volmer plot showing the change in relative intensity at 354 nm with addition of $Zn(CF_3COO)_2$. 0.1 Equivalents of $Zn(CF_3COO)_2$ was added between each measurement until saturation was reached. The excitation spectrum prior to titration is shown on the left.

Compounds 2.1 and 2.5 were also titrated with $Zn(CF_3COO)_2$ to observe the response. Both compounds show a decrease in emission intensity, however; 2.1 shows a red shift in emission, while 2.5 shows a slight blue shift.

For compound 2.5, the Lewis acidity of the zinc center is the dominating factor. The zinc ion withdraws electrons from the ligand, widening the optical bandgap, and therefore causing a bathochromic shift in emission. Decreasing the electron density on a

luminophore has been previously reported to cause a blue shift in emission. The details of this work are briefly described in the previous chapter.[21]

The sensitivity of 2.1 and 2.5 to the presence of metal ions demonstrates their potential as ligands in coordination chemistry. Unfortunately, isolation of the related zinc(II) and silver(I) compounds has been unsuccessful.

2.4 Conclusions

In summary, five benzimidazolyl functionalized linear and star-shaped molecules have been successfully synthesized and characterized. These compounds all have high electron affinities and a large HOMO-LUMO gap. Furthermore, this group of compounds displays high thermal stability, making them excellent candidates as electron transport/hole blocking materials in OLEDs. The results of our preliminary investigation on the triazine derivative molecule 2.3 confirmed that it is indeed an excellent electron transport/hole blocking material with performance comparable to the well known Alq_3 molecule.

Furthermore, molecular orbital calculations have been performed on a series of related tri-substituted benzene compounds in order to observe the effect on the physical properties. The results of these calculations are consistent with the empirical data available. Furthermore, they also clearly indicate that the positioning of the nitrogen atom has an important effect on the overall energies. Moving the nitrogen from the 7-position to the 3- position has a stabilizing effect on both the HOMO and the LUMO, and appears to slightly increase the size of the optical bandgap.

Finally, titration experiments were performed on compounds 2.1 and 2.5 in order to gain some understanding of the effect of metal coordination. It is clear that the ligands

do coordinate to the metal centers in solution, resulting in a decrease in fluorescent intensity by the heavy atom effect.[22]

1 a) J. Shen, C. Lee, T. Huang, J. Lin, Y. Tao, C. Chien, C. Tsai. *J. Mater. Chem*. 2005, **15,** 2455. b) Y. Shirota, *J. Mater. Chem.* 2000, **10,** 1. c) K. Naito, A. Miura. *J. Phys. Chem.* 1993, **97,** 6240.

2 J. Pang, Y. Tao, S. Freiberg, X. Yang, M. D'Iorio, S. Wang. *J. Mater. Chem*. 2002, **12,** 206.

3 M. Thelakkat, H. Schmidt. *Adv. Mater.* 1998, **10,** 219.

4 a) Y. Shirota, H. Inada. *J. Mater. Chem*. 1993, **4**, 319. b) Y. Shirota in *Organic electroluminescence*. Chapter 4, Z. H. Kafafi ed., Taylor & Francis Group, Boca Raton, FL, **2005**.

5 a) W.-L. Jia, T. McCormick, Y. Tao, J. P. Lu, S. Wang. *Inorg. Chem.* 2005, **44,** 5706. b) T. McCormick, W. L. Jia, S. Wang. *Inorg. Chem*. 2006, **45,** 147. c) S. W. Lai, M. C. W. Chan, S. M. Peng, C. M. Che. *Angew. Chem. Int. Engl.* 1999, **38,** 669. d)L. De La Durantaye, T. McCormick, W.-L. Jia, S. Wang. *Dalton Trans*. 2006, 5675.

6 Q. Liu, W.-L. Jia, S. Wang. *Inorg. Chem*. 2005, **44,** 1332.

7 I. Wu, J. Lin, Y. Tao, E. Balasubramaniam. *Adv. Mater.* 2000, **12,** 668.

8 W.-L. Jia, R. Wang, D. Song, S. Ball, A. McLean, S. Wang. *Chem. Eur. J.* 2005, **11**, 832.

9 a) A. Kulkarni, C. Tonzola, A. Babel, S. Jenekhe. *Chem. Mater*. 2004, **16,** 4556. b) J. Shi, C. Tang, C. Chen. U.S. Patent 5646948, **1997**. c) H. Shih, C. Line, H. Shih, C. Chen, *Adv. Mater*. 2002, **14,** 1409. d) Z. Gao, C. Lee, I. Bello, S. Lee, R. Chen, J. Shi, C. Tang, *Appl. Phys. Lett.* 1999, **74,** 865.

10 a) W. –H. Huang, W. -L. Jia, S. Wang. *Can. J. Chem.* **2006**, 84, 477. b) Q. Wu, J. A. Lavigne, Y. Tao, M. D'Iorio, S. Wang. *Chem. Mater*. **2001**, 13, 71.

11 *SHELXTL NT Crystal Structure Analysis Package*, Version 6.14; Bruker Axs, Analytical X-ray System, Madison, WI, 2000.

12 D. Song, Q. Wu, A. Hook, I. Kozin, S. Wang. *Organometallics.* 2001, **20**, 4683.

12 J. Elguero, F.H. Cano, L. Infantes, P. Cornago, M. D. Santa Maria, P. Cabildo, R.M. Claramunt, V. Milata. *Heterocycles.* 2001, **55,** 905.

14 A. P. Kulkarni, C. J. Tonzola, A. Babel, S. A. Jenekhe. *Chem. Mater.* 2004, **16,** 4556.

15 Q.D. Liu, M. S. Mudadu, R. Thummel, Y. Tao, S. Wang. *Adv. Funct. Mater.* 2005, **15,** 143.

16 T. Anthopoulos, J. Markham, E. Namdas, I. Samuel, S. Lo, P. Burn. *Appl. Phys. Lett.* ***2003***, 82, 4824.

17 a) W.-L. Jia, X. Feng, D. Bai, Z. Lu, S. Wang, G. Vamvounis. *Chem. Mater.* 2005, **17,** 164. b) C. Tang, S. Van Slyke. *Appl. Phys. Lett.* 1987, **51**, 913. c) C. Tang, S. Van Slyke, C. Chen. *J. Appl. Phys.* 1989, **65,** 3611.

18 Y. Y. Yuan, S. Han, D. Grozea, Z. H. Lu. *Appl. Phys. Lett.* 2006, **88**, 093503.

19 a) C. Seward, J. Chan, D. Song, S. Wang. *Inorg. Chem.* 2003, **42,** 1112. b) Y. Kang, C. Seward, D. Dong, S. Wang. *Inorg. Chem.* 2003, **42,** 2789.

20 L. De La Durantaye, T. McCormick, X.–Y. Liu, S. Wang. *Dalton Trans.* 2006, 5676.

21 Q. Liu, M. S. Mudadu, H. Schmider, R. Thummel, Y. Tao, S. Wang. *Organometallics.* 2002, **21**, 4743.

22 C. Seward, W.-L. Jia, R.–Y Wang, G. D. Enright, S. Wang. *Angew. Chem. Int. Ed.* 2004, **43,** 2933.

Chapter 3:

Exploration of the Properties of Benzimidazole Based, Hetero-Substituted Molecular Stars

3.1 Introduction

In light of the facile synthesis and utility of 2,4,6-trisbenzimidazolyl-1,3,5-triazine (2.3), other triazine molecules employing 2,2'-dipyridylamino (DPA), 2-(2'-pyridyl)benzimidazolyl (PBM) and benzimidazolyl functional groups were designed.

DPA is interesting because it is a known blue emitter[1] and can function as a *N,N'*-chelate ligand.[2,3,4] Previously reported molecular stars employing the DPA derivative displayed moderate to bright blue emission, with quantum yields varying between 16 % and 78 %.[1] Furthermore, the coordination chemistry of this functional group has been explored with a variety of transition metals, including zinc(II)[2] and silver(I)[3] metal ions. Work with these complexes has demonstrated a variety of interesting coordination motifs, and has shown that DPA derivatives can potentially function as fluorescent sensors for both metal ions.[4,5] A zinc complex of 1,3,5-tris(*p*-(2,2'-dipyridylamino)phenyl)benzene has also been demonstrated as an effective sensor for benzene.[2c]

2-(2'-Pyridyl)benzimidazolyl (PBM) derivatives, similar to DPA derivatives, are also interesting as blue emitters, and have also been applied as *N,N'-chelate* ligands. For example, coordination of PBM derivatives to copper(I) has resulted in a series of complexes with interesting phosphorescent and photophysical properties analogous to those of similar previously reported 9,10-phenanthroline complexes.[6,7] The PBM

complexes with copper(I) have also been applied as triplet emitters in orange emitting devices.[7,8]

In addition to copper(I), PBM derivative complexes with platinum(II)[9] and ruthenium(II)[10] have also been characterized as potential triplet emitters. In particular, ruthenium(II) complexes with known PBM derivatives have been applied in electroluminescent devices.[10] Finally the potential utility of PBM derivatives as sensors for the biologically relevant zinc(II) cation has also been previously demonstrated.[11] Some of the details of these investigations have been presented in chapter 1.

Because of the diverse and interesting chemistry of DPA, PBM and benzimidazolyl derivative compounds, two new compounds combining these functional groups were synthesized and characterized. These complexes were then intended to be further used to coordinate different metal ions, and produce novel hetero-bimetallic compounds. Toward this goal, a copper(I) complex with one of these ligands has been isolated, and its photophysical properties have been investigated. A detailed discussion of these results is to follow.

3.2 Experimental

3.2.1 General syntheses, characterizations and physical measurements.

The general procedures for synthesis, characterization and measurement of physical properties are the same as reported previously in chapter 2, with the following exceptions. The low temperature ^{1}H, ^{13}C and ^{31}P NMR were recorded on a Bruker Avance 500 spectrometer. Emission lifetimes were measured on a Photon Technologies International Phosphorescent lifetime spectrometer, Time Master C631F equipped with a Xenon flash lamp and digital emission photo multiplier tube using a band pathway of 5

nm for excitation and 2 nm for emission. UV-Vis absorption titrations were performed using a procedure analogous to the fluorescent titrations described in chapter 2, with absorption spectra being recorded instead of emission spectra.

Synthesis of 2,4-dichloro-6-dipyridylamino-1,3,5-triazine (3.1): A flask was charged with 2,4,6-trichloro-1,3,5-triazine (0.750 g, 4.1 mmol) and 2,2'-dipyridylamine (0.660 g, 4.0 mmol) in 60 mL of toluene. The resulting suspension was stirred for 30 minutes before addition of sodium hydroxide (0.155 g, 3.9 mmol), and then refluxed in toluene for 24 hours. The resulting mixture was poured into water, extracted with methylene chloride (3x 60 mL) and dried over magnesium sulfate. The solvent was evaporated, and the product isolated by column chromatography using THF:hexane (1:1) as the mobile phase. A colorless powder of 3.1 was obtained (670 mg, yield 53%). ^{1}H NMR (300 MHz, CD_2Cl_2, 298 K, ppm) δ: 8.50 (dd, 2H, J_1 = 1.2 Hz, J_2 = 4.8 Hz), 7.90 (ddd, 2H, J_1 =1.2 Hz , J_2 =1.2 Hz, J_3 =8.1 Hz), 7.55 (d, 2H, J = 8.1 Hz), 7.34 (ddd, 2H, J_1 = 1.2 Hz, J_2 = 4.8 Hz, J_3 =7.5 Hz).

Synthesis of 2,4-bisbenzimidazolyl-6-(2,2'-dipyridylamino)-1,3,5-triazine (3.2): Intermediate 3.1 (300 mg, 0.93 mmol) was dissolved in 35 mL of toluene. A suspension of benzimidazole (277 mg, 2.35 mmol) in 30 mL toluene was slowly added to this solution. The mixture was stirred for 30 minutes before addition of sodium hydroxide (93 mg, 2.35 mmol), and then refluxed for 24 hours. The resulting mixture was poured into water, extracted with methylene chloride (3 x 40 mL) and dried over magnesium sulfate. The solvent was evaporated, and the product isolated by column chromatography using THF:hexane (1:1) as the mobile phase. A colorless powder of 3.2 is obtained (230 mg, yield 52%). The product was further purified by recrystallization from ethyl acetate.

^{1}H NMR (400 MHz, CD_2Cl_2, 298 K, ppm) δ: 9.00 (s, 2H), 8.62 (d, 2H, J = 3.6 Hz), 8.00 (td, 2H, J_1 = 2 Hz, J_2 = 8 Hz), 7.87, (d, 2H, J = 7.2 Hz), 7.80 (t, 4H, J = 7.2 Hz), 7.45 (dd, 2H, J_1 = 4.8 Hz , J_2 = 7.2 Hz), 7.38 (t, 2H, J = 7.2 Hz), 7.26 (t, 2H, J = 8 Hz). ^{13}C NMR (100 MHz, CD_2Cl_2, 298 K, ppm) δ:149.9, 142.0, 138.7, 125.2, 124.8, 123.5, 123.1, 120.9, 116.2. *Anal Calc for* $C_{27}H_{18}N_{10}$: C, 67.21.90, H, 3.76, N, 29.03 *Found* C, 66.96, H 3.76, N, 28.83.

Synthesis of 2-(2,2'-dipyridylamino)-4,6-(2-(2'-pyridyl)benzimidazolyl)-1,3,5-triazine (3.3): Intermediate 3.1 (250 mg, 0.78 mmol) was dissolved in 35 mL of toluene. To it was added a suspension of 2-(2'-pyridyl)benzimidazole (380 mg, 1.95 mmol) in 30 mL toluene. The mixture was stirred for 30 minutes before addition of sodium hydroxide (80 mg, 1.95 mmol), and then refluxed for 24 hours. At the end of the reflux, the reaction solution turned pink. The pink solution was poured into water, extracted with methylene chloride (3x 35 mL) and dried over magnesium sulfate. The solvent was evaporated, and the product isolated by column chromatography using THF:hexane (3:1) as the mobile phase. A colorless powder of 3.2 was obtained (230 mg, yield 52%). The product was further purified by recrystallization from ethyl acetate. ^{1}H NMR (CD_2Cl_2, δ, ppm, 298 K): 8.52 (d, 2H, J = 5.0 Hz), 8.43 (dd, 2H, J_1 = 1.5 Hz, J_2 = 5.0 Hz), 7.93 (d, 2H, J = 8.0 Hz), 7.80 (d, 2H, J = 8 Hz), 7.79 (td, 2H, J_1 = 1.5 Hz, J_2 = 8.0 Hz), 7.65 (td, 2H, J_1 = 1.5 Hz, J_2 = 8 Hz), 7.56 (d, 2H, J = 8.5 Hz), 7.38 (td, 2H, J_1 = 1Hz, J_2 = 8Hz) 7.277-7.255 (m, 8H). ^{13}C NMR (100 MHz, CD_2Cl_2, 298 K, ppm) δ:164.7, 164.5, 154.2, 152.5, 150.8, 149.3, 149.3, 143.4, 138.3, 137.0, 135.0, 125.2, 124.5, 124.3, 124.2, 122.9, 122.6, 120.6, 114.33. HRMS. *calcd* for M-H ($C_{37}H_{24}N_{12}H^{+}$): 637.2335 *found*:637.2342

Synthesis of Cu(3.3)(PPh_3)$_2$$BF_4$ (3.4): Compound 3.3 (60 mg, 0.09 mmol) was dissolved in 5 mL of CH_2Cl_2. In a separate vial, $[Cu(CH_3CN)_2(PPh_3)_2]BF_4$ (0.142 g, 0.19 mmol) was dissolved in 5 mL of CH_2Cl_2. The contents were mixed and the resulting yellow solution was stirred for 30 minutes. 2 mL of toluene was then layered on top, and allowed to diffuse slowly into the solution. The solvent was then allowed to slowly evaporate, producing yellow crystals of 3.4 (0.148 g, 79 % yield). ^{1}H NMR (500 MHz, CD_2Cl_2, 253 K, ppm) δ: 8.53 (d, 2H, J = 8.0 Hz), 8.19 (d, 2H, J = 4.0 Hz), 7.97 (t, 2H, J = 7.5 Hz), 7.88 (d, 2H, J = 5.0 Hz), 7.72 (d, 2H, J = 8.5 Hz), 7.50 (d, 2H, J = 8.0 Hz), 7.37 (t, 12H, J = 7.5 Hz), 7.32 (d, 2H, J = 8 Hz), 7.257-7.29 (m, 30 H), 7.13-7.10 (m, 24H), 6.95 (t, 2H, J = 8.0 Hz), 6.71 (t, 2H, J = 5.0 Hz). ^{13}C NMR (500 MHz, CD_2Cl_2, 253, ppm) δ: 133.5, 133.4, 133.4, 132.4, 130.7, 129.3. ^{31}P{^{1}H} (500 MHz, CD_2Cl_2, 253 K, ppm) δ: 3.01. *Anal Calc* for $C_{109}H_{84}B_2Cu_2F_8N_{12}P_4$: C, 65.90, H, 4.26, N, 8.46 *Found* C, 65.35, H 4.53, N, 8.46.

3.3 Results and Discussion

3.3.1 Synthesis and characterization.

Two new hetero-substituted molecular stars have been synthesized using procedures similar to the one used to prepare compound 2.3 in chapter 2. Intermediate 3.1 was first isolated from the reaction of 2,4,6-trichloro-1,3,5-triazine and 2,2'-dipyridylamine. This intermediate was then used in subsequent steps with either benzimidazole or 2-(2'-pyridyl)benzimidazole to prepare 3.2 or 3.3 respectively, as illustrated in Figure 3-1.

Compounds 3.2 and 3.3 are substantially more soluble than the related compound 2.3, reported in chapter 2. Furthermore, compound 3.3 has 3 separate *N*,*N*'-chelate sites.

Therefore, coordination of both 3.2 and 3.3 to zinc(II), platinum(II), palladium(II) and copper(I) was attempted. Despite this, only compound 3.4, which is isolated from the reaction of 3.3 with two equivalents of $[Cu(CH_3CN)_2(PPh_3)_2]BF_4$, was successfully isolated and characterized.

Compounds 3.1 to 3.4 were isolated in moderate to good yields and characterized using ^1H NMR. The final products, 3.2, 3.3 and 3.4, were further characterized by ^{13}C NMR, and either elemental analysis or high resolution mass spectrometry. Compound 3.4, containing two triphenylphosphine groups, was also characterized by $^{31}P\{^1H\}$ NMR.

At room temperature, the solution state structure of 3.4 appears to be fluxional, resulting in significant broadening of signals in the ^1H NMR spectrum. Because of this, NMR experiments for 3.4 have been performed at 253 K, at which temperature the structure appears to stabilize. The variable temperature NMR data are presented and discussed in detail below.

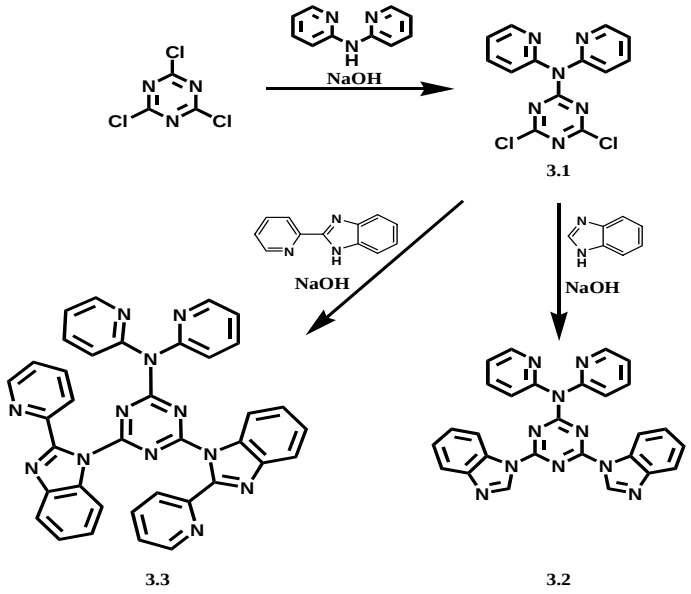

Figure 3-1: Procedure for ligand synthesis. All reactions were performed in toluene under reflux for 24 hours. Full synthetic details are available in the experimental section.

Single crystals suitable for X-ray crystallography were obtained for 3.3 and for its copper complex 3.4. Their structures were determined using X-ray diffraction methods. 3.3 crystallized in the monoclinic $P2_1$ space group (Figure 3-2) in the presence of a single well ordered water molecule. The water molecule is involved in hydrogen bonding interactions with nearby PBM functional groups, with the shortest hydrogen bond distance being ~2.00 Å. Furthermore, there is evidence of extensive π–π interactions between the molecules with the shortest atomic contact distance being 3.4 Å. These π–π interactions cause the molecule to stack along the *a* axis, as depicted in Figure 3-3.

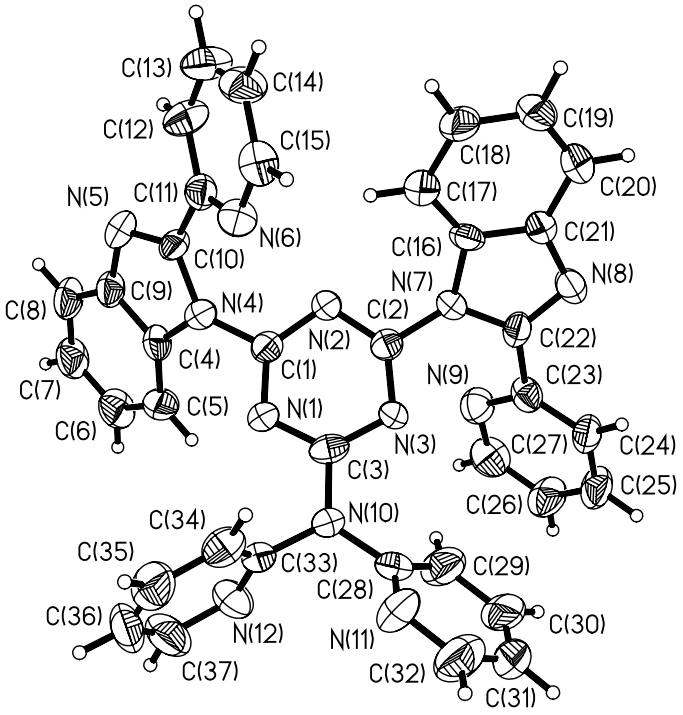

Figure 3-2: Crystal structure for 3.3 crystallized in the $P2_1$ space group with labeling scheme.

Table 3-1: Crystal Data and structure refinement for 3.3

Identification code	3.3	
Empirical formula	C37 H26 N12 O	
Formula weight	654.70	
Temperature	298(2) K	
Wavelength	0.71073 Å	
Crystal system	Monoclinic	
Space group	P2(1)	
Unit cell dimensions	a = 6.0077(6) Å	α= 90°.
	b = 22.128(3) Å	β= 95.062(2)°.
	c = 11.7628(14) Å	γ = 90°.
Volume	1557.7(3) $Å^3$	
Z	2	
Density (calculated)	1.396 Mg/m^3	
Absorption coefficient	0.091 mm^{-1}	
F(000)	680	
Crystal size	0.2 x 0.2 x 0.1 mm^3	
Theta range for data collection	1.74 to 28.42°.	
Index ranges	-7<=h<=8, -29<=k<=27, -15<=l<=15	
Reflections collected	11538	
Independent reflections	6829 [R(int) = 0.0512]	
Completeness to theta = 28.42°	96.2 %	
Absorption correction	Empirical	
Max. and min. transmission	1.000 and 0.710	
Refinement method	Full-matrix least-squares on F^2	
Data / restraints / parameters	6829 / 1 / 458	
Goodness-of-fit on F^2	0.731	
Final R indices [I>2sigma(I)]	R1 = 0.0419, wR2 = 0.0481	
R indices (all data)	R1 = 0.1505, wR2 = 0.0610	
Absolute structure parameter	-0.4(18)	
Largest diff. peak and hole	0.208 and -0.177 $e.Å^{-3}$	

Table 3-2: Crystal Data and structure refinement for 3.4

Identification code	3.4	
Empirical formula	C123 H102 B2 Cu2 F8 N12 P4	
Formula weight	2172.75	
Temperature	298(2) K	
Wavelength	0.71073 Å	
Crystal system	Triclinic	
Space group	P-1	
Unit cell dimensions	a = 13.170(3) Å	α= 112.60(3)°.
	b = 22.233(4) Å	β= 94.55(3)°.
	c = 22.710(5) Å	γ = 107.15(3)°.
Volume	5724(2) $Å^3$	
Z	2	
Density (calculated)	1.261 Mg/m^3	
Absorption coefficient	0.494 mm^{-1}	
F(000)	2248	
Crystal size	0.30 x 0.20 x 0.10 mm^3	
Theta range for data collection	1.92 to 20.48°.	
Index ranges	-10<=h<=10, -21<=k<=21, -22<=l<=22	
Reflections collected	31818	
Independent reflections	10545 [R(int) = 0.0708]	
Completeness to theta = 20.48°	92.2 %	
Absorption correction	Semi-empirical from equivalents	
Max. and min. transmission	0.9523 and 0.8660	
Refinement method	Full-matrix least-squares on F^2	
Data / restraints / parameters	10545 / 0 / 1261	
Goodness-of-fit on F^2	0.990	
Final R indices [I>2sigma(I)]	R1 = 0.0601, wR2 = 0.1456	
R indices (all data)	R1 = 0.1093, wR2 = 0.1656	
Largest diff. peak and hole	0.390 and -0.333 $e.Å^{-3}$	

Table 3-3: Selected Bond lengths [Å] for 3.3.

N(4)-C(1)	1.406(4)	N(10)-C(33)	1.432(4)
N(7)-C(22)	1.380(4)	C(22)-C(23)	1.485(4)
N(10)-C(3)	1.361(4)	C(10)-C(11)	1.462(5)
N(10)-C(28)	1.428(4)		

Table 3-4: Selected Bond lengths [Å] and angles [°] for 3.4.

Cu(1)-N(5)	2.087(6)	Cu(2)-P(4)	2.247(2)
Cu(1)-N(6)	2.109(5)	Cu(2)-P(3)	2.280(3)
Cu(1)-P(1)	2.244(2)	N(5)-Cu(1)-N(6)	79.7(3)
Cu(1)-P(2)	2.262(3)	P(1)-Cu(1)-P(2)	120.54(8)
Cu(2)-N(11)	2.112(5)	N(11)-Cu(2)-N(12)	79.3(3)
Cu(2)-N(12)	2.124(6)	P(4)-Cu(2)-P(3)	119.99(9)

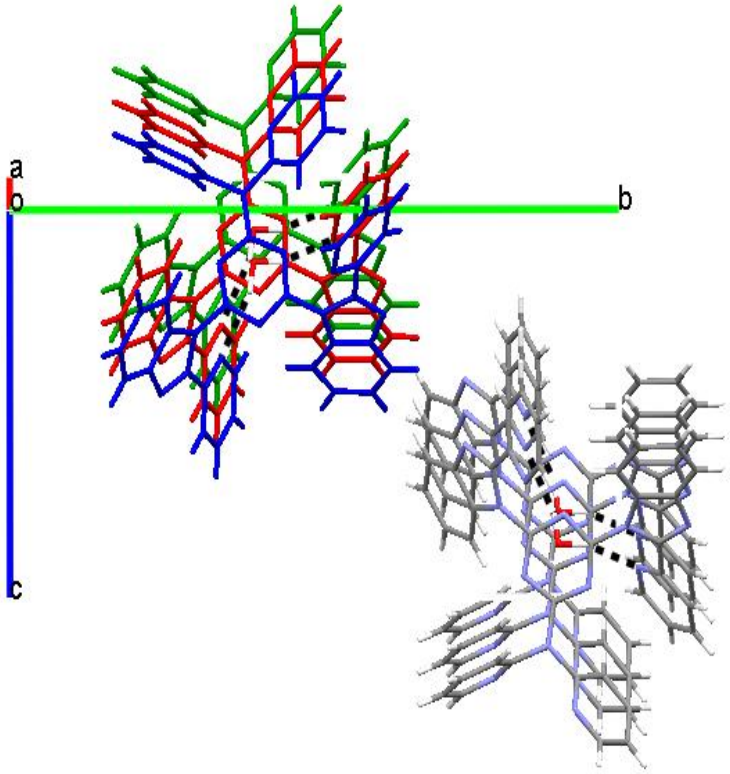

Figure 3-3: Packing diagram for 3.3 projected down the *a* axis.

3.4 crystallizes in the triclinic $P\bar{1}$ space group (Figure 3-4), and cocrystallizes with a single molecule of toluene. The BF_4^- anions are disordered but have been successfully refined. Furthermore, there is an edge to face π–π interaction between the pyridyl groups on the DPA moiety and nearby phenyl groups from the triphenylphosphine. The shortest atomic contact is 3.9 Å. It is also interesting to note that the copper ion binds preferentially to the 2-(2'-pyridyl)benzimidazolyl site as opposed to the open dipyridylamino site.

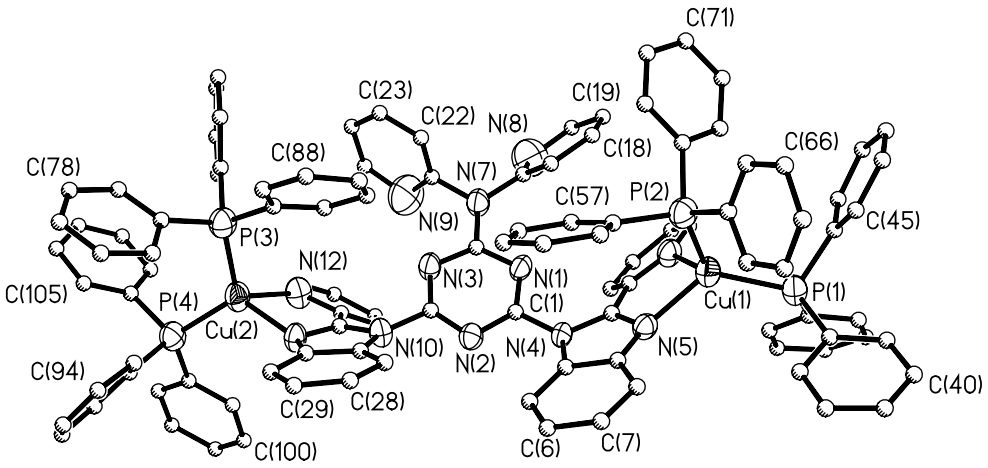

Figure 3-4: Crystal structure for 3.4 crystallized in the P-1 space group with partial labeling scheme. Hydrogen atoms, BF_4 anions and co-crystallized toluene have been removed for clarity.

3.3.2 Photophysical Properties

As demonstrated in Figure 3-5, compounds 3.2 and 3.3 absorb primarily in the 200 – 350 nm range of the UV-Vis spectrum with similar features. Based on the magnitude of the extinction coefficients, these absorptions can be assigned as $\pi \rightarrow \pi^*$ transitions.

Compound 3.4 also absorbs in the 200 nm to 350 nm region of the spectrum, and has an additional absorption band centered at approximately 405 nm. This is consistent with a MLCT absorption band which has been frequently observed for compounds of this type, and is responsible for the yellow color of the complex.[6,7,8]

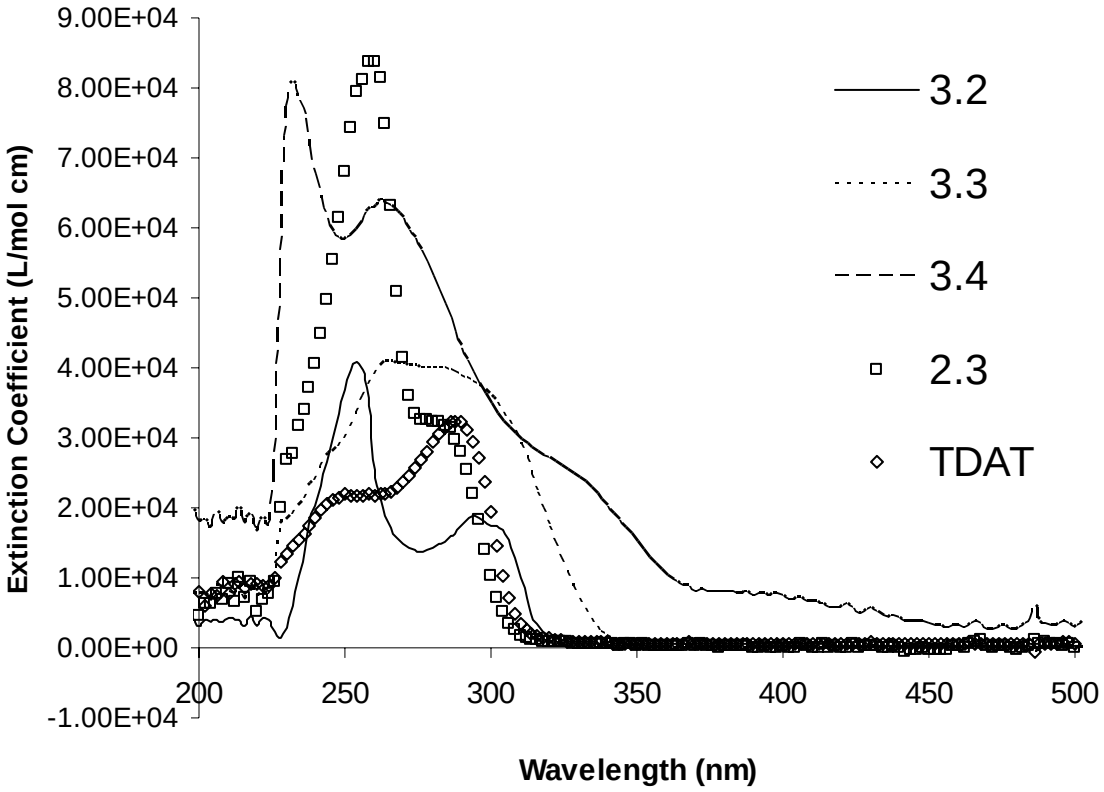

Figure 3-5: UV-Vis absorption data for 2.3, 3.2-3.4 and TDAT. All data were collected in CH_2Cl_2 at a concentration of ~ 10^{-6} M.

The absorption spectrum for compound 3.3 is slightly red shifted compared to 3.2. Furthermore, compared to the previously reported compound 2,4,6-tris(2,2'-dipyridylamino)-1,3,5-triazine (TDAT) and to compound 2.3, the absorption spectra for 3.2 and 3.3 are both slightly red shifted.[12] Apparently the hetero-substituted molecular

stars have optical bandgaps which are smaller than those previously observed in the homo-substituted stars.

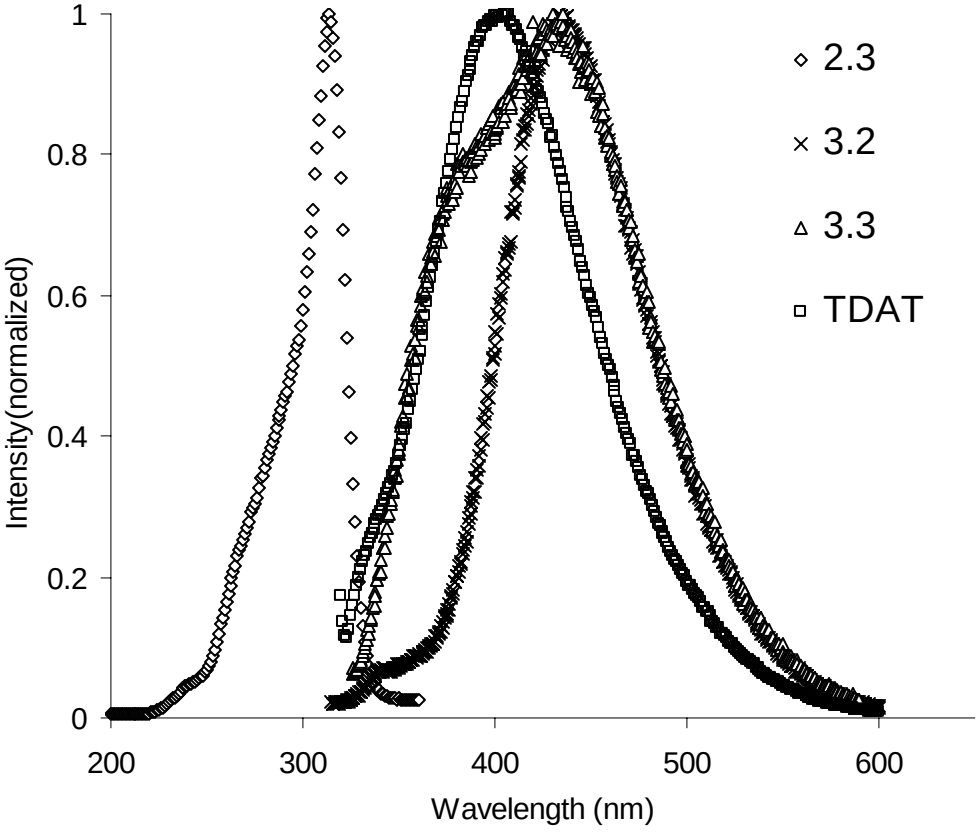

Figure 3-6: Emission spectra for compounds 2.3, 3.2, 3.3 and TDAT in CH_2Cl_2 at a concentration of 10^{-5} M.

The emission spectra for compounds 2.3, 3.2, 3.3 and TDAT are illustrated in Figure 3-6. TDAT has an emission maximum at 405 nm and compound 2.3 has an emission maximum at 384 nm. Comparatively, 3.2 and 3.3 have emission maxima at 431 nm and 433 nm, respectively, demonstrating a remarkable and unexpected red shift in emission compared to the related compounds.

The relative broadness and the appearance of an additional shoulder at 385 nm in the emission spectrum of 3.3 suggests the possibility of a secondary charge transfer based

emission . To test this hypothesis, solvatochromic experiments were performed on the emission and absorption spectra for 3.2 and 3.3. The absorption spectra of 3.2 and 3.3 are both insensitive to solvent polarity (Figure 3-7 and Figure 3-8 respectively), while the emission spectra show a red shift in λ_{max} as the solvent polarity increases (Figure 3-9 and Figure 3-10 respectively). This is consistent with an excited state which is more polarized than the ground state.[2a]

Careful examination of Figure 3-9 reveals that for 3.2 the emission maximum shifts from 433 nm in CH_2Cl_2 to 452 nm in acetonitrile. For compound 3.3, the maximum shift is from 431 nm in CH_2Cl_2 to 454 nm in acetonitrile. It is interesting that the spectrum for 3.3 in DMF clearly reveals a marked increase in the intensity of the shoulder peak at 365 nm, suggesting that this solvent favors an alternate emission pathway.

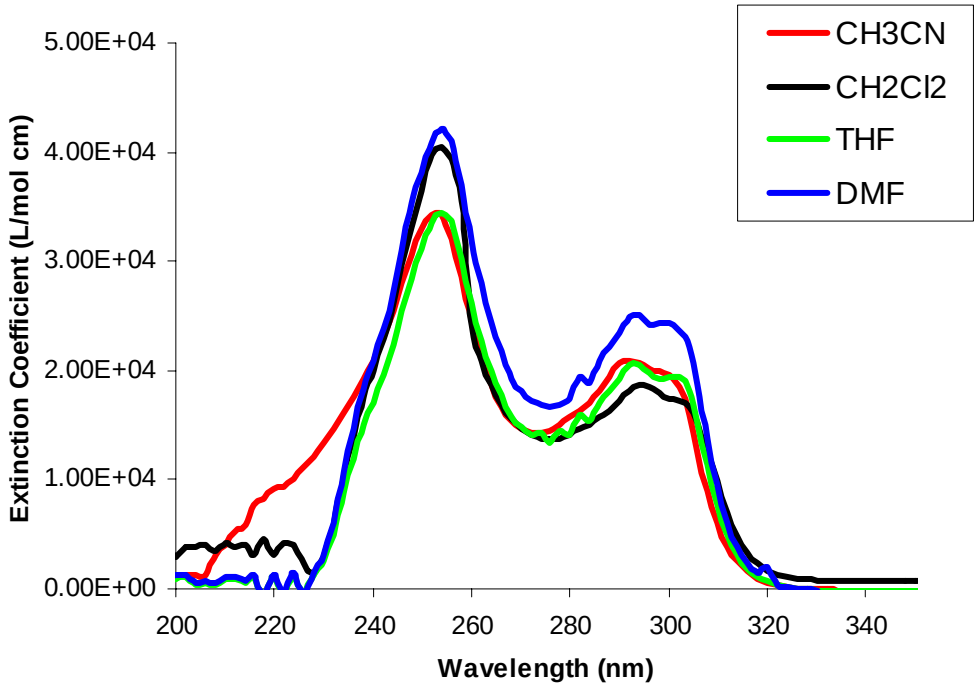

Figure 3-7: Solvatochromic absorption data for compound 3.2. All spectra were recorded at a concentration of 10^{-6} M.

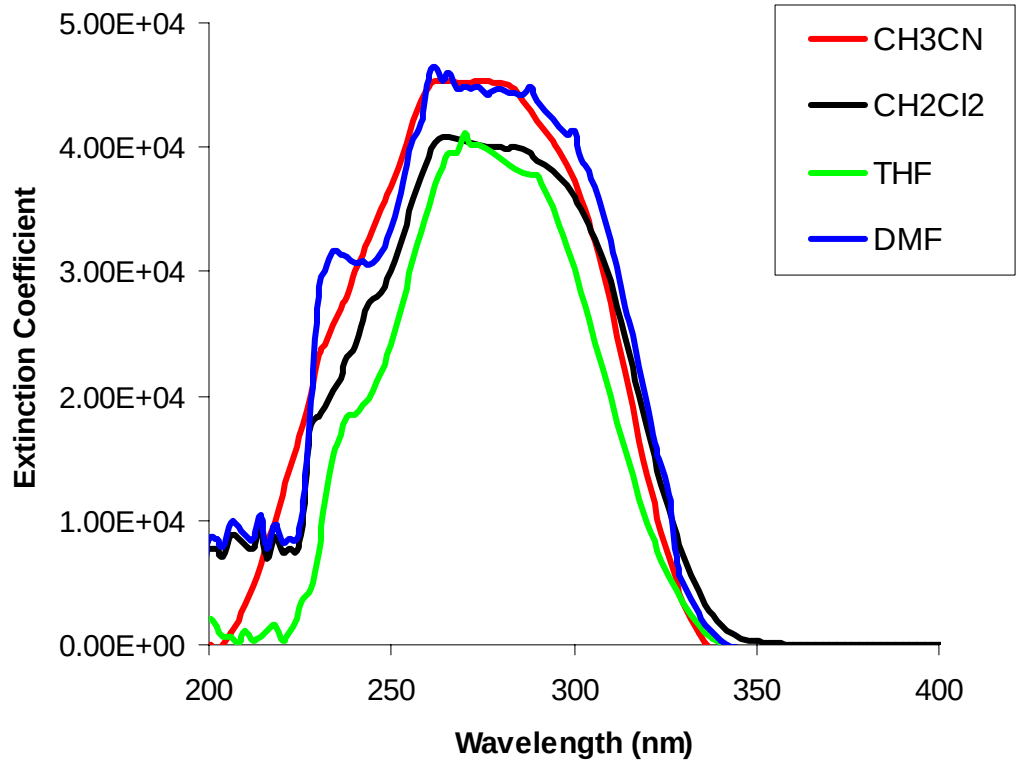

Figure 3-8: Solvatochromic absorption data for compound 3.3. All spectra were recorded at a concentration of 10^{-6} M.

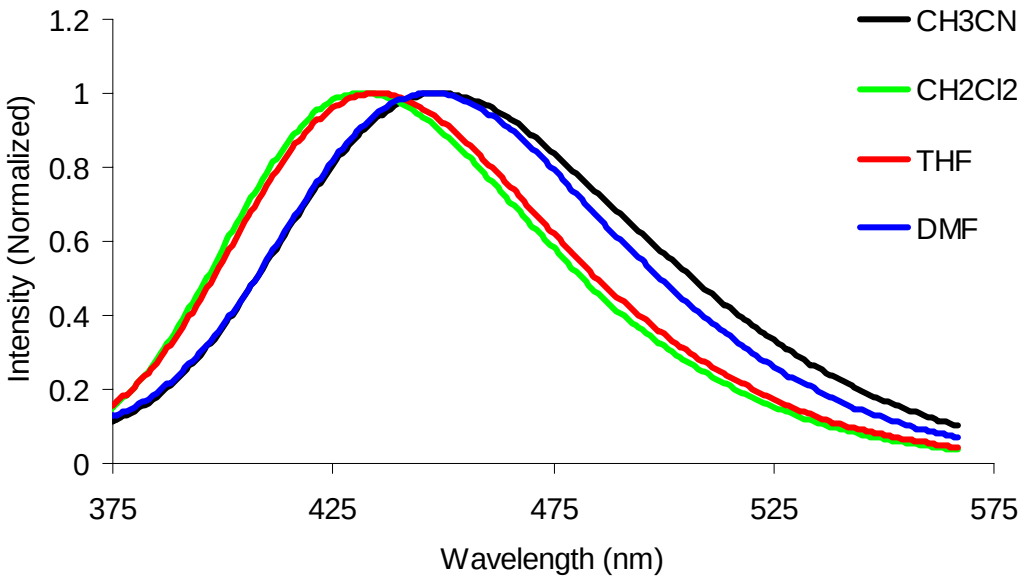

Figure 3-9: Solvatochromic emission spectrum for compound 3.2. All spectra were recorded at a concentration of 10^{-5} M.

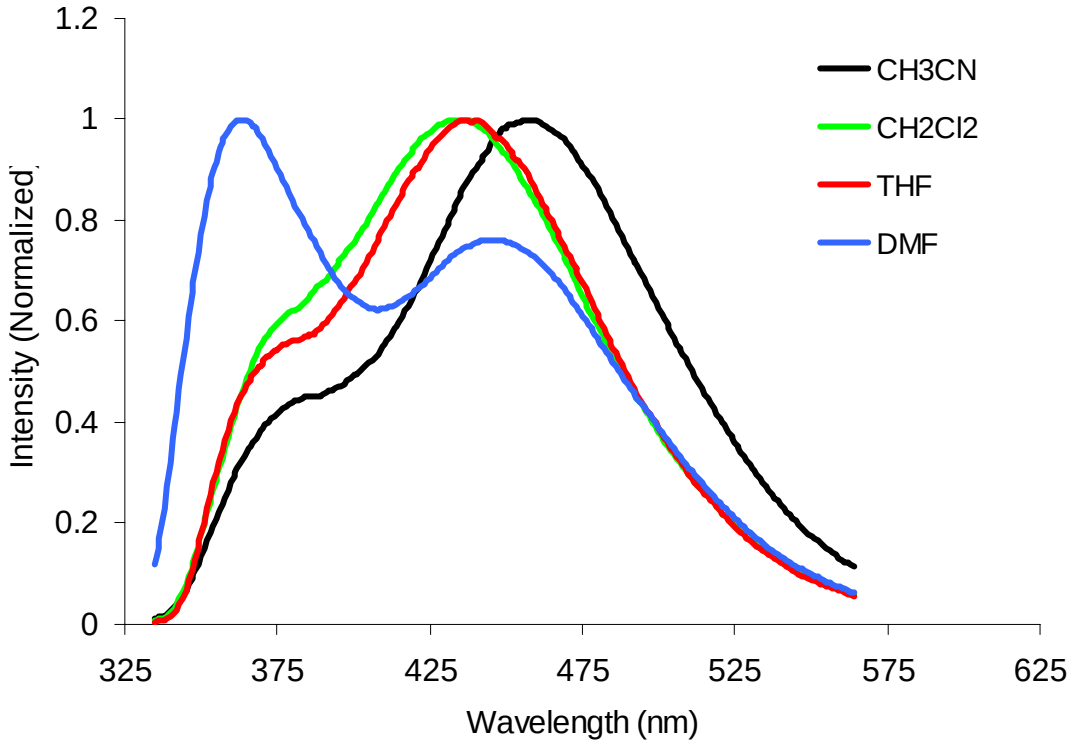

Figure 3-10: Solvatochromic emission spectrum for compound 3.3. All spectra were recorded at a concentration of 10^{-5} M.

The phosphorescent emission for compounds 3.3 and 3.4 was also studied. The phosphorescent spectra are displayed in Figure 3-11. The room temperature spectra for 3.4 in a thin film and as a thin film doped into PMMA are essentially identical with emission maxima at approximately 558 nm, while the emission for 3.4 at 77 K in methylene chloride and as a thin film is red shifted, with an emission maximum at approximately 568 nm. Similar bathochromic shifts have been previously reported at low temperature in related systems. The substantial lowering of the temperature apparently results in a reduced population of the vibrational energy levels in the excited state, resulting in an overall reduction of the emission energy.

The phosphorescent decay lifetimes for 3.4 were examined at room temperature as a pure thin film, and as a film doped in PMMA and at 77 K as a pure thin film and in methylene chloride at 77 K. The data are summarized in Table 3-5.

The decay lifetimes for 3.3 in methylene chloride at 77 K and for 3.4 as a pure film at room temperature and at 77 K were approximated by a simple one component decay. When 3.4 is doped in PMMA at room temperature, or in frozen methylene chloride, a second component is required to obtain a good fit to the experimental data. Furthermore, it is interesting that in PMMA at room temperature, the second, shorter component only appears to play a small role in the decay, as demonstrated by the relatively small weight contribution (2.8%). In methylene chloride at 77 K, however; the weight of the second component is considerably more substantial (43%). This differs from previously reported PBM derivative complexes, in which the second component is reported to have a small contribution.

When the emission spectrum for 3.3 is taken after a delay of 120 μs, a weak green phosphorescent emission is observed, with an emission maximum at 511 nm. The copper complex, 3.4, shows a more intense orange phosphorescence with an emission maximum at 568 nm. This demonstrates that the ligand based phosphorescence is distinctly different from that of the complex, suggesting that the phosphorescent emission in 3.4 originates from the ^{3}MLCT excited state.

Table 3-5: Phosphorescent data for 3.3 and 3.4.

	λ_{max} (nm)	τ (μs)
3.3 (CH_2Cl_2, 77 K)[a]	511	1233 (61)
3.4 (thin film, 298 K)	559	10.5 (0.17)
3.4 (thin film, 77K)	568	293.9(0.14)
3.4 (PMMA, 298 K)[b]	559	78.78 (2.7), 17.41 (0.90)
3.4 (CH_2Cl_2, 77 K)[a]	566	566.1 (4.0), 209.5 (3.3)

[a]Data collected in CH_2Cl_2 at a concentration of 10^{-6}M. [b]Data collected as a thin film of 10% by mass of 3.4 doped in PMMA.

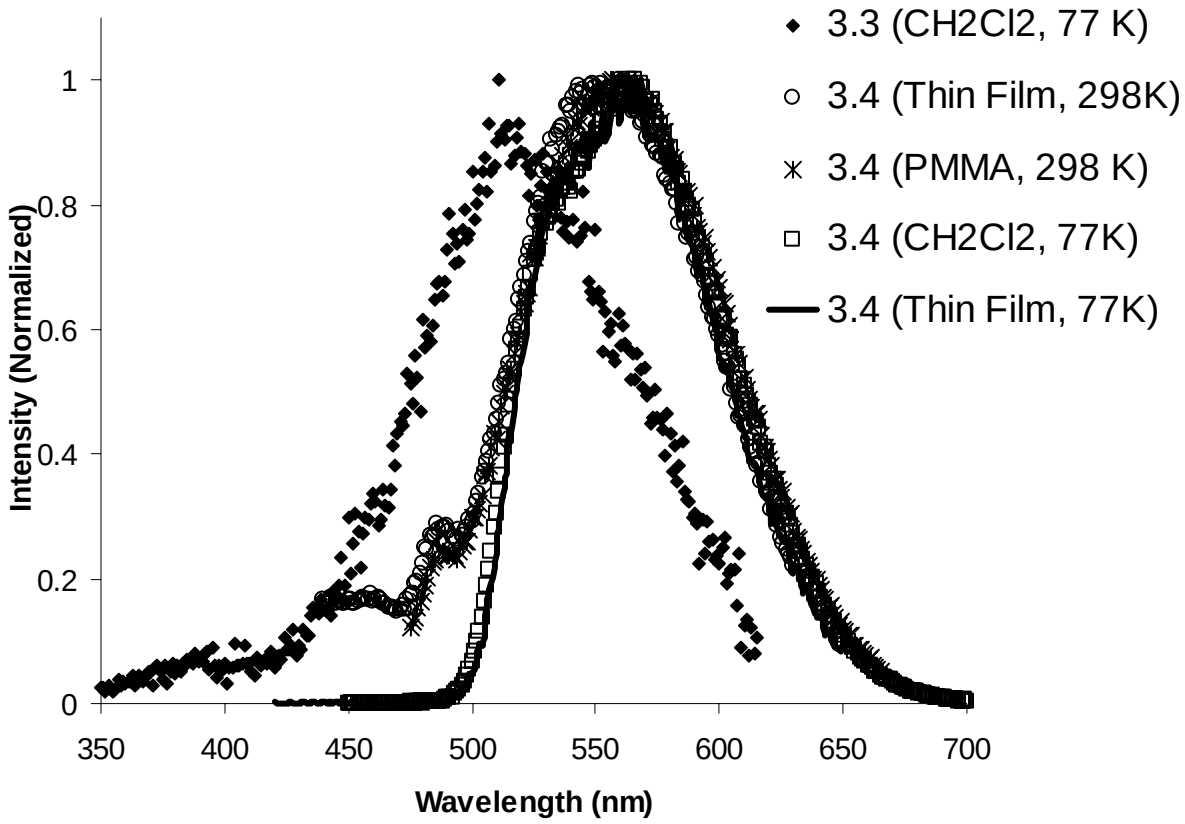

Figure 3-11: Phosphorescent spectra for 3.3 in CH_2Cl_2 glass at 77 K at a concentration of 10^{-5} M. For 3.4 the phosphorescent spectra were obtained in CH_2Cl_2 glass at a concentration of 10^{-5} M at 77 K, as a pure thin film, and as a film of 3.4 doped in PMMA (10% 3.4 by mass in PMMA). The excitation wavelengths were 320 nm and 371 nm for 3.3 and 3.4 respectively. Spectra were collected after 150 and 500 μs for 3.3 and 3.4 respectively.

3.3.3 Electrochemical properties

The electrochemical properties of 3.2 and 3.3 were evaluated by cyclic voltammetry. A mixture of freshly distilled methylene chloride and dry DMF was used as the solvent for 3.2, and dry acetonitrile was used as the solvent for 3.3. After calibration with the $FeCp_2/FeCp_2^+$ oxidation potential, the observed oxidation potentials were used to estimate the HOMO energy levels for each compound. The LUMO energy levels were subsequently estimated using the optical bandgap determined by UV-Vis-spectroscopy. The data are summarized in Table 3-6.

Neither compound is stable upon oxidation, indicating that unlike the compounds presented in chapter 2, these are not useful as charge transport materials. The photophysical and electrochemical data are summarized in Table 3-6. Compared to compound 2.3 in chapter two, the EAs for 3.2 and 3.3 are lower. It is apparent that the incorporation the DPA moiety raises the LUMO energy level. Moreover, this effect is more pronounced in 3.3, because of the additional modification of the benzimidazolyl group.

Table 3-6: Photophysical and electrochemical data for compounds 3.2 and 3.3.

	λ_{em} (nm)[a]	Φ[b]	E_{ox} (V)[c]	Optical bandgap (eV)[a]	HOMO (eV)	LUMO (eV)	HOMO-LUMO gap[d] (eV)
3.2	433	0.07	1.19	3.88	-5.44	-1.56	4.54
3.3	431	0.10	1.07	3.65	-5.41	-1.76	4.27

[a] Measured in CH_2Cl_2 at a concentration of 10^{-6} M. [b] Fluorescent quantum yields were measured relative to anthracene. [c] For 3.2 measured in CH_2Cl_2, for 3.3, measured in CH_3CN and measured versus a Ag/AgCl electrode. [d]Obtained from theoretical molecular orbital calculations.

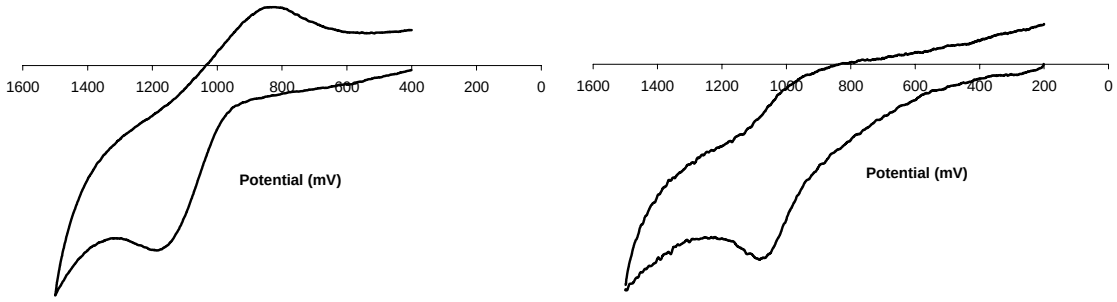

3.2 **3.3**

Figure 3-12: Cyclic voltammetry curves for 3.2 (left) in CH_2Cl_2-DMF and 3.3 (right) in acetonitrile. The oxidation was measured relative to the Ag/AgCl reference electrode.

3.3.4 Theoretical Molecular Orbital Calculations

Molecular orbital calculations have been performed on compound 3.2 and 3.3 to further understand the electronic properties of these compounds. Calculations were performed using density functional theory at the B3LYP level of theory, employing a 6-311^{++}G** basis set. The molecular orbital (MO) diagrams can be seen in Figure 3-13.

The MO diagrams clearly show that the HOMO orbitals are primarily centered on the benzimidazolyl and PBM moieties for 3.2 and 3.3 respectively. It is noteworthy that the electron density in the LUMO orbitals is dispersed over the entire structure, indicating a significant shift in electron density in the excited state. Therefore, the molecular orbital calculations support the conclusions drawn by the solvatochromic experiment, suggesting a charge transfer based excitation and emission.

Finally, the energies of the molecular orbitals for 3.2 and 3.3 were also calculated. The trend in the calculated bandgaps is in agreement with that obtained from the UV-Vis

data, and show that 3.2 has a larger bandgap than 3.3. It should be noted that for 3.2 there are two degenerate HOMO-1 molecular orbitals, and for 3.3 there are two degenerate HOMO energy levels.

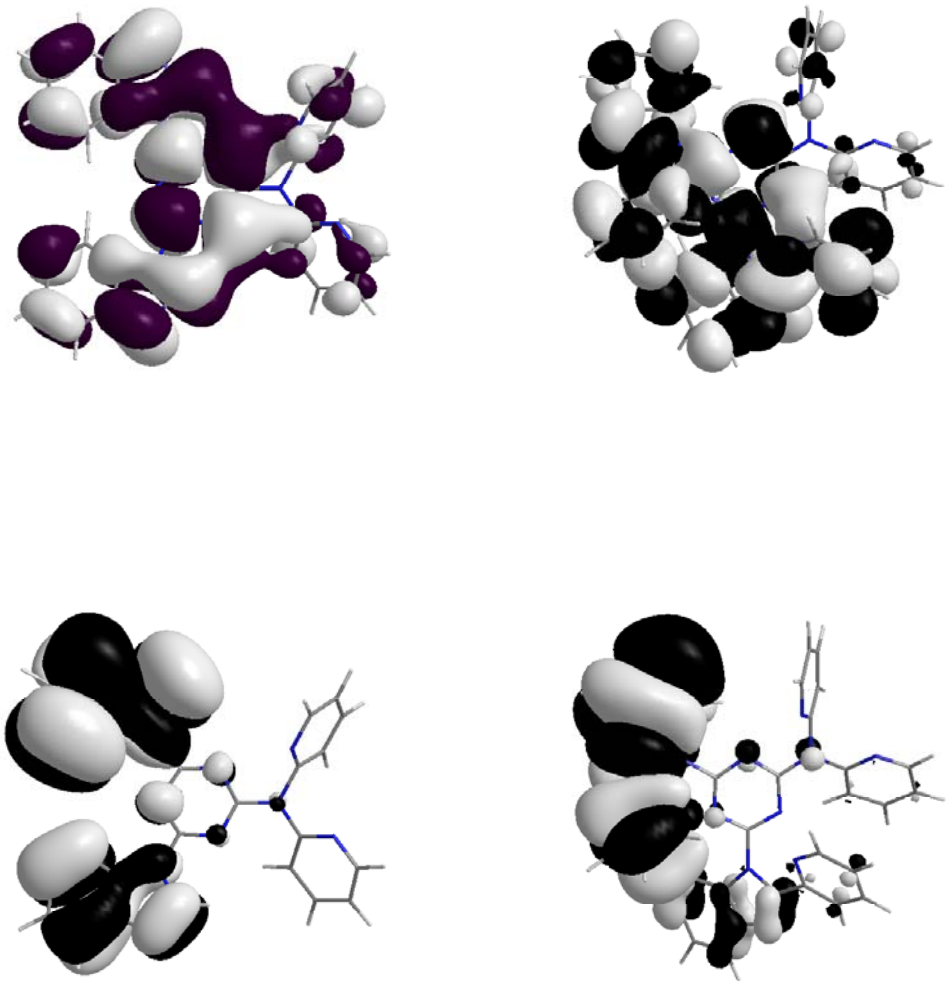

Figure 3-13: Molecular Orbital diagrams for 3.2 (left) and 3.3 (right). The HOMO diagrams (bottom) clearly show that the electron density is primarily focused on the benzimidazolyl and 2-(2'-pyridyl)benzimidazolyl moieties respectively, while the LUMO (top) shows electron density which is dispersed over the entire molecule.

3.3.5 Variable Temperature NMR Data

Room temperature ^{1}H NMR experiments for 3.4 revealed broad and unresolved signals. Therefore, variable temperature NMR was used in order to better resolve the spectrum.

Temperature dependant NMR spectra have been previously reported for related copper(I)[7b] and platinum(II) complexes employing the PBM functional group. The temperature dependence in these instances was a result slow interconversion of the *syn* and *anti* conformational isomers in the solution state, generally resulting in two sets of distinct chemical shifts, corresponding to separate isomers. The broadening of the NMR signals in 3.4 was believed to have a similar origin.

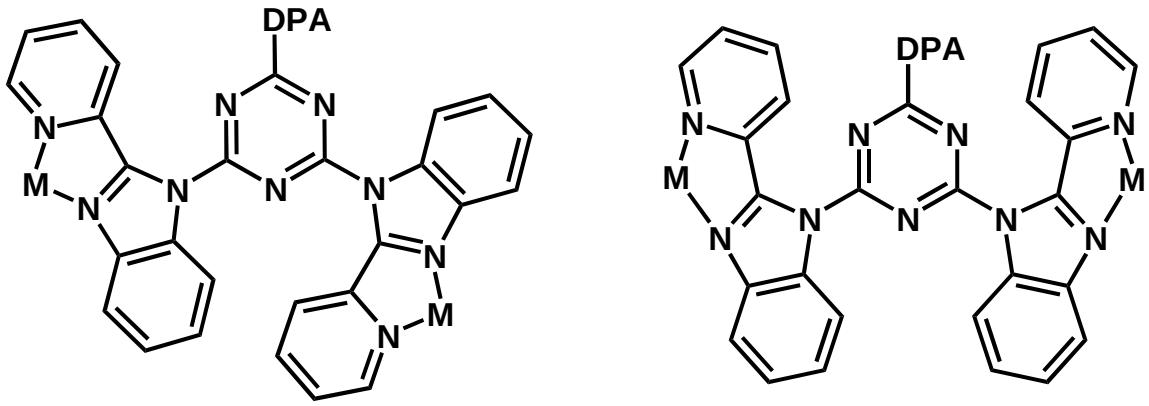

ANTI **SYN**

Figure 3-14: Illustrative diagram of the *syn* and *anti* conformations of 3.4. DPA represents the dipyridylamino group, and M is meant to represent the $[Cu(PPh_3)_2]^+$.

Decreasing the temperature to 253 K results in a well resolved spectrum which is consistent with the X-ray structure of 3.4. Based on an integration of 42 proton signals, corresponding to half of C_s symmetric molecule, there appears to be only a single isomer

at this temperature. At room temperature, it seems that the 2-(2'-pyridyl)benzimidazolyl groups rotate freely, resulting in a broadening of the NMR spectrum. When the temperature is lowered, the molecule no longer possesses sufficient energy to rotate, resulting in resolution of a single isomer. The resolved isomer is most likely the *syn* isomer, since the crystal structure indicates that this is the favored conformation.

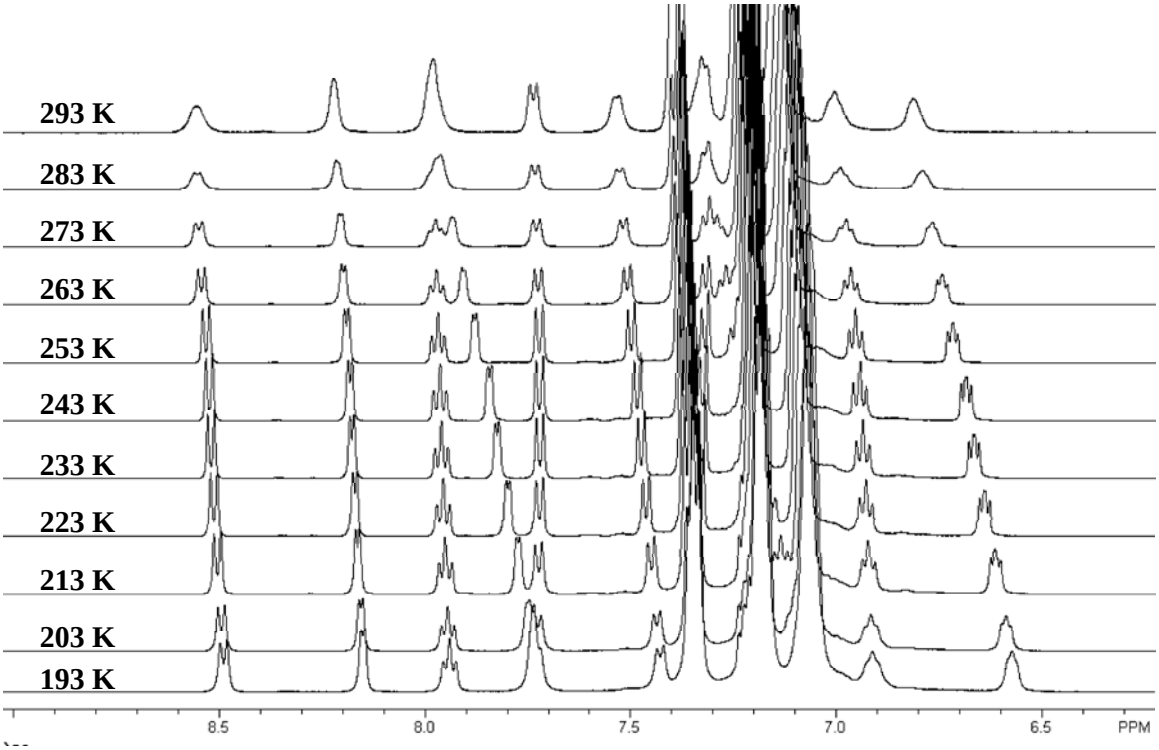

Figure 3-15: Low temperature NMR spectra for 3.4.

3.3.7: Metal Ion Titrations

In order to explore the utility of ligand 3.3 and the open binding site on 3.4, titration experiments with silver nitrate and zinc trifluoroacetate were performed. Silver(I) is interesting because it tends to elicit changes in absorption and fluorescence, and because of the diversity of coordination modes previously observed for silver complexes.[3,4] Zinc(II) was explored for similar reasons, and because of the utility of the

previously reported PBM functionalized molecules as fluorescent zinc sensors. The reasons for the interest in the sensing of zinc ions have been discussed in detail in chapter 1.

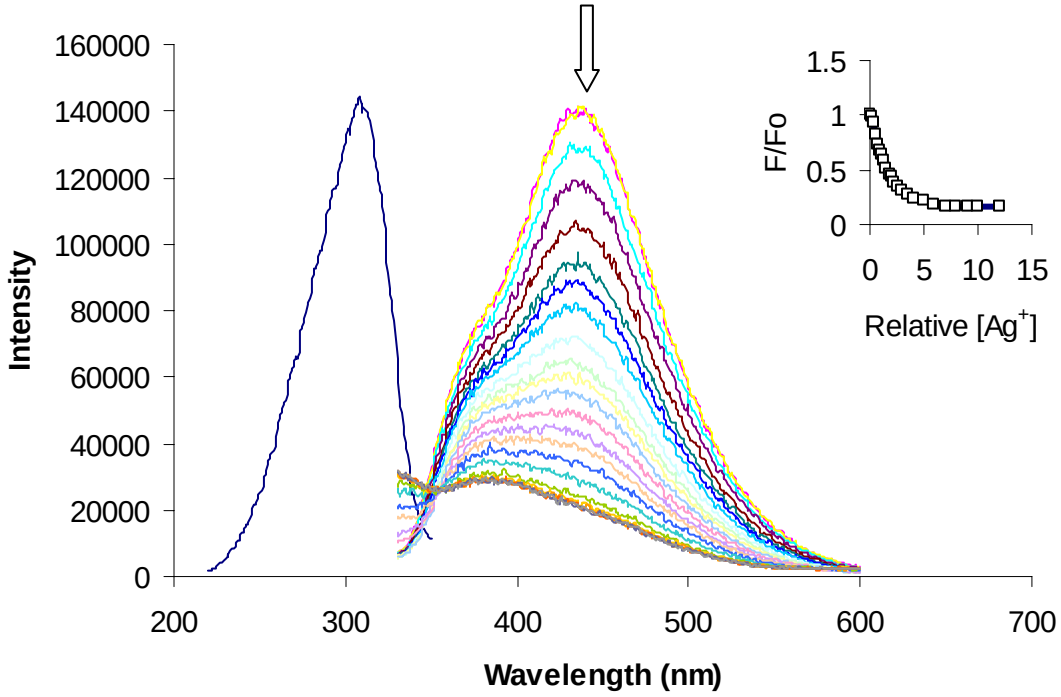

Figure 3-16: Fluorescent titration of 3.3 in CH_2Cl_2 (2.1×10^{-5}M) with $AgNO_3$ in CH_3CN (1.1×10^{-2}M). Inset: Stern-Volmer plot of relative fluorescent intensity at 433 nm versus relative concentration of metal ions. 0.1 equivalents of $AgNO_3$ was added until saturation was achieved. The excitation spectrum prior to titration is shown on the left.

As has been previously reported,[3,4,13] titration of 3.3 with $AgNO_3$ results in quenching of the ligand's normal fluorescence. As shown in Figure 3-16, quenching is complete upon addition of 6 equivalents of silver ions, and the fluorescence is reduced to ~16% of its original intensity.

Two effects are observed when 3.3 is titrated with zinc ions. Initially, the ligand fluorescence is quenched, until approximately 0.5 equivalents of metal ions have been

added. Addition of another 0.1 equivalents of Zn(II) results in fluorescent enhancement. This trend continued until two full equivalents of zinc ions had been added, at which point the fluorescent intensity had increased by more than 800%. Continued addition of zinc beyond two equivalents does not result in any further change in fluorescence intensity.

It seems that unlike copper(I), zinc(II) binds preferentially to the DPA functional group. The initial quenching may be due to binding of Zn(II) to the DPA site, which is known to display fluorescent quenching in the presence of zinc(II).[4] Coordination to the PBM site appears to become more favorable at higher ion concentrations, resulting in the observed fluorescent enhancement. This type of fluorescent enhancement has also been previously reported for PBM derivatives. [11]

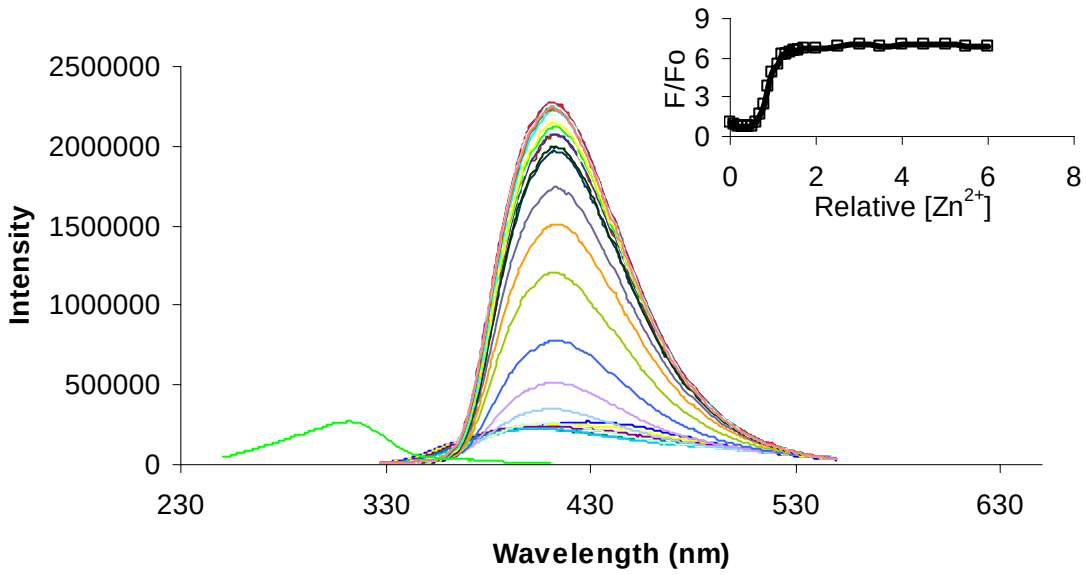

Figure 3-17: Fluorescent titration of 3.3 in CH_2Cl_2 (2.1×10^{-5}M) with $Zn(CF_3COO)_2$ in THF (1.0×10^{-2}M). Inset: Stern-Volmer plot of relative intensity at 431 nm versus relative concentration of metal ions. 0.1 equivalents of $Zn(CF_3COO)_2$ was added until saturation was achieved. The excitation spectrum prior to titration is shown on the left.

In order to confirm that binding of zinc(II) to the DPA group would in fact quench ligand fluorescence, TDAT was titrated with $Zn(CF_3COO)_2$ and the fluorescent response was observed. The titration data are presented in Figure 3-18 and do in fact confirm that coordination of Zn(II) to DPA causes fluorescent quenching.

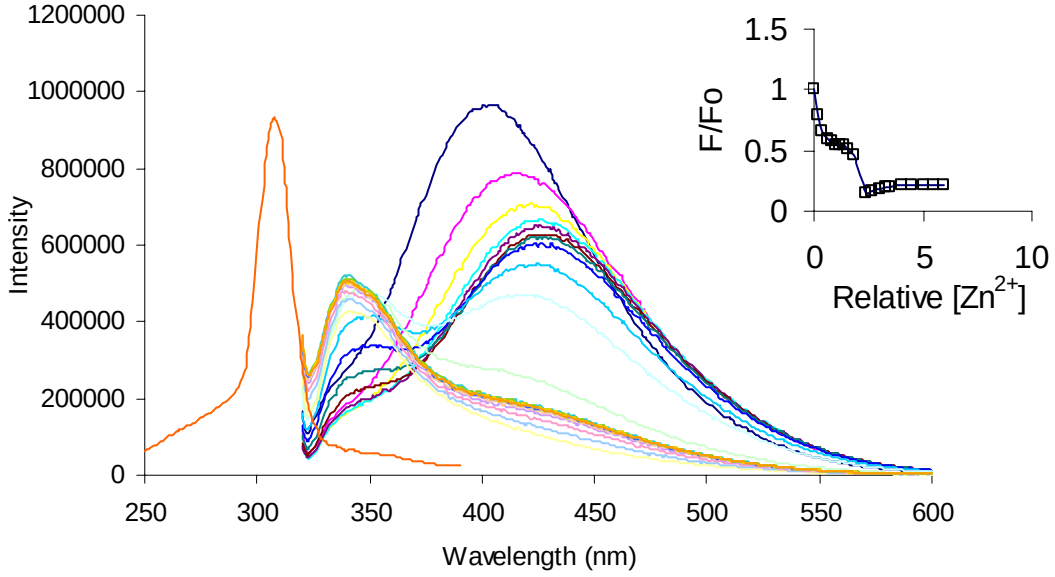

Figure 3-18: Fluorescent titration of TDAT in CH_2Cl_2 (2.5×10^{-4}M) with $Zn(CF_3COO)_2$ in THF (1.5×10^{-1}M). Inset: Stern-Volmer plot of relative intensity at 403 nm versus relative concentration of metal ions. 0.1 equivalents of $Zn(CF_3COO)_2$ was added until saturation was achieved. The excitation spectrum prior to titration is shown on the left.

While the impact of titration of 3.3 with zinc ions is interesting, it does not suggest that 3.3 would be a useful zinc sensor. The simultaneous existence of two opposing fluorescent responses will prevent determination of zinc concentration at low concentrations. Therefore, the homo-substituted PBM derivatives are still better for quantitative sensing of zinc ions.

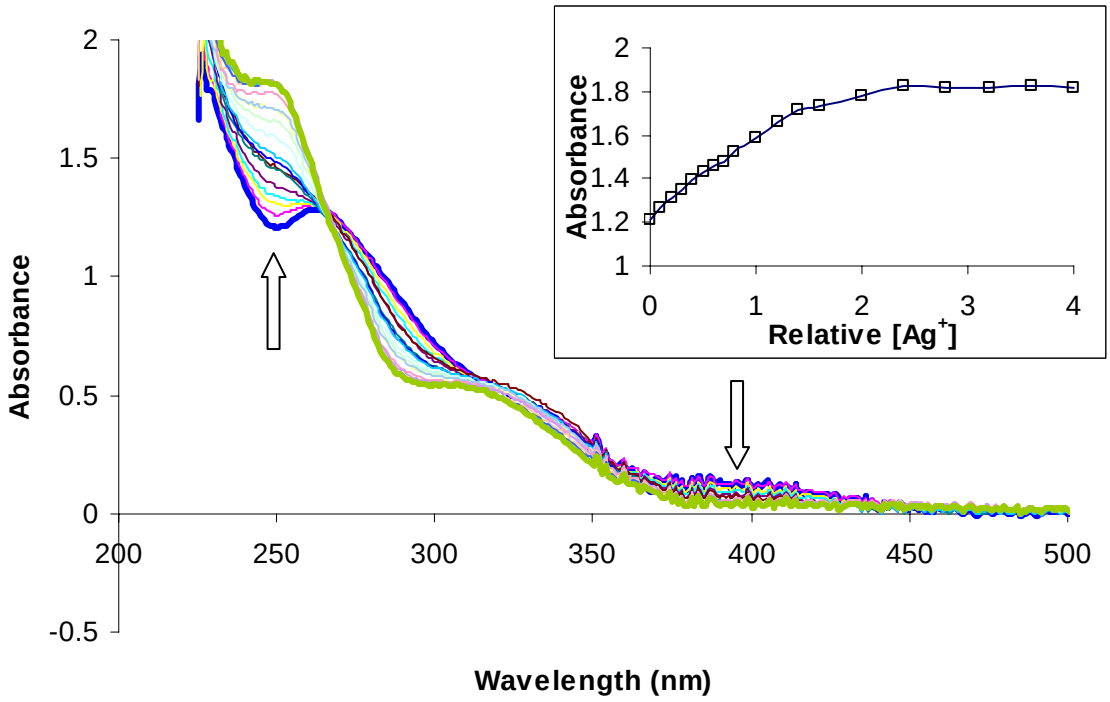

Figure 3-19: UV-Vis titration of complex 3.4 in CH_2Cl_2 (2.0×10^{-5}M) with $AgNO_3$ in CH_3CN (1.1×10^{-2}M). Inset: Plot of relative absorbance at 246 nm versus relative concentration of metal ions. 0.1 equivalents of $AgNO_3$ was added until saturation was achieved.

Because complex 3.4 is not fluorescent in solution under ambient conditions, the change in absorption with respect to metal ion concentration was recorded instead of the fluorescent response. As illustrated in Figure 3-19, titration of 3.4 with $AgNO_3$ affects the absorption spectrum in two ways. As the metal ion concentration increases, the absorption peak at 265 nm slowly shifts to 248 nm, and the metal to ligand charge transfer band centered at 400 nm slowly disappears. It is also noteworthy that the concentration of silver ions continues to affect the absorbance until two full equivalents of silver have been added.

The hypsochromic shift in the absorption band at 265 nm could be a result of a change in the energy levels of the molecular orbitals. Silver(I), like zinc(II), is a Lewis

acid, and will have an electron withdrawing effect upon coordination. Therefore, the ion can cause a stabilization of the HOMO orbital, and a thereby widen the optical bandgap.[14]

The disappearance of the charge transfer band suggests that the silver ions may in fact replace the copper ions in the coordination complex. The fact that the change in absorbance is not complete until the addition of two full equivalents of $AgNO_3$ further supports this hypothesis.

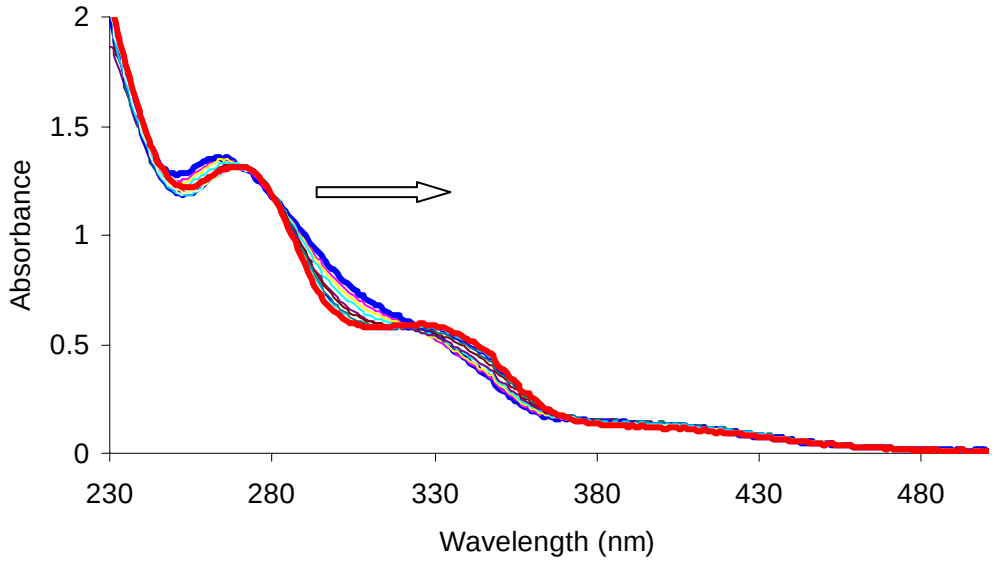

Figure 3-20: UV-Vis titration of complex 3.4 in CH_2Cl_2 (2.0×10^{-5}M) with $Zn(CF_3COO)_2$ in THF (1.0×10^{-2}M). 0.1 equivalents of $Zn(CF_3COO)_2$ was added until saturation was achieved.

The effect of titration with zinc (II) is depicted in Figure 3-20 and is less profound. Trifluoroacetate binds more strongly to zinc ions than nitrate does to silver ions, so this trend is expected. The charge transfer band is only slightly affected by addition of zinc, clearly demonstrating that zinc ions do not replace the copper ions. The addition of zinc causes an increase in intensity of the absorption band centered at 330 nm, and a slight red

shift in the absorption band at 268 nm. The effect on the absorption spectrum is complete upon addition of 1 full equivalent of zinc ions, suggesting that they are chelating to the DPA site.

3.4: Conclusions

A pair of novel molecular stars have been prepared and fully characterized. Because of their poor electrochemical stability and low fluorescent quantum yield, these compounds are not useful as materials for OLED applications.

Despite this, the coordination of compound 3.3 to a variety of metal ions has been explored. The presence of two distinct binding sites on a single molecular star provides a unique opportunity to observe the binding preference for different metal ions. For example, complete characterization of complex 3.4 clearly demonstrates that copper(I) binds preferentially to the PBM functional group. Furthermore, the UV-Vis titration experiment of complex 3.4 with $AgNO_3$ suggests that silver ions have a similar preference. This makes sense since the two ions are isoelectronic, and belong to the same group.

Zinc ions appear to bind more readily to the DPA functional group. This is suggested by the initial quenching of fluorescence of 3.3 at low concentrations of zinc, which has been previously observed for chelation of DPA to zinc ions. It is not until larger concentrations of zinc(II) are applied, and the DPA sites presumably become occupied, that the fluorescent enhancement, typical PBM chelation to zinc(II), is observed.

Finally, the phosphorescent properties of complex 3.4 have been carefully explored. The phosphorescent emission observed from complex 3.4 is distinctly different

from the phosphorescent emission observed from the free ligand. This suggests that the phosphorescence originates from the ^{3}MLCT excited state. Unfortunately, the phosphorescent lifetimes determined for 3.4 are substantially longer than those reported for related complexes, suggesting that 3.4 is also not appropriate for use as an emitter material in OLED applications.

1 J. Pang, Y. Tao, S. Freiberg, X.–P. Yang, M. D'iorio, S. Wang. *J. Mater. Chem.* 2002, **12,** 206.

2 a) W.–L. Jia, D.–R. Bai, T. McCormick, Q.–D. Liu, M. Motala, R.–Y. Wang, C. Seward, Y. Tao, S. Wang. *Chem. Eur. J.* 2004, **10,** 994. b) W. Yang, H. Schmider, Q. Wu, Y. Zang, S. Wang. *Inorg. Chem.* 2000, **39,** 2397. c) J. Pang, E. J.–P. Marcotte, C. Seward, R. S. Brown, S. Wang. *Angew. Chem. Int. Ed.* 2001, **40,** 4042. d) C. Seward, J. Pang, S. Wang. *Eur. J. Chem.* 2002, **6,** 1390. e) W.–L. Jia, T. McCormick, Q.–D. Liu, H. Fukutani, M. Motala, R.-Y. Wang, Y. Tao, S. Wang. *J. Mater. Chem.* 2004, **14**, 3344.

3 C. Seward, J. Chan, D. Song, S. Wang. *Inorg. Chem.* 2003, **42,** 1112.

4 Y. Kang, C. Seward, D. Song, S. Wang. *Inorg. Chem.* 2003, **42,** 2789.

5 C. Seward, W.–L. Jia, R.-Y. Wang, G. D. Enright, S. Wang. *Angew. Chem. Int. Ed.* 2004, **43,** 2933.

6 a)S**.–**M. Kuang, D. G. Cuttell, D. R. McMillin, P. E. Fanwick, R. A. Walton. *Inorg. Chem.* 2002**, 41,** 3313. b) A. Juris, R. Ziessel. *Inorg. Chim. Acta.* 1994, **225,** 251. c)M. K. Eggleston, D. R. McMillin, K. S. Koenig, A. Pallenberg. *J. Inorg. Chem.* 1997, **36,** 172. c) J. R. Kirchhoff, D. R. McMillin, W. R., Robinson, D. R. Powell, A. T. McKenzie, S. Chen. *Inorg. Chem.* 1985, **24,** 3928. d) K. Saito, T. Arai, N. Takahashi, T. Tsukuda, T. Tsubomura. *Dalton Trans.* 2006, 4444. e) K. Saito, T. Tsukuda, T. Tsubomura, *Bull. Chem. Soc. Jpn.* 2006, **79,** 437.

7 a) W.–L. Jia, T. McCormick, Y. Tao, J.–P. Liu, S. Wang. *Inorg. Chem.* 2005, **44,** 5706. b)T. M. McCormick, W.–L. Jia, S. Wang, *Inorg. Chem.* 2006, **45,** 147.

8 Q. Zhang, Q. Zhou, Y. Cheng, L. Wang, D. Ma., X. Jing, F. Wang. *Adv. Mater.* 2004, **16**, 432.

9 Q.–D. Liu, W.–L. Jia, S. Wang. *Inorg. Chem.* 2005, **44,** 1332.

10 W.-L. Jia, Y. –F. Hu, J. Gao, S. Wang. *Dalton Trans.* 2006, 1721.

11 L. De La Durantaye, T. McCormick, X.–Y. Liu, S. Wang. *Dalton Trans.* 2006, 5675.

12 J. Pang, Y. Tao, S. Freiberg, X.–P. Yang, M. D'iorio, S. Wang. *J. Mater Chem.* 2002, **12,** 206.

13 W.–L. Jia, R.–Y. Wang, D. Song, S. J. Ball, A. B. McLean, S. Wang. *Chem. Eur. J.* 2005, **11,** 832.

14 Q. Liu, M. S. Mudadu, H. Schmider, R. Thummel, Y. Tao, S. Wang. *Organometallics.* 2002, **21**, 4743.

Chapter 4

Summary and Prospective Efforts:

4.1 Summary and conclusions

The work presented in this thesis began in September 2004 with the intention of exploring benzimidazolyl functionalized ligands for applications in OLEDs. A series of seven new compounds have been synthesized and fully characterized using NMR spectroscopy and either elemental analysis or high resolution mass spectrometry. Furthermore, the previously reported 2,4,6-trisbenzimidazolyl-1,3,5-triazine has been fully characterized as an electron transport material for OLED applications.

It has been determined that benzimidazolyl compounds generally possess low lying LUMO energy levels and are reasonably stable to reduction. Furthermore, molecular stars incorporating this functionality are thermally stable. It has been further demonstrated that this class of compounds can function as excellent electron transport materials which perform similarly to Alq_3 a well known ETM. Moreover, unlike Alq_3, the benzimidazolyl derivatives possess large optical bandgaps, and do not emit substantially in the visible spectrum, making them potentially excellent host materials for other emitters.

The benzimidazolyl compounds are also fluorescent in the solution state. While coordination complexes have not been isolated for these ligands, their sensitivity toward metal ion complexation has been explored via a series of fluorescent titrations. It has been demonstrated that both silver(I) and zinc(II) ions quench the ligand based fluorescence, suggesting that these compounds could function as turn-off sensors for either metal ion. This is particularly important for zinc(II) because of its biological

relevance and the importance of being able to accurately sense concentrations of this ion. These titrations also helped reveal the benefits of incorporation of multiple fluorophores into a single molecule, since 2.5 was generally sensitive to a wider range of metal ion concentrations than 2.1.

Finally, a detailed comparison of benzimidazolyl derivatives and related indolyl and 7-azaindolyl compounds has been explored, both theoretically and empirically. It has been demonstrated that incorporation of the second heteroatom into the structure of the indolyl ring has a dramatic impact on the electronic properties of related compounds. It has also been demonstrated that the positioning of the heteroatom has an important influence on the electronic properties of these compounds, such that benzimidazolyl compounds typically display larger optical bandgaps and lower LUMO energy levels than previously reported, related 7-azaindolyl derivatives.

The compounds described in chapter 3 are equally interesting. Replacing one of the of the benzimidazolyl groups with a 2,2'-dipyridylamine (DPA) group has a dramatic effect on solubility. Moreover, replacing the other two benzimidazolyl groups with 2-(2'-pyridyl)benzimidazolyl (PBM) groups further enhances said solubility, and results in a molecule possessing three separate chelation sites.

These compounds were also characterized electrochemically, and found to be considerably less stable than their homo-substituted counterparts. Therefore, these compounds were not considered as potential charge transport materials. Furthermore, while both compounds are blue emitters, owing to the presence of the DPA functionality, neither is sufficiently bright to suggest application as an emitting material.

Despite this, exploration of the coordination chemistry of 3.3 has proven intersting. Isolation of single crystals of a copper(I) complex with 3.3 revealed a preference for coordination to the PBM group as opposed to the DPA. Complex 3.4 displays a MLCT based orange phosphorescence, typical of previously explored related compounds.

Furthermore, fluorescent and UV-Vis metal ion titrations were performed on 3.3 and 3.4 respectively. It has been demonstrated that the ligand fluorescence is sensitive to the presence of the metal ions. The impact of metal ion titration on the UV-Vis spectrum of the copper complex has also been explored. The data suggest that zinc(II) ions will coordinate to the open DPA site on 3.4 and therefore only slightly change the absorbance. Silver(I) ions on the other hand appear to prefer binding to the PBM groups, such that they displace the coordinated copper ions, and completely quench MLCT absorption. Therefore, while the compounds presented in chapter 3 are not promising as OLED materials, they do present an excellent opportunity to explore some of the fundamentals of inorganic chemistry.

4.2 Future Research

Continuation of related work should focus on further device characterization of homo-substituted benzimidazolyl compounds from chapter 2 and on further exploration of the coordination chemistry of the hetero-substituted triazine stars reported in chapter 3.

It has been suggested that the wide optical bandgap observed in the benzimidazolyl derivatives makes them suitable as host materials for other emitters. Therefore, further work exploring the possibility of using 2.3 as a host material for blue emitters is certainly warranted.

In addition to this, further characterization of the benzimidazolyl derivative compounds is also of interest. It has been shown that the use of triethylamine in column chromatography can facilitate the isolation of benzimidazolyl derivatives. The syntheses and purification of 2.1, 2.2 and 2.4 should be optimized to improve the yields, and then these compounds should be explored as electron transport and host materials. While 2.3 does have the highest electron affinity, 2.2 and 2.5 have larger optical bandgaps, which could make them more effective host materials. Therefore further exploration of the applications of the other derivatives is warranted.

Continuation of the coordination chemistry with 3.2 and 3.3 is also of interest. Both compounds possess Lewis basic nitrogen sites which can be used to bind to metals. The titration data suggest a preference for zinc(II) binding to the DPA functional group, and for silver(I) to bind to the PBM functional group. Confirmation of these conclusions is best done through preparation of zinc(II) and silver(I) complexes in different metal to ligand ratios in order to determine the true preference for the binding. Furthermore, NMR studies to determine possible fluxionality in solution is also of interest. Finally, preparation of similar complexes with 3.2 would also be interesting.

In addition to this, mixed metal complexes derived from the copper(I) complex 3.4 are also worth examining. First, preparation of a complex by adding two equivalents of $AgNO_3$ to the copper complex is crucial, in order to verify that silver does in fact displace copper during the UV-Vis titrations. Furthermore, mixed metal complexes incorporating both copper(I) and zinc(II) could be interesting to characterize, in order to completely understand what is happening during the titration.

Continuation of this work to include other transition metals such as ruthenium(II) and platinum(II) is also interesting. These metals are known to show intense orange ^{3}MLCT type emission, and have shown great potential as phosphorescent emitters in OLED applications. Perhaps complexes of 3.2 or 3.3 and these metals will generate compounds which are more promising as triplet emitters. Clearly, there are still a great number of interesting experiments which are left to be done on this system.